



Broadening the 1D dissolution: new nanosheets and new media

Doctoral Thesis

submitted to obtain the academic degree of Doctor of Natural Sciences

(Dr. rer. nat.)

of the Bayreuth Graduate School of Mathematical and Natural
Sciences (BayNAT)

of the University of Bayreuth

Volodymyr Dudko

from Pavlohrad, Ukraine

Bayreuth, 2023

This doctoral thesis was prepared at the department of Inorganic colloids for electrochemical energy storage (former *Inorganic Chemistry I*) at the University of Bayreuth from (09/2019) until (05/2023) and was supervised by Prof. Dr. *Josef Breu*.

This is a full reprint of the thesis submitted to obtain the academic degree of Doctor of Natural Sciences (Dr. rer. nat.) and approved by the Bayreuth Graduate School of Mathematical and Natural Sciences (BayNAT) of the University of Bayreuth.

Type of dissertation: Cumulative thesis

Date of submission: 11.05.2023

Date of defence: 14.12.2023

Acting director: Prof. Dr. Jürgen Köhler

Doctoral committee:

Prof. Dr. Josef Breu (reviewer)

Prof. Dr. Markus Retsch (reviewer)

Prof. Dr. Seema Agarwal (chairman)

Prof. Dr. Leonid Ionov

Table of content

Contents

Table of content.....	1
List of abbreviations.....	2
1 Summary	3
2 Zusammenfassung.....	3
3 Introduction	6
3.1 Synthetic hectorite as a model system.....	7
3.2 Mechanism and driving forces	7
3.3 How to trigger delamination by 1D dissolution	15
4 Synopsis	24
4.1 Osmotic Delamination: A Forceless Alternative for the Production of Nanosheets Now in Highly Polar and Aprotic Solvents	25
4.2 Delamination by repulsive osmotic swelling of synthetic Na-hectorite with variable charge in binary DMSO-water mixtures	27
4.3 Spontaneous Delamination of Affordable Natural Vermiculite as a High Barrier Filler for Biodegradable Food Packaging	29
5 Own contribution.....	33
6 References	34
7 Osmotic delamination: Forceless alternative for the production of nanosheets now in highly polar and aprotic solvents.....	42
8 Delamination by repulsive osmotic swelling of synthetic Na-hectorite with variable charge in binary DMSO-water mixtures.....	56
9 Spontaneous Delamination of Affordable Natural Vermiculite as a High Barrier Filler for Biodegradable Food Packaging.....	80
10 List of publications and conferences	105

List of abbreviations

2D Two-dimensional

1D One-dimensional

DMSO Dimethyl sulfoxide

PXRD (Powder) x-ray diffraction

NMR Nuclear magnetic resonance

PLA Polylactic acid

SAXS Small angle X-ray scattering

3D three-dimensional

DMAE 2-(dimethylamino)ethanol

TBA tetrabutylammonium

TMA tetramethylammonium

C4 n-butylammonium

C3 n-propylammonium

Na-Hec sodium Hectorite

vol% volume percent

PVDC poly(vinylidene dichloride)

PBAT poly(butylene adipate terephthalate)

PBSA poly(butylene succinate-co-butylene adipate)

NMF N-methyl formamide

1 Summary

The potential of 2D materials in various fields of material science and chemistry is undeniable. However, their large-scale production poses challenges due to low yield, uncontrollable defects, and high-energy input in state-of-the-art exfoliation methods. Balancing high quality and high yield has always been a tradeoff. In this thesis, I explore an alternative method for producing 2D nanosheets called 1D dissolution (historically known as osmotic swelling), which is a thermodynamically driven process with numerous benefits. It yields a high aspect ratio and defect-free nanosheets with a quantitative yield. In this thesis, I have focused on the expanding phenomenon of 1D dissolution to organic solvents and understanding its main driving forces using synthetic hectorite as a model system.

First, the importance of steric pressure is demonstrated. It is caused by the interlayer cation and the right combination of the solvent parameters, which leads to the synergistic effect of 1D dissolution. In this case, the complexation of the interlayer Na^+ by 15-crown-5 and 18-crown-6 caused the 1D dissolution in the number of highly polar solvents like ethylene carbonate, propylene carbonate, glycerol carbonate, N-methylformamide, and N-methylacetamide. The crucial parameters for the solvents were found to be a high dipole moment and a high dielectric constant. This highlights the key role of electrostatic interactions in the 1D dissolution process. Second, the role of a strong hydrogen bonding network of water-DMSO mixture for the delamination of highly charged clays was investigated. Hectorite shows a well-defined 1D dissolution window, where the phenomenon of 1D dissolution is observed and outside of this composition, swelling is limited only to crystalline. We applied the PXRD and ^{23}Na solid-state NMR to study solvation behavior and uncovered the key role of the solvation environment. The water and DMSO molecules form molecular assemblies, which act as a single solvation unit and exert a bigger steric pressure on the interlayer space, leading to 1D dissolution.

Finally, we explored the transferring of knowledge, obtained from studying the synthetic hectorite as a model system, to more relevant and affordable natural analogs –vermiculites. The paper reports an improved delamination protocol based on the use of butyl amine as the cation and organic acids as the counter anion. Organic acids in this case act as a complexing agent to the Mg^{2+} cations, which are commonly found in natural vermiculites and impede the 1D dissolution process. After the successful ion exchange, the 1D dissolution is extended to highly polar organic solvents, which allows the processing of vermiculite nanosheets as a nanocomposite with PLA- one of the most promising biodegradable polymers. The resulting nanocomposite boosts the barrier performance to the level of commercially available multilayer metalized films.

2 Zusammenfassung

Das Potential von 2D-Materialien in verschiedenen Bereichen der Materialwissenschaft und Chemie ist unbestreitbar. Die großflächige Produktion stellt jedoch aufgrund geringer Ausbeute, unkontrollierbarer Defekte und des hohen Energieaufwands bei State-of-the-Art-Exfoliationsmethoden eine Herausforderung dar. Ein Ausgleich zwischen hoher Qualität und hoher Ausbeute war schon immer ein Kompromiss. In dieser Arbeit wird eine alternative Methode zur Herstellung von 2D-Nanosheets namens 1D-Auflösung (historisch bekannt als osmotische Quellung) untersucht, die ein thermodynamisch gesteuerter Prozess mit zahlreichen Vorteilen ist. Sie liefert Nanosheets mit hohem Aspektverhältnis und ohne Defekte mit quantitativer Ausbeute. In dieser Arbeit wurde die Ausdehnung des Phänomens der 1D-Auflösung auf organische Lösungsmittel und das Verständnis ihrer wichtigsten treibenden Kräfte unter Verwendung synthetischer Hectorite als Modellsystem untersucht.

Zunächst wird die Bedeutung des sterischen Drucks demonstriert. Dieser wird durch das Zwischenschichtkation und die richtige Kombination der Lösungsmittelparameter erzeugt, was zum synergistischen Effekts der 1D-Auflösung führt. In diesem Fall verursachte die Komplexierung des Zwischenschicht- Na^+ durch 15-Krone-5 und 18-Krone-6 die 1D-Auflösung in einer Reihe von stark polarisierten Lösungsmitteln wie Ethylencarbonat, Propylencarbonat, Glycerolcarbonat, N-Methylformamid und N-Methylacetamid. Die entscheidenden Parameter für die Lösungsmittel waren ein hohes Dipolmoment und eine hohe Dielektrizitätskonstante. Dies unterstreicht die wichtige Rolle elektrostatischer Wechselwirkungen im Prozess der 1D-Auflösung.

Zweitens wurde die Rolle des starken Wasserstoffbrückenbindungsnetzwerks einer Wasser-DMSO-Mischung für die Delamination von stark geladenen Tonen untersucht. Hectorit zeigt ein klar definiertes Fenster für die 1D-Auflösung, in dem das Phänomen der 1D-Auflösung beobachtet wird, und außerhalb dieser Zusammensetzung ist die Quellung auf kristalline Strukturen beschränkt. Wir haben die PXRD und ^{23}Na -Festkörper-NMR angewendet, um das Solvationsverhalten zu untersuchen und die wichtige Rolle der Solvationsumgebung aufzudecken. Die Wasser- und DMSO-Moleküle bilden molekulare Assemblierungen, die als einzelne Solvatationseinheit wirken und einen größeren sterischen Druck auf den Zwischenschichtraum ausüben, was zur 1D-Auflösung führt.

Schließlich wurde das Wissen, welches durch die Untersuchung des synthetischen Hectorits als Modellsystem gewonnen wurde, auf relevantere und erschwinglichere natürliche Analoge - Vermikulite - angewendet. Die Arbeit berichtet über ein verbessertes Delaminierungsprotokoll auf Basis der Verwendung von Butylamin als Kation und organischer

2 Zusammenfassung

Säuren als Gegenion. Organische Säuren wirken in diesem Fall als Komplexmierungsmittel für die Mg^{2+} -Kationen, die in natürlichen Vermikuliten häufig vorkommen und den 1D-Auflösungsprozess hindern. Nach dem erfolgreichen Ionenaustausch wird die 1D-Dissolution auf hochpolare organische Lösungsmittel ausgeweitet, so dass die Vermikulit-Nanoschichten als Nanokomposit mit PLA - einem der vielversprechendsten biologisch abbaubaren Polymere - verarbeitet werden können. Das resultierende Nanokomposit erhöht die Barriereigenschaften auf ein Niveau von kommerziell erhältlichen metallisierten Mehrschichtfolien.

3 Introduction

The properties of materials at the nanoscale can differ significantly from those of bulk materials. For example, materials that are unreactive in bulk form can become catalytically active at the nanoscale¹, thanks to quantum size effects that modulate their electronic structure. Many of these intriguing properties are rooted in quantum and surface phenomena².

Two-dimensional (2D) materials, in particular, exhibit unique properties due to their extreme anisotropy. These materials typically consist of stacked nanosheets, known as tactoids, which can be hundreds of nanometers to micrometers wide but only a few nanometers thick³. The anisotropy of individual nanosheets results in a high surface-to-volume ratio⁴ and a pronounced directional dependence of properties, such as moduli^{5, 6}.

Since the ground-breaking work of Novoselov and Geim on monolayer graphene almost two decades ago, there has been a growing interest in 2D materials⁷⁻¹¹. Hundreds of 2D materials have been isolated and studied¹²⁻¹⁹, finding applications in catalysis^{2, 20}, electronics²¹, sensors²², biomedical fields²³, and more²⁴⁻²⁸. Despite this progress, there is still a lack of an effective and universal approach to delaminate and produce 2D materials with a monodisperse thickness on a large or industrial scale.

The story of delaminated materials goes back much further in scientific history. Clay^{29, 30} and graphene oxide^{29, 31, 32} were likely the first 2D materials known to humanity. When certain clay minerals are immersed in water, they can disperse homogeneously to form a viscous suspension consisting of nanometer-thick clay sheets, a phenomenon called "osmotic swelling"^{29, 33-37} that was thoroughly studied in the 1960s. This historic term suggests that the process is related to osmotic pressure, but it was later discovered that the initial phases of repulsive osmotic delamination have more to do with the dissolution of ionic crystals. Clay tactoids separate into individual single-layer nanosheets at distances of hundreds of nanometers³⁸ through a spontaneous process³⁸⁻⁴¹, requiring no additional energy input to completely delaminate the pristine layered material. Osmotic swelling allows for the maximization of yield, obtaining nanosheets with strictly monolayer thickness and a unique mesophase with the liquid crystalline state of the nanosheets. If only every 2D material could be prepared using a similar approach! The state-of-the-art process-liquid phase exfoliation⁴²⁻⁴⁵ relies on high-power ultrasonification, to separate nanosheets, but it is a brute-force method. Instead, this thesis will strictly focus on purely thermodynamically driven and therefore spontaneous delamination processes that do not require any input of shear force. Unfortunately, these processes are currently regarded as niche and are mainly known in the clay science community. Historically, it was referred to as "osmotic swelling," but in its initial steps, the process has nothing to do with osmotic pressure

3 Introduction

and instead resembles the dissolution of ionic solids. For layered ionic materials, this dissolution is limited to the stacking direction of the nanosheets, and therefore, labeling one-dimensional (1D) dissolution is suggested. This thesis will explore the widening of 1D dissolution to the organic solvents and uncover new strategies for the 1D dissolution triggering.

3.1 Synthetic hectorite as a model system

To get the full understanding and avoid false positive or false negative results it is needed to start with a well-defined and easy to work with material. Redox-active compounds like Li-MoS₂⁴⁶ or K-graphite⁴⁷ are not suitable because of their high redox activity and enormous sensitivity to oxygen and water. Natural clays have inhomogeneous charge density and defects that impede 1D dissolution in many cases⁴⁸⁻⁵¹. For this reason, synthetic hectorite is chosen as a model system for studying 1D dissolution.

Synthetic hectorite is the 2:1 smectites of the stoichiometric formula $[\text{Na}_{0.5}]^{\text{inter}}[\text{Mg}_{2.5}\text{Li}_{0.5}]^{\text{oct}}[\text{Si}_4]^{\text{tet}}\text{O}_{10}\text{F}_2$ ^{52, 53}. It consists of two tetrahedral sheets, that sandwich the octahedral layer. Nanosheets have permanent charged, caused by the isomorphous substitution of Mg²⁺ to Li⁺ and the negative charge is compensated by the interlayer cation, in the case of synthesized material- Na⁺.

Interlayer cation is relatively mobile and can be exchanged for other positively charged species. This changes the interaction energy with the solvent system and can be used to manipulate the 1D dissolution process.

Synthetic hectorite has a high phase purity and charge homogeneity, meaning that 1D dissolution and the crystalline swelling process occur homogeneously through the whole material and can be tracked using PXRD, NMR, or SAXS.

Charge homogeneity and phase purity are achieved by the elaborate synthetic procedure involving melt synthesis and long-term annealing to ensure the superior properties of the crystals⁵². Upon immersion of the crystalline powder into water, the nanosheets separate into hundreds of nanometers forming a nematic liquid crystalline phase even at very diluted concentrations³⁸. This liquid crystallinity is the first indication of 1D dissolution that can be easily verified under the cross-polarized light due to the characteristic birefringence of the nematic phase.

3.2 Mechanism and driving forces

The unique characteristic of 2D materials lies in their anisotropic chemical bonding. In two dimensions, the bonding is strong and partially covalent. In the third direction, there are weaker, but still cohesive, non-covalent interactions that result in stacks of nanosheets (Figure 1). Compared to ionic layered solids that are held together by Coulomb attraction (Figure 1)⁵⁴,

3 Introduction

cohesive interactions in van der Waals crystals are considerably weaker⁵⁵. However, this Coulomb attraction can be reversed to repulsion, which is the fundamental principle behind osmotic swelling and 1D dissolution.

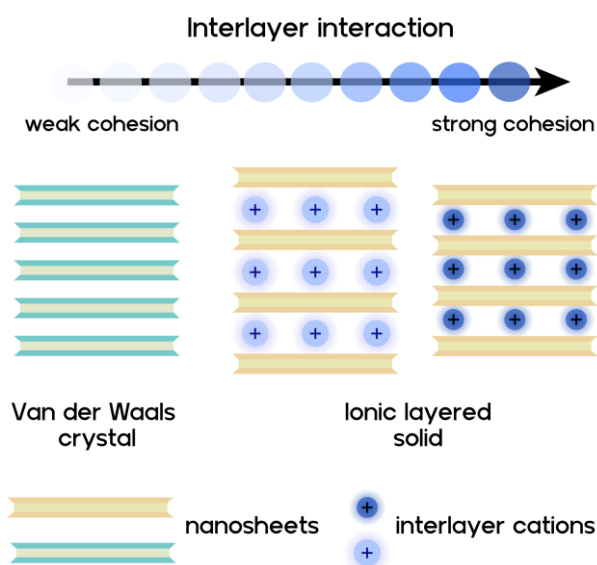


Figure 1. Types of layered compounds and relative strength of cohesive interactions holding together the nanosheets in the stack. Reproduced with permission⁵⁶. Copyright 2021, Wiley-VCH GmbH.

Layered materials exhibit weak interactions in the stacking direction, allowing for soft, intracrystalline reactions that are topotactic, meaning that the periodicity in the stacking direction can be altered while maintaining the 2D structure of the nanosheets (Table 1). In the case of anionic layers, ion exchange with bulky cations can increase the d-spacing and weaken the cohesive interaction. Similarly, the solvation of interlayer ions, known as crystalline swelling, can also increase the d-spacing and enhance the shear lability^{57, 58}.

Unlike osmotic swelling, crystalline swelling refers to a distinct phase transition with a defined stoichiometry. Depending on the type of interlayer ion and the activity of the swelling agent, the solvent is incorporated into the interlayer space in discrete steps (e.g. one-, two-, or three-layer hydrate in hectorites)⁵². Swelling and de-swelling in the crystalline swelling regime exhibit a hysteresis as expected for a first-order phase transition. If the basal surfaces carry functional groups, such as silanol groups found in zeolites, molecules can be covalently attached, leading to an irreversible increase in the d-spacing (Table 1).

Table 1. Topotactic intra-crystalline reactions (e.g. intercalation: e.g. grafting, ion-exchange, swelling) increase the basal spacing and thus decrease the cohesive energy in the stack.

3 Introduction

Type of reaction	Grafting	Ion-exchange	Swelling	
			Crystalline	1D dissolution
Reversibility	irreversible	reversible	reversible	reversible
Bonding type	covalent	ionic interaction, non-covalent	stepwise non-covalent	quasi-continuous non-covalent
Type of interactions of adjacent nanosheets	cohesive	cohesive	cohesive	repulsive

One of the key features of layered crystals is the strong anisotropy of chemical bonding, resulting in weak interactions in the stacking direction. As long as the nanosheets are cohesively stacked, energy input is required to obtain exfoliated materials through a top-down process. Liquid phase exfoliation is currently the most established and widely used method for exfoliating such cohesively stacked layered crystals. This process relies on strong shear forces applied to suspensions⁵⁴, which can thin down the stacks to individual nanosheets⁵⁹.

It should be noted, however, that liquid phase exfoliation cannot achieve delamination, as defined by Gardolinski and Lagaly⁶⁰ for clay minerals, where exfoliation refers to the decomposition of large aggregates into smaller particles, while delamination refers to the separation of individual layers of particles.

The diverse range of scientific communities interested in 2D materials has led to various terminologies being used to describe layered compounds and nanosheets. To establish a common ground and clarify the terminology, the following terms are proposed:

- Tactoid: a stack of layers; since individual layers are stacked with frequent faults or even in a completely random way, these stacks of layers lack a strict crystallographic phase relationship and consequently should not be referred to as crystals, but as tactoids.
- Intercalation: Incorporation of atoms, ions, or molecules into a layered host structure. It is a topotactic reaction with the 2D structure where the layers remain essentially unchanged, while the inserted material is present between the layers. Intercalation commonly involves ion exchange or solvation reactions.
- Interlayer refers to the region between the two adjacent layers in a tactoid.

3 Introduction

- (Intracrystalline) swelling involves an increase in the basal spacing of a layered compound to accommodate H₂O or other solvent or gaseous molecules within the interlayer.
- Exfoliation: slicing of tactoids into thinner stacks with multimodal thickness distributions
- Delamination: exfoliation of layered material to the level of individual, single-layer nanosheets; a state in which translational symmetry along the stacking direction is completely destroyed.

High-power ultrasonication is the most commonly used method to overcome cohesion forces required to obtain 2D materials (First line Table 2). However, this brute force approach mechanically breaks weak van der Waals bonds and lacks control over the thickness distribution of the resulting materials. Liquid phase exfoliation, on the other hand, generates dispersions of 2D materials consisting of single, double, and multilayer nanosheets^{13, 54, 61, 62}. This method is also energy-intensive, challenging to scale⁶³, and often provides only a modest yield of nanosheets. Additionally, the excess energy required for exfoliation may cause the nanosheets to break, resulting in aspect ratios far from the potential maximum determined by the pristine layered material's inherent diameter⁶⁴. Furthermore, the collapse of cavities produced by ultrasonication results in high local temperatures, potentially producing radicals that may chemically modify the nanosheets' surface⁶⁵.

Table 2. Comparison of advantages and disadvantages of different exfoliation methods and 1D dissolution.

Exfoliation method	Type of materials accessible ^l	Advantages	Disadvantages
Mechanical ^{62, 63, 66, 67}	2 D van der Waals crystals like graphene, boron nitride, black phosphorous, metal dichalcogenides	Suitable for most 2D materials, simple equipment, easy to use, universal	Low yield, high energy input, low aspect ratio, defects, and functional groups may be introduced, and broad thickness distribution

3 Introduction

Hydrothermal ⁶⁸	Materials that show crystalline swelling, potentially after redox-modification rendering the materials more shear labile: metal dichalcogenides, metal hydroxides, metal oxides, MXenes	Moderate yield, narrow lateral size distribution	Defects may be introduced, requires special equipment, non-universal.
Electrochemical ⁶⁹	As above, crystalline swelling is, however, triggered by redox modification by an external field: graphene, black phosphorous, metal dichalcogenides, MXenes, metal oxides	High yield, narrow thickness distribution.	2D materials must be electrically conductive, requires high-quality crystals, requires electrochemical equipment
1D dissolution	Silicates, zeolites perovskites, acids. oxides	Strictly monolayers, quantitative yield, the direct formation of electrostatically stabilized liquid crystalline phase,	Limited to ionic layered solids, requires a special protocol for every material, non-universal.

3 Introduction

		no surfactants required	
--	--	-------------------------	--

a) All materials referred to here are of layered morphology.

In contrast, a few rare ionic-layered materials exhibit osmotic swelling, a thermodynamically spontaneous process for delamination that has been known for some time⁷⁰. Examples of such materials include layered transition metal oxides, layered antimony phosphates, graphene oxide, layered zeolites, or smectites. This process, also known as "one-dimensional dissolution" (1D dissolution), is based on repulsive interactions between charged nanosheets and results in complete delamination with a 100% yield. The resulting suspensions are colloidally stable and consist solely of individual nanosheets. One of the advantages of this process is that it preserves the aspect ratio of the starting material and does not introduce additional defects to the nanosheet structure. Furthermore, it is a gentle process that does not require high energy input. A comparison of the common exfoliation methods and 1D dissolution can be found in Table 2.

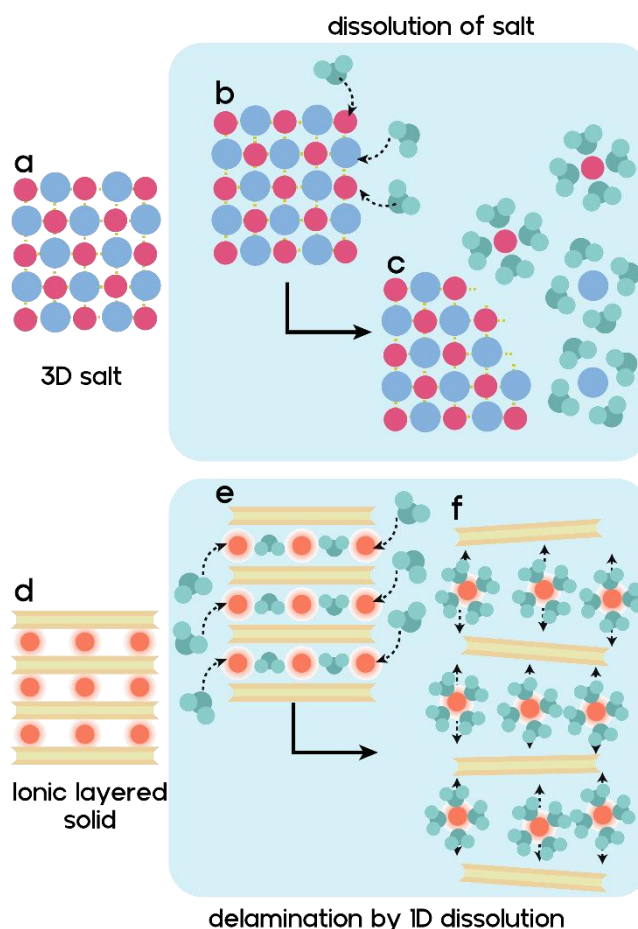


Figure 2. Schematic of the dissolution of a 3D crystalline salt and the 1D dissolution of a layered material. Crystalline salt **a.** upon immersion in water it starts to readily dissolve **b.** until

3 Introduction

complete dissolution with the formation of c. a homogeneous solution of ions. Ionic layered solid d. upon immersion into the solvent, solvent molecules start to solvate the interlayer ions e. and upon reaching the critical threshold separation 1D dissolution into a nematic liquid crystalline suspension takes place f. Reproduced with permission⁵⁶. Copyright 2021, Wiley-VCH GmbH.

The delamination process through osmotic swelling shares similarities with the dissolution of salts (Figure 2a). When an ionic crystal, such as sodium chloride, is immersed in water, it dissolves due to the solvation of the ionic constituents on its surface by water molecules, resulting in the separation of solvated ions (Figure 2b). The strong electrostatic attraction between positively and negatively charged ions must be overcome by the interaction with the solvent molecules (Figure 2c). Dissolution is driven in part by the enthalpy of solvation, and the entropy increase during the dissolution process may allow for crystals to dissolve even with an endothermic enthalpy of dissolution. Overall, dissolution is a thermodynamically driven process (exergonic) in which all enthalpic and entropic contributions involved override the lattice energy.

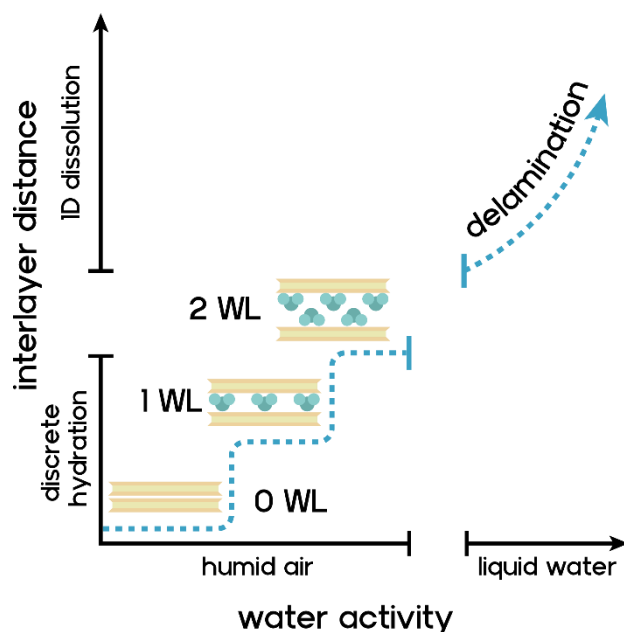
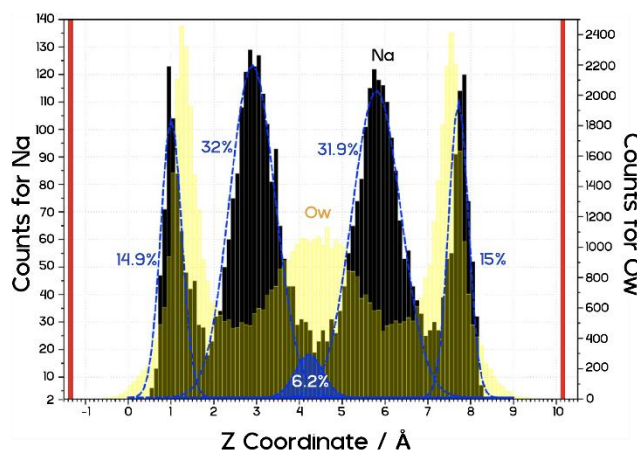


Figure 3. Schematic illustration of the transition of crystalline swelling to delamination via 1D dissolution as a function of water activity. Reproduced with permission⁵⁶. Copyright 2021, Wiley-VCH GmbH.

3 Introduction

Repulsive osmotic swelling is a process similar to the dissolution of salts, but it is limited to 1D due to the anisotropic nature of layered compounds (Figure 2d). For this process to be spontaneous, the solvent must overcome the adhesive interaction between the interlayer ions and the charged nanosheets. At low activity, solvent molecules initially solvate the interlayer ions in discrete steps (Figure 2e) and increase the separation distance of the nanosheets. To demonstrate the essential ingredients of 1D dissolution, I will focus on the swelling of 2:1 layered silicates (clay minerals) with water. The initial swelling of clay minerals occurs in discrete steps referred to as crystalline swelling (Figure 2e and Figure 3)⁷¹. However, if the uptake of solvent molecules exceeds the limit of crystalline swelling and increases beyond a critical threshold of separation, the interaction between adjacent nanosheets in the stack changes from attractive to repulsive, and the nanosheets separate themselves to equal distances (Figure 2f), much larger than what is found in the crystalline swelling regime (Figure 3). For 1D dissolution to be triggered, the interlayer cations must leave the symmetrical position in the middle of the interlayer space and segregate into the Helmholtz-layers belonging to one of the two adjacent clay layers formerly circumscribing the interlayer space. This process requires monovalent interlayer ions and is fostered by the translational entropy contribution of interlayer species (ions and solvent molecules). As a result, overlapping diffuse double layers electrostatically repel adjacent clay layers in the stack (Figure 4)³⁸. At this point, the separation of nanosheets is h/Φ , where h is the thickness of individual nanosheets and Φ is the volume content of clay in the aqueous suspension. This means that all available solvent molecules are incorporated between the nanosheets, giving a maximum separation distance, which indicates a repulsive interaction. If the separation distance as a function of clay volume fraction follows the h/Φ relationship for a given clay, this is sound experimental evidence for its complete delamination by spontaneous 1D dissolution.



3 Introduction

Figure 4. Histogram of the z -distribution of Na^+ (black bars) and water molecules (“Ow”, yellow bars) in the interlayer space of hectorite already swollen beyond the threshold separation as obtained by molecular dynamic simulation (NVT, 300 K). Red bars represent the plane of basal oxygen atoms of the tetrahedral layers. The five blue Gaussians are the deconvoluted peaks of the Na^+ locations. Reproduced with permission⁵⁶. Copyright 2021, Wiley-VCH GmbH.

Once the nanosheets are separated at the threshold separation of 2D ionic crystals, they remain parallel to each other and cannot rotate due to their smaller separation compared to their diameter. This marks the formation of a uniform nematic liquid crystal suspension, which is a single phase. The transition from the crystalline swollen phase to the nematic liquid crystal phase at the onset of 1D dissolution corresponds to a phase transition. The discrete d -spacing of the swollen phase corresponds to the molecular dimensions of its interlayer species, whereas the separation in the nematic liquid crystal phase is determined by the volume fraction of dispersed clay in a quasi-continuous manner.

The yield of delamination is 100% as it is a thermodynamically driven, spontaneous phase transition. However, delamination does not always produce an isotropic suspension, and only high aspect ratio blocks allow for the observation of anisotropic liquid crystals. Even at low volume fractions, birefringent nematic suspensions are expected for fully delaminated 2D crystals due to the free rotation of nanosheets being restricted by their high aspect ratio.

3.3 How to trigger delamination by 1D dissolution

Typically, materials require the exchange of specific interlayer ions to initiate the transition from crystalline swelling to 1D dissolution. However, synthetic Na-hectorite clay is an exception since the solvation enthalpy of its interlayer cation is already high enough to exceed the threshold separation required for repulsive 1D dissolution to occur³⁸. Nonetheless, increasing the layer charge from $x=0.5$ (hectorite $[\text{Na}_{0.5}]^{\text{inter}}[\text{Mg}_{2.5}\text{Li}_{0.5}]^{\text{oct}}[\text{Si}_4]^{\text{tet}}\text{O}_{10}\text{F}_2$) to $x=0.7$ (vermiculite-type $[\text{Na}_{0.7}]^{\text{inter}}[\text{Mg}_{2.5}\text{Li}_{0.3}]^{\text{oct}}[\text{Si}_4]^{\text{tet}}\text{O}_{10}\text{F}_2$) strengthens the Coulombic interactions between the charged nanosheets and interlayer ions, making it difficult to reach the threshold with just the hydration of interlayer cations. In such cases, the threshold separation can still be achieved with the assistance of bulky interlayer cations that exert steric pressure³⁹⁻

41.

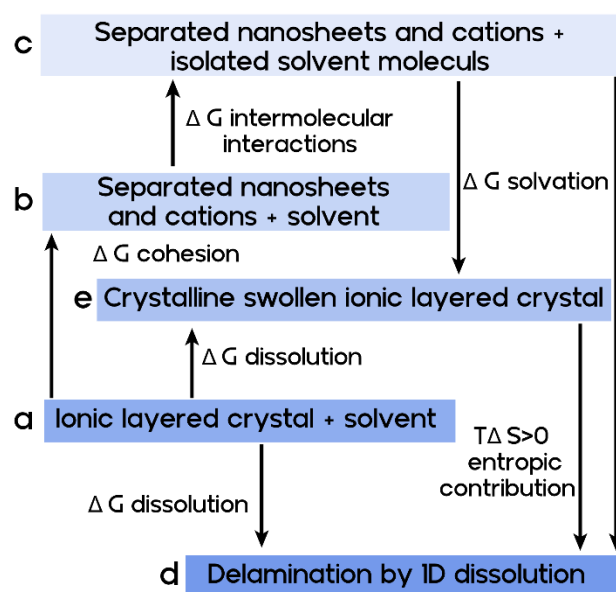


Figure 5. Thermodynamic scheme of 1D dissolution **a.** Ionic layered tactoid immersed into the solvent, **b.** The increase of free energy upon separation of the nanosheets is denoted as the energy of cohesion. **c.** The increase of free energy upon breaking of the interaction between solvent molecules is denoted as the energy of intermolecular interactions. **d.** Decrease of free energy upon solvation of ionic layered crystal with solvent molecules, leading to crystalline swollen ionic layered crystal. **e.** Decrease of free energy upon 1D dissolution. Reproduced with permission⁵⁶. Copyright 2021, Wiley-VCH GmbH.

The process of 1D dissolution is complex and involves several simultaneous steps. To simplify this process, it can be broken down into individual steps. Initially, unsolved ionic layered tactoids are dispersed in a solvent (Figure 5a). To separate solvent molecules from charged nanosheets and interlayer ions (Figure 5c), two endergonic steps are required. First, the nanosheets and interlayer ions must be separated from each other (cohesion energy) (Figure 5b). Second, intermolecular interactions of solvent molecules must be broken (Figure 5c). The solvation energy of both interlayer ions and the basal surfaces of nanosheets compensates for these unfavorable steps. If the solvation energies are higher than the cohesion energy, the 2D ionic tactoid spontaneously dissolves in the stacking direction (1D dissolution, Figure 5e). However, if the solvation energies are lower, we end up with a crystalline swollen, ionic-layered solid tactoid where the interlayer cations are solvated (Figure 5d). The entropy of the 1D dissolved state is higher than that of the crystalline swollen state dispersed in the excess solvent. Increasing the temperature can make 1D dissolution favorable⁷². The cohesion energy can also be reduced by either decreasing the layer charge or by exchanging with bulky ions, as the leading term of cohesion is electrostatic in nature. The layer charge density of nanosheets is

3 Introduction

therefore one of the keys to achieving 1D dissolution. As a general rule of thumb, it is more difficult to delaminate highly charged solids due to stronger electrostatic attraction. For instance, 1D dissolution in water is possible for low-charged 2:1 layered silicates with a charge density of < 2.3 charges/nm² and Na⁺ as the interlayer cation (e.g., synthetic hectorite³⁸) or certain natural, purified montmorillonites²⁹. Charge densities > 2.3 charges/nm² prevent 1D dissolution due to excessive electrostatic attraction³⁹.

In 2:1 layered silicates like hectorite or montmorillonite that carry no acidic groups at the basal surface, the layer charge can be lowered by the Hofmann–Klemen⁷³ effect. This effect occurs when small interlayer cations migrate into empty octahedral sites of the 2:1-layer⁷⁴. In layered crystalline silicic acids and in zeolites that carry silanol groups at the basal surfaces, the charge density can be modified by adjusting the pH of the dispersion, which affects the degree of protonation of these acidic groups. The same applies to layered metal oxides that carry acidic groups at the basal surface, such as titanates of lepidocrocite type or niobates of layered Ruddlesden–Popper type oxidic perovskites⁷⁵⁻⁷⁷.

As mentioned earlier, the cohesion energy can be effectively reduced by increasing the interlayer distance, particularly through exchange with bulky ions. Here, bulky refers to ions with lower charge density than the nanosheets⁷⁸. In such cases, the interlayer ions compensate for the charge by pushing the nanosheets apart, thereby increasing the interlayer distance and weakening cohesion (Figure 6a). The complexation of inorganic interlayer cations can also lead to a similar expansion of interlayer distance. It should be noted that ion exchange significantly affects the solvation energy. Bulky ions with low solvation energy do not favor 1D dissolution³⁹⁻⁴¹. Table 3 lists suitable cations that offer sufficient bulkiness and high solvation energy and have been successfully used to achieve 1D dissolution, along with their corresponding charge equivalent areas.

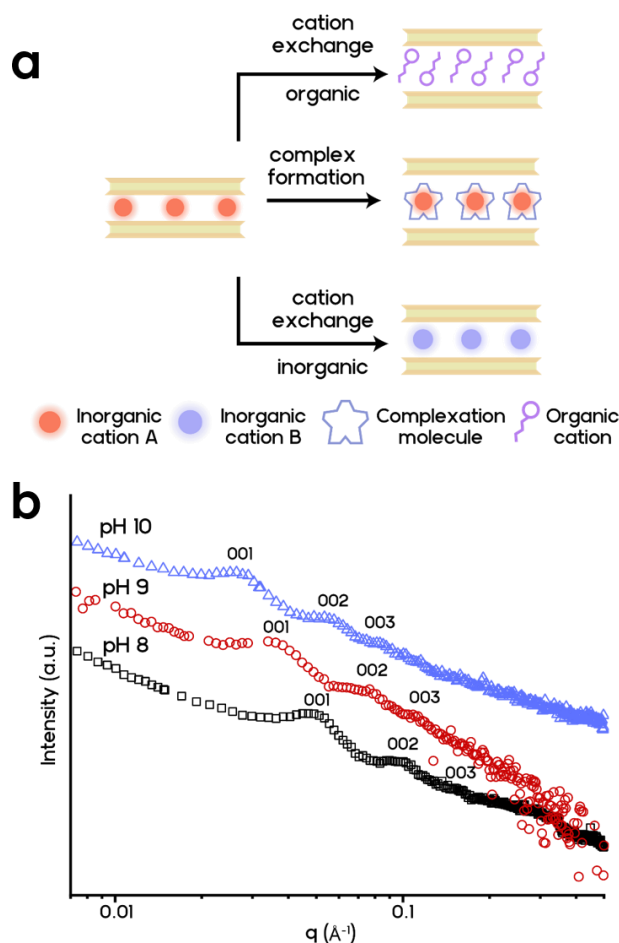


Figure 6. a. Approaches that help to push layered materials above the threshold separation and thus trigger 1D dissolution. **b.** SAXS curves of Ilerite suspensions were recorded at different pH values. Reproduced with permission⁵⁶. Copyright 2021, Wiley-VCH GmbH.

By using crystallographic data and structural compositions, I calculated the charge density of various ionic layered compounds, which is listed in Table 3. However, it is important to note that some of the cations listed in Table 3 serve as buffer systems⁷⁹, and if used in combination with layered compounds that carry acidic groups at the basal surface, the charge density of the layers will be modified according to the effective pH in the suspension. In our calculations for Table 3, I have assumed a degree of protonation derived from the structural formula as obtained at the pH of synthesis. In addition, the pH for quaternary amines may be adjusted by adding a base.

The organic base used in the intercalation process can significantly impact the swelling process and influence the morphology and properties of the final nanosheet suspension. For example, when layered titanates are intercalated with 2-(dimethylamino)ethanol (DMAE), a stable and reversible 100-fold expansion within the interlayer gallery can be achieved (Figure 6b).⁸⁰

3 Introduction

It is worth noting that the charge equivalent areas of the organic ions mentioned systematically exceed those of the layered compounds, in contrast to small ions like Li^+ and Na^+ . This means that organic cations capable of triggering 1D dissolution have larger charge equivalent areas than the charge density of the layered compound. For example, the relatively low-charged $\text{H}_{0.13}^{\text{inter}} \text{Mn}^{\text{III/IV}}\text{O}_2$ (1.8 charge/ nm^2) requires the sterically demanding TBA (1.1 charge/ nm^2) to trigger 1D dissolution. However, for more highly charged layer compounds, several significantly smaller organic cations are known to trigger 1D dissolution. For instance, $\text{H}^{\text{inter}} \text{Ca}_2\text{Nb}_3\text{O}_{10}$ (6.7 charge/ nm^2) undergoes 1D dissolution with the much smaller TMA (3.4 charge/ nm^2) as the interlayer ion (Table 3).

Table 3: Some 1D dissolved combinations of organo-cations (Cation) and layered compounds: To trigger repulsive osmotic swelling, the cation must be intercalated into the respective layered compound by cation exchange. The cations are TBA, DMAE, C4 (n-butylammonium), C3 (n-propylammonium), and TMA. In the case of hydroxonium-intercalated layer compounds, the cation exchange is carried out by the corresponding tertiary amines as the base, or for quaternary ammonium ions by their hydroxide salts as the base.

	Cation	Name/ chemical formula (before cation exchange)	Charge density [charges/ nm^2]	The charge density of layered compound ^{b)} [charges / nm^2]	Ratio ^{c)}
1	TBA	birnessite ^{81, 82} $\text{H}_{0.13}^{\text{inter}} \text{MnO}_2$	1.1	1.8	1.6
2	TBA	Calciumniobate ^{83, 84} $\text{H}^{\text{inter}} \text{Ca}_2\text{Nb}_3\text{O}_{10}$	1.1	6.7	6.0
3	TBA	lepidocrite type Titanate ^{76, 85} $\text{H}_{0.8}^{\text{inter}} \text{Ti}_{1.2}\text{Fe}_{0.8}\text{O}_4$	1.1	7.1	6.4
4	TBA	α -Zirconiumphosphate ^{86, 87} $\text{Zr}(\text{H}^{\text{inter}} \text{PO}_4)$	1.1	8.3	7.5
5	DMAE	Calciumniobate ^{83, 84} $\text{H}^{\text{inter}} \text{Ca}_2\text{Nb}_3\text{O}_{10}$	2.6	6.7	2.5
6	DMAE	lepidocrite type Titanate ⁷⁶ $\text{H}_{0.8}^{\text{inter}} \text{Ti}_{1.2}\text{Fe}_{0.8}\text{O}_4$	2.6	7.1	2.7

3 Introduction

7	C4	vermiculite ⁸⁸⁻⁹⁰ Na,Mg _{x=0.64} ^{inter} [Mg _{2.36} Fe _{0.48} Al _{0.16}] ^{oct} <Si _{2.72} Al _{1.28} > ^{tetr} O ₁₀ (OH) ₂	2.6	2.6	1.0
8	C3	Caliumhexaniobate ^{91, 92} K ₄ ^{inter} Nb ₆ O ₁₇	3.2	7.1	2.2
9	TMA	Calciumniobate ^{83, 84} H ^{inter} Ca ₂ Nb ₃ O ₁₀	3.4	6.7	1.9
10	TBA	MCM-56 ⁹³ 1xSiO ₂ :0.04xAl ₂ O ₃ :0.093xNa ₂ O:0.3xHMI:16 H ₂ O	1.1	1.4	1.3
11	Meglu mine	ilerite Na ₈ [Si ₃₂ O ₆₄ (OH) ₈].32 H ₂ O (pH 10)	1.5	1.3	1.2

- The maximum projected area of the cations (calculation: Chemicalize.com⁹⁴) was taken as the charge equivalent area. The charge equivalent areas for C4 and C3 were taken from the literature.⁷⁵
- Calculated for the given compositions and the quoted structural 2D dimensions. For compounds with acidic groups, the degree of protonation was assumed as represented by the structural formula obtained at the pH of synthesis. The charge density of vermiculite was calculated by a formula given in the literature: $24 \text{ \AA}^2 / x$ ³⁹.
- The ratio of charge density of layered compound and countercation used for 1D dissolution

The recent delamination of Ilerite (also known as NaRUB-18 or orthosilicate (Na₈[Si₃₂O₆₄(OH)₈].32 H₂O),) provides a great example of how effective pH of the suspension, charge density, and steric pressure all play a subtle role in triggering 1D dissolution^{95, 96}. The 50% deprotonated sodium form of Ilerite contains acidic OH-groups that are exposed at the basal surfaces of the layers, altering the pH and layer charge density. By ion exchange at a certain pH, the influence of pH on layer charge and resulting swelling/dissolution behavior can be examined. As the pH decreases, silanol groups become increasingly protonated, resulting in a decrease in the layer charge density. Charge equivalent areas for Ilerite basal surfaces were calculated to correlate layer charge density with pH and swelling/dissolution tendency. The

3 Introduction

calculated charge equivalent areas decrease by 27% from pH 7 to 10, and for delamination by 1D dissolution, the charge equivalent area of the interlayer cation should be larger than that of the layered material. A bulky cation like megluminium, which remains protonated at higher pH values and offers strong hydrogen bonding to water as a swelling agent, is suitable for triggering delamination by 1D dissolution. Meglumine-ilerite at pH 8-10 resulted in a nematic phase with separation of adjacent nanosheets >13 nm, while at pH 7, only a crystalline swollen suspension was obtained. The onset of the phase transition into the nematic liquid crystalline phase as a function of pH, along with the accompanying delamination and the separation of nanosheets to large distances, can easily be followed by small-angle X-ray scattering (SAXS). Comparing the behavior of Na-hectorite exchanged with different alkali cations also illustrates the solvation energy of interlayer ions, which is concomitantly modified with steric pressure. K^+ , Ru^+ , or Cs^+ (322 kJ/mol and lower)⁹⁷ rather gives crystalline swollen suspensions, while 1D dissolution is observed with high hydration enthalpy cations like Li^+ or Na^+ .

Table 4. Nanosheet characteristics of layered compounds mentioned in the text

Compound	Group	Basal planes	Porosity of nanosheets	Source of nanosheet charge	Special features
Birnessite $H_{0.13}^{inter} MnO_2$	hydrous manganese dioxide	acidic	impermeable	deprotonation	semiconducting, redox-active
Calciumniobate ^{83, 8483, 8483, 8483, 84} $H^{inter} Ca_2Nb_3O_{10}$	Ruddlesden–Popper perovskites	inert	impermeable	isomorphous substitution	semiconducting, photocatalytic, dielectric
Lepidocrite type Titanate $H_{0.8}^{inter} Ti_{1.2}Fe_{0.8}O_4$	transition metal oxides	inert	impermeable	isomorphous substitution	semiconducting, photocatalytic, ferromagnetic
α -Zirconiumphosphate $Zr(H^{inter} PO_4)$	Layered acid	acidic	impermeable	deprotonation	solid-state ion conductive

3 Introduction

Na-Hectorite $[\text{Na}_{0.5}]^{\text{inter}}[\text{Mg}_{2.5}\text{Li}_{10.5}]^{\text{oct}}[\text{Si}_4]^{\text{tet}}\text{O}_{10}\text{F}_2$	2:1 clay	inert	impermeable	isomorphous substitution in octahedral or tetrahedral layer	insulating, high aspect ratio
Illerite $\text{Na}_8[\text{Si}_{32}\text{O}_{64}(\text{OH})_8] \cdot 32 \text{H}_2\text{O}$	Na-silicate	acidic	microporous	deprotonation	insulating, well-defined nanoporosity
Vermiculite $\text{Na}, \text{Mg}_{x=0.64}^{\text{inter}}[\text{Mg}_{2.36}\text{Fe}_{0.48}\text{Al}_{0.16}]^{\text{oct}} < \text{Si}_{2.72}\text{Al}_{1.28} >^{\text{tet}}\text{O}_{10}(\text{OH})_2$	2:1 clay	inert	impermeable	isomorphous substitution in the octahedral layer	insulating, high temperature resistant, Fenton's reagent
Caliumhexaniobate $\text{K}_4^{\text{inter}} \text{Nb}_6\text{O}_{17}$	Ruddlesden–Popper perovskites	inert	impermeable	isomorphous substitution	dielectric, photocatalytic
layered antimony phosphates $\text{H}_3^{\text{inter}} \text{Sb}_3\text{P}_2\text{O}_{14}$	layered acid	acidic	impermeable	deprotonation	insulating, ion-conductive
MCM-56, $1x\text{SiO}_2:0.04x\text{Al}_2\text{O}_3:0.093x\text{Na}_2\text{O}:0.3x\text{HMI}:16 \text{H}_2\text{O}$	layered zeolites	acidic	microporous	isomorphous substitution in the tetrahedral layer	insulating, well-defined nanoporosity
Graphene oxide $\text{C}_x\text{H}_y\text{O}_z$	Carbon-based	acidic	microporous	deprotonation	insulating, high degree of functionality

3 Introduction

Beidellite (Na,Ca _{0.5}) _{0.3} Al ₂ (Si, Al) ₄ O ₁₀ (OH) ₂ ·4H ₂ O	2:1 clay	inert	impermeable	isomorphous substitution in octahedral or tetrahedral layer	insulating, high temperature resistant
Nontronite (CaO _{0.5} ,Na) _{0.3} Fe ³⁺ ₂ (Si,Al) ₄ O ₁₀ (OH) ₂ ·nH ₂ O	2:1 clay	inert	impermeable	isomorphous substitution in octahedral or tetrahedral layer	insulating, high temperature resistant, Fenton's reagent

By altering the dispersion medium, the solvation energy can be significantly altered. The dielectric constant, dipole moment, and the ability to create hydrogen bonding^{78, 98-100} appear to be the key solvent parameters for initiating 1D dissolution. Initially, only water and aqueous solvent mixtures were deemed suitable for 1D dissolution. However, with solvent combination optimization, the water content can be lowered to as little as 3 vol%⁹⁸. To achieve 1D dissolution in entirely water-free media, it was necessary to employ the complexation of interlayer cations. The use of crown ethers with a high complex building constant with Na⁺ successfully extended 1D dissolution into organic solvents, such as propylene carbonate, ethylene carbonate, glycerol carbonate, methyl formamide, and methyl acetamide, for the first time. The mastery of spontaneous delamination by 1D dissolution depends on finding the right balance between the charge of the layered material, the properties of the interlayer ion (solvation energy, equivalent area), and the solvent's properties⁷⁸.

4 Synopsis

The present work contains three publications. For further publications I contributed to, please see the list of publications.

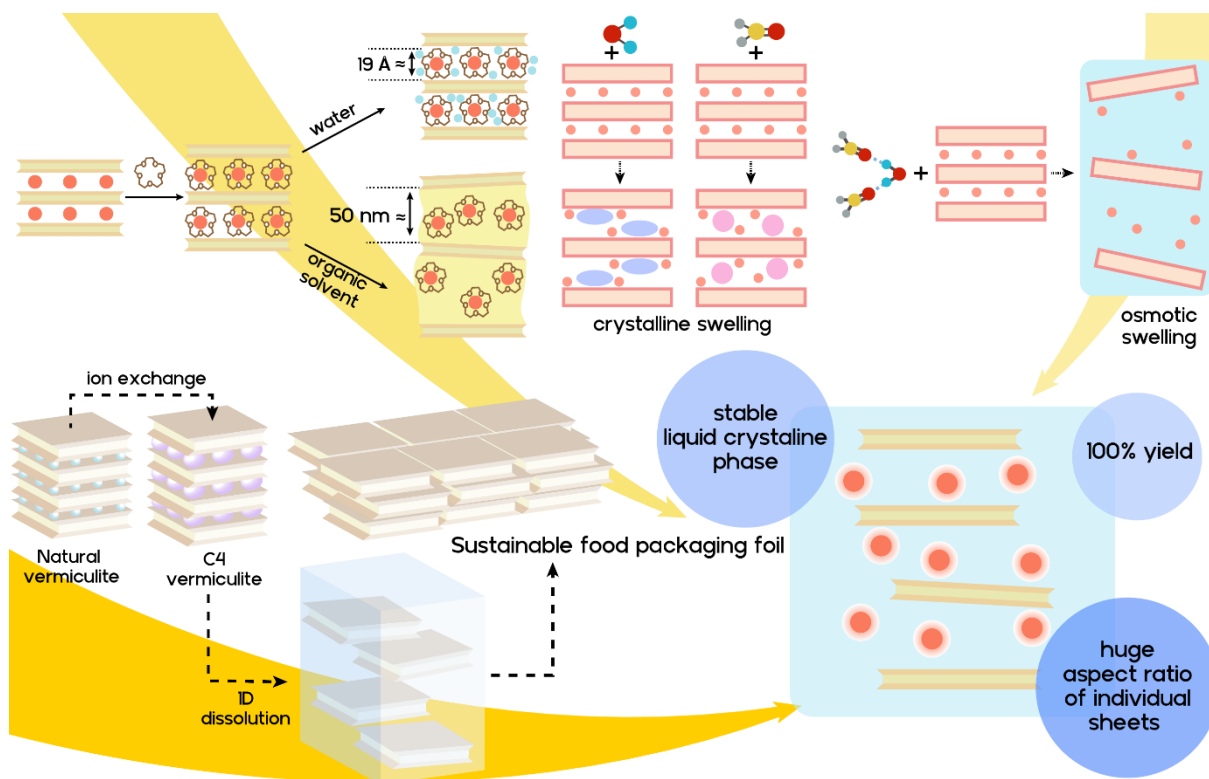


Figure 7. Graphical synopsis of the thesis highlighting the broadening of 1D dissolution

All the work is based on the expanding on phenomenon of 1D dissolution and understanding the main driving forces, which allows to transfer of this concept to the organic solvents, the smectites with the higher surface charge, and the more affordable natural vermiculites (Figure 7).

The publication “Osmotic Delamination: A Forceless Alternative for the Production of Nanosheets Now in Highly Polar and Aprotic Solvents” highlights the importance of the steric pressure caused by interlayer cation and the right combination of the solvent parameters to provide the synergistic effect. In this case, the complexation of the interlayer Na^+ by 15-crown-5 and 18-crown-6 caused the 1D dissolution in the number of highly polar solvents like ethylene carbonate, propylene carbonate, glycerol carbonate, N-methylformamide, and N-metylacetamide. The crucial parameters for the solvents were found to be high dipole moment and high dielectric constant. This highlights the key role of electrostatic interactions in the 1D dissolution process.

4 Synopsis

The publication “Delamination by repulsive osmotic swelling of synthetic Na-hectorite with variable charge in binary DMSO-water mixtures” studies the unusual behavior of the highly charged hectorites in the water-DMSO mixture. Hectorite shows a well-defined 1D dissolution window, where the phenomenon of 1D dissolution is observed and outside of this composition, swelling is limited only to crystalline. We applied the PXRD and ^{23}Na solid-state NMR to study solvation behavior and uncovered the key role of the solvation environment. The water and DMSO molecules form molecular assemblies, which act as a single solvation unit and exert a bigger steric pressure on the interlayer space, leading to 1D dissolution.

The last publication titled “Spontaneous Delamination of Affordable Natural Vermiculite as a High Barrier Filler for Biodegradable Food Packaging” explores the transferring of the knowledge, obtained from studying the synthetic hectorite as a model system to more relevant and affordable natural analogs –vermiculites. The paper reports improved delamination protocol based on the use of butyl amine as a cation and organic acids as a counter anion. Organic acids in this case act as a complexation agent to the Mg^{2+} cations, which are commonly found in natural vermiculites and impede the 1D dissolution process. After the successful ion exchange, the 1D dissolution is extended to the highly polar organic solvents, allowing to process of the vermiculite nanosheets as a nanocomposite with PLA- one of the most promising biodegradable polymers. The resulting nanocomposite boosts the barrier performance to the level of commercially available multilayer metalized films.

4.1 Osmotic Delamination: A Forceless Alternative for the Production of Nanosheets Now in Highly Polar and Aprotic Solvents

Traditionally, liquid-phase exfoliation is used to produce mono- or few-layer nanosheets by exploiting the anisotropy in the mechanical strength of layered materials to create thinner stacks using shear forces. An alternative method, 1D dissolution or osmotic swelling, has long been known but is rare and limited to 1D ionic crystals, where layers carry a charge compensated by counterions residing between them. However, this method is limited to a handful of ionic layered compounds. 1D dissolution is a thermodynamically allowed process that does not require mechanical force, allowing for gentle delamination. This method preserves the aspect ratio inherent in the platelet diameter of the non-delaminated layered starting material.

However, extending 1D dissolution to more attractive but highly reducing 2D compounds like Li-MoS₂ or K-graphite requires two major steps, including using a suspension medium with a large redox stability window that is inert in redox reactions and sufficient swelling capacity. Additionally, all handling must be done strictly in an inert atmosphere. To tackle the first step, synthetic clay, sodium fluorohectorite, is used to mimic negatively charged nanosheets held

4 Synopsis

together by interlayer cations that can be solvated. These high aspect ratio nanosheets are already applied as fillers in polymer nanocomposites, where they improve mechanical properties, decrease gas permeability and enhance flame retardancy and thermal conductivity. Solution blending, where both filler and polymer are dissolved/dispersed in the same solvent, offers the best control over homogeneity. However, 1D dissolution could only be achieved in aqueous media, limiting the choice of polymers.

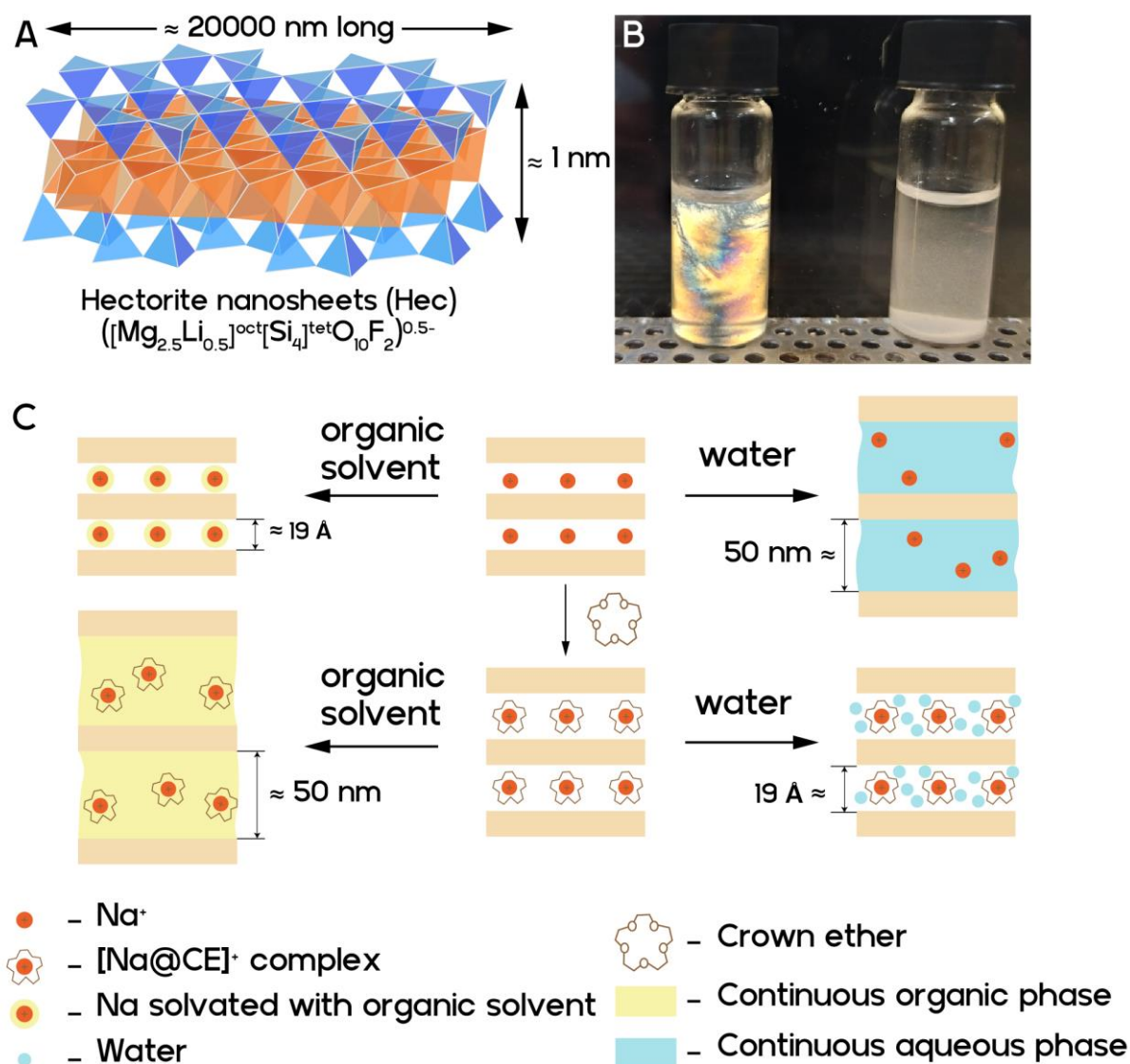


Figure 8. A Schematic illustration of the structure of negatively charged unilamellar hectorite nanosheets. B (left) Birefringent suspension of osmotically swollen Crown Ether (CE)-modified Na-Hec in NMF and (right) crystalline swollen CE-modified Na-Hec in water. C schematic illustration of delamination process

By transferring repulsive osmotic delamination of Na-Hec (Figure 8 A). to (aprotic), water-free organic solvents, the range of nanosheets accessible through 1D dissolution can be extended to

4 Synopsis

redox-active intercalation compounds (Figure 8 B). This will allow for a wider range of polymers for nanocomposite applications, including more hydrophobic matrices like biodegradable polyesters. Additionally, this system could work with moisture-sensitive precursors and potentially be used as "superionic" battery electrolytes.

Above mentioned approach involves suspending the ionic layered solid in an appropriate solvent with a high dipole moment and dielectric constant, and a high interaction energy with the interlayer ionic species.

Crown ether completes the first solvation shell because of the high selectivity toward Na^+ cation, which fits perfectly to the crown ethers' cavity (Figure 8 C). This yields interlayer space more hydrophobic and promotes intercalation of the solvent molecules, hence expanding interlayer space beyond crystalline swelling. The high dielectric constant and dipole moment of the solvent molecules ensure the formation of the electrical double layer to stabilize the nanosheets in suspension. We have characterized this process using PXRD and SAXS. This regime allows for easy processing of the nanosheets. Nematic suspensions in water-free organic solvents expand the range of polymer matrices for making ordered nanocomposites via solution blending. In this paper, we have reported 1D dissolution, assisted by crown ethers in highly polar solvents like cyclic carbonates and amides.

4.2 Delamination by repulsive osmotic swelling of synthetic Na-hectorite with variable charge in binary DMSO-water mixtures

Swelling of highly charged silicates, particularly beyond crystalline swelling, is becoming increasingly challenging, if not impossible, due to the strong electrostatic interactions between counter cations and anionic nanosheets. To trigger osmotic swelling in vermiculite-type 2:1 layered silicates, a complete cation exchange is required with a bulky and hydrophilic organic cation or with monovalent cations of high hydration enthalpy like Li^+ . These observations highlight the complexity of the interactions accompanying repulsive osmotic swelling, which generally goes through two distinct phases: crystalline and osmotic.

However, natural 2:1 layered silicates (smectites and vermiculites) suffer from compositional inhomogeneity, making it difficult to interpret observed basal spacing. To overcome this, synthetic clay minerals synthesized from the melt are preferred as model compounds, characterized by phase purity, charge homogeneity, and a wide range of layer charges. By studying the repulsive osmotic swelling of two such synthetic clay minerals, 0.5 Hec ($[\text{Na}_{0.5}]^{\text{inter}}[\text{Mg}_{2.5}\text{Li}_{0.5}]^{\text{oct}}[\text{Si}_4]^{\text{tet}}\text{O}_{10}\text{F}_2$) and 0.7 Hec ($[\text{Na}_{0.7}]^{\text{inter}}[\text{Mg}_{2.3}\text{Li}_{0.7}]^{\text{oct}}[\text{Si}_4]^{\text{tet}}\text{O}_{10}\text{F}_2$), we show that changes in the composition of the dispersion medium can lead to significant alterations in swelling behaviour (Figure 9 C).

4 Synopsis

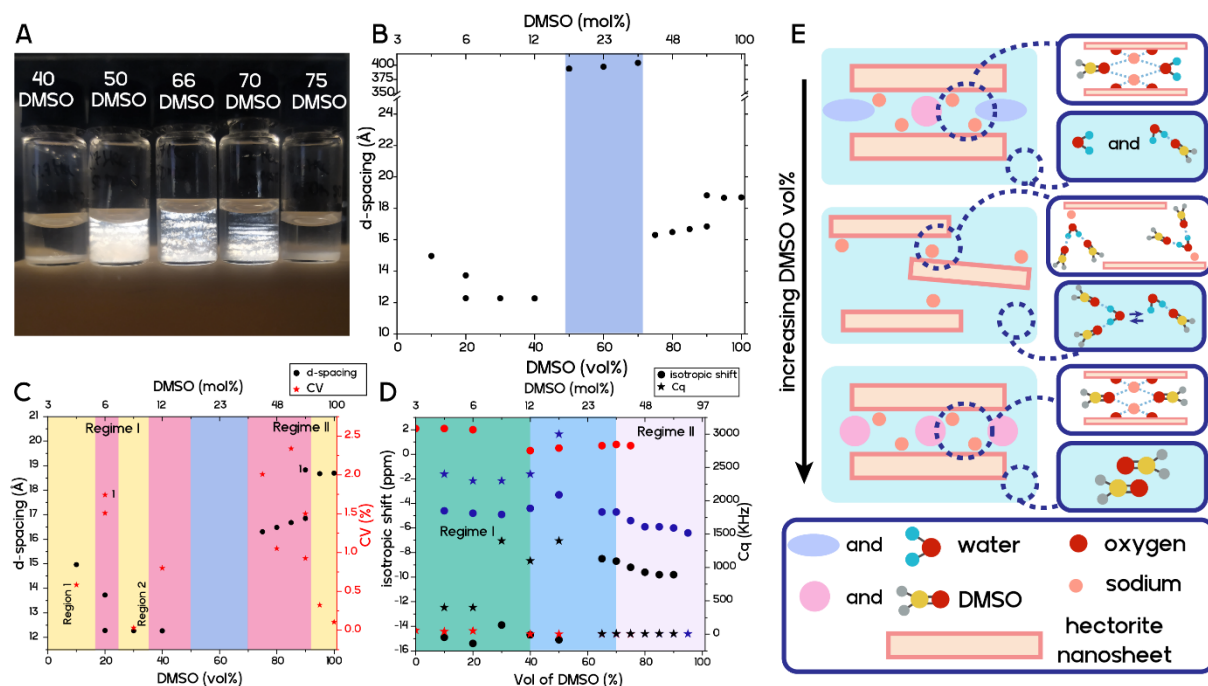


Figure 9. Swelling behavior of 0.7 Hec in water–DMSO mixtures. A. Photo in cross-polarized light of the suspension of 0.7 Hec in the region of 40 vol % to 75 vol % of DMSO featuring the transition from crystalline (40 vol %) to osmotic (50–70 vol %) (the d -spacing corresponds to around 2.8 ± 0.1 vol %) and back to crystalline (75 vol %) swelling. B. Drastic change of d -spacing when going from crystalline swelling regime I to the nematic liquid crystalline suspension and back to crystalline swelling regime II. The blue area indicates the water–DMSO composition range in which osmotic swelling is triggered. C. d -values and the CV in crystalline swollen regime I and regime II as a function of water–DMSO composition. The areas mark rational d -values observed for distinct solvates as indicated by CV values <0.7 , while the red area refers to the transition zone where both different swelling states coexist in a random interstratification as indicated by CV values >0.7 . D. Diagram of ^{23}Na MAS-NMR features as a function of water–DMSO composition. Two crystalline swelling regimes I and II (green and purple) and the osmotically swelling regime (blue). Filled circles indicate the position of the isotropic shift, and the star of the respective color indicates the quadrupole coupling constant, C_q . E. Schematic representation of the swelling behavior of 0.7 Hec in water–DMSO mixtures

Specifically, we observe repulsive osmotic swelling in a mixture of water and DMSO, while in both pure water and pure DMSO swelling is restricted to crystalline swelling. The onset of osmotic swelling is attributed to changes in the first and second coordination/solvation sphere,

4 Synopsis

as indicated by significant changes in the ^{23}Na MAS-NMR spectra (Figure 9 D). We propose a mechanism of synergistic solvation of the first solvation shell of interlayer cations, which resembles the dominant 1HB cluster present in solvent mixtures of the particular composition range (Figure 9 E). This leads to the thermodynamically favored formation of the second solvation shell in the interlayer space, which in turn overrules the strong electrostatic attraction between anionic nanosheets and interlayer cations.

We report for the first time the repulsive osmotic delamination of the sodium form of the vermiculite-type synthetic hectorite, which was previously considered impossible due to strong electrostatic interactions. This delamination occurs only within a narrow range of 50 to 70 vol% DMSO in the binary water-DMSO mixture (Figure 9 A and B). We propose that this is fostered by strong intermolecular interaction between water and DMSO molecules, which, however, become weaker again with increasing DMSO content, eventually leading to the substitution of the water molecules in the first solvation shell and a concomitant collapse of osmotic swelling to ordinary crystalline swelling (Figure 9 E).

Overall, this study provides a fundamental understanding of spontaneous, repulsive osmotic swelling and opens new avenues for the use of high aspect ratio nanosheets in nanocomposites, super-ion conductors, and hybrid organic-inorganic functional structures.

4.3 Spontaneous Delamination of Affordable Natural Vermiculite as a High Barrier Filler for Biodegradable Food Packaging

Innovative packaging is crucial in preventing food waste, but it poses problems when considering end-of-life scenarios. According to the United Nations Food and Agricultural Organisation, global food wastage amounts to 1.3 billion tons, leading to the release of 3.3 billion tonnes of CO_2 equivalent to greenhouse gases into the atmosphere yearly. While materials like polyethylene, poly(vinylidene dichloride) (PVDC), and polyamide prevent food waste by preserving freshness and preventing contamination, consumers are becoming increasingly aware of plastic pollution and microplastic contamination.

There is a growing movement to replace traditional plastics with biodegradable alternatives to promote environmental preservation and human health. However, current coated and chemically treated paper alternatives are unrecyclable and non-compostable. Biodegradable packaging that provides lightweight, convenient protection with high-performance properties to reduce food waste is needed. Although bio-based and biodegradable packaging is essential, it must have properties that reduce food waste for the entire system to have a positive environmental impact. Consumers are unwilling to pay more for environmentally friendly

4 Synopsis

packaging, so practical and low-cost solutions are necessary. Multilayer strategies and surface hydrophobization strategies can address the challenge of the poor and moisture susceptible barrier properties of bio-based and biodegradable materials.

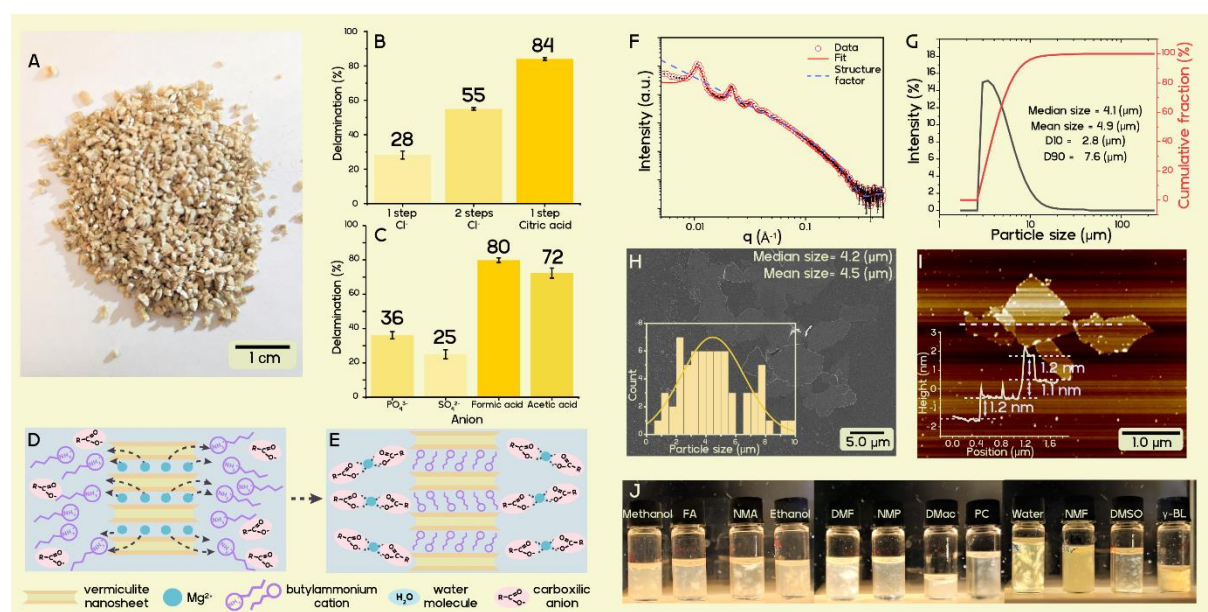


Figure 10. Schematic representation of osmotic swelling of natural vermiculites. A. Photo of thermally expanded natural vermiculite. B. Delamination yield observed by a one-step ion exchange with butylammonium chloride or citrate as compared to a two-step ion exchange first to Na⁺ followed by butylammonium chloride. C. Delamination yield observed by a one-step ion exchange with different inorganic and organic salts of butylammonium. D. Schematic of ion exchange process in presence of carboxylic acid anions E. The proposed process of ion exchange that leads to enhanced delamination yield. Magnesium cations form complexes with carboxylic acid anions, increasing the hydrophilicity and reducing the tendency to re-enter the interlayer space. F. SAXS intensity of vermiculite gel, indicating a liquid crystalline order in the nematic suspension in NMF. G Static light scattering number weighted size distribution indicating a mean size of 4.9 μm H SEM photo of vermiculite nanosheets on a Si wafer. Inset: Particle size distribution measured from the SEM image indicating a mean size of 4 ± 1 μm. I Topographic AFM image of vermiculite nanosheets and height profile from the single nanosheets indicating a height of ~1.2 nm. J. Photos of nematic suspensions of vermiculite in various solvents obtained by diluting a vermiculite/NMF gel, viewed under cross-polarized light, and reducing the tendency to re-enter the interlayer space.

Thin nanocomposite barrier coatings using clay nanosheets are another approach that provides improved barrier performance at a lower cost. The use of natural clay is an inexpensive and sustainable filler that reduces the overall cost of the packaging. However, the most commonly

4 Synopsis

applied clay minerals, montmorillonite, and Laponite, with an aspect ratio of <150 and 20, respectively, are insufficient. Synthetic hectorites or natural vermiculites (Figure 10 A), which have much larger aspect ratios, are more promising.

Osmotic swelling is an effective method for the production of barrier nanosheets, and it is a thermodynamically allowed process that does not require any mechanical force, unlike ultrasound-driven liquid-phase exfoliation methods. The most attractive options for the polymer component of a nanocomposite coating are commercially produced biodegradable polymers like polylactic acid (PLA), poly(butylene succinate-co-butylene adipate) (PBSA), and poly(butylene adipate terephthalate) (PBAT). Natural vermiculites are particularly appealing as a clay component in a nanocomposite barrier system because of their abundant global production and cost-effectiveness. Although vermiculites have a higher charge density compared to montmorillonite, they have the same layer structure and a higher potential aspect ratio. However, the dominant divalent interlayer cation Mg^{2+} of vermiculites forms a strong and symmetrical electrostatic interaction with adjacent nanosheets, hindering their swelling. By exchanging it with bulky organocations, vermiculite swelling can be facilitated (Figure 10 B to E).

This article presents a straightforward ion exchange method for repulsive osmotic delamination of natural vermiculite in N-methyl formamide (NMF) and its mixtures (Figure 10 F to J). The method yields a high delamination yield (80%wt) while preserving the nanosheets' high aspect ratio compared to ultrasonication-assisted methods. The resulting nanosheets can be easily blended with biodegradable polymers such as PLA. Doctor blading of a polymer/clay suspension yields nanocomposite coatings that improve the gas barrier properties of natural, fully biodegradable, and highly hygroscopic wood-based nanocellulose paper substrates by 90.2% and 97.8%, respectively. The PLA-vermiculite-coated nanocellulose system provides a biodegradable alternative to traditional high-performance food packaging with oxygen and water transmission rates of $1.30 \text{ cm}^3 \text{ m}^2 \text{ day}^{-1} \text{ atm}^{-1}$ and $1.74 \text{ g m}^{-2} \text{ day}^{-1}$, respectively. Furthermore, the manufacturing process involves only simple and scalable unit operations, making it suitable for commercial implementation in the future.

According to our research, the process of modifying vermiculite through delamination and transfer to organic solvents creates an excellent nanosheet filler for biodegradable food packaging. This solution addresses two main challenges that have hindered the widespread adoption of biodegradable polymers: poor barrier properties and high cost. Our calculations show that the cost of producing 1 kg of delaminated vermiculite on a laboratory scale is below \$1, which is more affordable than PBSA or PLA (which cost \$3.5 and \$2 per kg in 2019,

4 Synopsis

respectively). By using a strategy that is already employed by the packaging industry for commodity polymers, which involves adding inert fillers such as carbon black or CaCO_3 to reduce the cost of the final product, we can overcome the challenges of implementing biodegradable materials. A nanocomposite containing 50% vermiculite by weight is projected to cost approximately \$2 per kg for PBSA and \$1.5 per kg for PLA, making it competitive with commonly used materials in the packaging industry like polyethylene and polypropylene.

5 Own contribution

Dudko, V., Ottermann, K., Rosenfeldt, S., Papastavrou, G., & Breu, J. (2021). Osmotic Delamination: A Forceless Alternative for the Production of Nanosheets Now in Highly Polar and Aprotic Solvents. *Langmuir*, 37(1), 461–468. doi: 10.1021/acs.langmuir.0c03113

I have designed and performed the experiments. K.O. and G.P. assisted with the AFM measurements. S.R. assisted with SAXS measurements. J.B. and I wrote the manuscript with input from other authors.

Dudko, V., Rosenfeldt, S., Siegel, R., Senker, J., Matejdes, M., & Breu, J. (2022). Delamination by Repulsive Osmotic Swelling of Synthetic Na-Hectorite with Variable Charge in Binary Dimethyl Sulfoxide–Water Mixtures. *Langmuir*, 38(35), 10781–10790. doi: 10.1021/acs.langmuir.2c00965

The manuscript was written through the contributions of me, J.B., and M.M. R.S. and J.S. assisted with NMR measurements. S.R. assisted with the XRD and SAXS measurements. All authors have approved the final version of the manuscript.

Dudko, V., Timmins, R. L., Khoruzhenko, O., Röhrl, M., Greve, C., Rosenfeldt, S., ...Breu, J. (2022). Spontaneous delamination of affordable natural vermiculite as a high barrier filler for biodegradable food packaging. *Mater. Adv.*, 3(24), 9052–9062. doi: 10.1039/D2MA00734G

I and R. T. contributed equally to this work. J. B., S. A., and R. T. conceived and supervised the research. I optimized the vermiculite delamination and performed the transfer to organic solvents. I and O. K. performed the characterization of the nanosheets. Investigation of delamination progress by SAXS was done by me and S. R. R. T. and M. R. performed foil fabrication and barrier measurements. I, R. T., O. K., and J. B. wrote the manuscript. All authors discussed the results and commented on the manuscript.

6 References

1. Haruta, M., When Gold Is Not Noble: Catalysis by Nanoparticles. *Chem. Rec.* **2003**, *3* (2), 75–87.
2. Baig, N.; Kammakakam, I.; Falath, W., Nanomaterials: a review of synthesis methods, properties, recent progress, and challenges. *Mater. Adv.* **2021**, *2* (6), 1821–1871.
3. Guo, S.; Dong, S., Graphene nanosheet: synthesis, molecular engineering, thin film, hybrids, and energy and analytical applications. *Chem. Soc. Rev.* **2011**, *40* (5), 2644–2672.
4. Zhao, M.; Huang, Y.; Peng, Y.; Huang, Z.; Ma, Q.; Zhang, H., Two-dimensional metal–organic framework nanosheets: synthesis and applications. *Chem. Soc. Rev.* **2018**, *47* (16), 6267–6295.
5. Dörres, T.; Bartkiewicz, M.; Herrmann, K.; Schöttle, M.; Wagner, D.; Wang, Z.; Ikkala, O.; Retsch, M.; Fytas, G.; Breu, J., Nanoscale-Structured Hybrid Bragg Stacks with Orientation- and Composition-Dependent Mechanical and Thermal Transport Properties: Implications for Nacre Mimetics and Heat Management Applications. *ACS Appl. Nano Mater.* **2022**, 2022.
6. Wang, Z.; Rolle, K.; Schilling, T.; Hummel, P.; Philipp, A.; Kopera, B. A. F.; Lechner, A. M.; Retsch, M.; Breu, J.; Fytas, G., Tunable Thermoelastic Anisotropy in Hybrid Bragg Stacks with Extreme Polymer Confinement. *Angew. Chem. Int. Ed.* **2020**, *59* (3), 1286–1294.
7. Geim, A. K., Random Walk to Graphene (Nobel Lecture). *Angew. Chem. Int. Ed.* **2011**, *50* (31), 6966–6985.
8. Novoselov, K. S., Graphene: Materials in the Flatland (Nobel Lecture). *Angew. Chem. Int. Ed.* **2011**, *50* (31), 6986–7002.
9. Geim, A. K., Graphene: Status and Prospects. *Science* **2009**.
10. Geim, A. K.; Novoselov, K. S., The rise of graphene - Nature Materials. *Nat. Mater.* **2007**, *6* (3), 183–191.
11. Novoselov, K. S.; Geim, A. K.; Morozov, S. V.; Jiang, D.; Zhang, Y.; Dubonos, S. V.; Grigorieva, I. V.; Firsov, A. A., Electric Field Effect in Atomically Thin Carbon Films. *Science* **2004**.
12. Colson, J. W.; Dichtel, W. R., Rationally synthesized two-dimensional polymers - Nature Chemistry. *Nat. Chem.* **2013**, *5* (6), 453–465.
13. Coleman, J. N.; Lotya, M.; O'Neill, A.; Bergin, S. D.; King, P. J.; Khan, U.; Young, K.; Gaucher, A.; De, S.; Smith, R. J.; Shvets, I. V.; Arora, S. K.; Stanton, G.; Kim, H.-Y.; Lee, K.; Kim, G. T.; Duesberg, G. S.; Hallam, T.; Boland, J. J.; Wang, J. J.; Donegan, J. F.; Grunlan, J. C.; Moriarty, G.; Shmeliov, A.; Nicholls, R. J.; Perkins, J. M.; Grievson, E. M.; Theuwissen,

6 References

- K.; McComb, D. W.; Nellist, P. D.; Nicolosi, V., Two-Dimensional Nanosheets Produced by Liquid Exfoliation of Layered Materials. *Science* **2011**, *331* (6017), 568–571.
14. Rao, C. N. R.; Matte, H. S. S. R.; Maitra, U., Graphene Analogues of Inorganic Layered Materials. *Angew. Chem. Int. Ed.* **2013**, *52* (50), 13162–13185.
 15. Cong, H.-P.; Chen, J.-F.; Yu, S.-H., Graphene-based macroscopic assemblies and architectures: an emerging material system. *Chem. Soc. Rev.* **2014**, *43* (21), 7295–7325.
 16. Tedstone, A. A.; Lewis, D. J.; O'Brien, P., Synthesis, Properties, and Applications of Transition Metal-Doped Layered Transition Metal Dichalcogenides. *Chem. Mater.* **2016**, *28* (7), 1965–1974.
 17. Tan, C.; Cao, X.; Wu, X.-J.; He, Q.; Yang, J.; Zhang, X.; Chen, J.; Zhao, W.; Han, S.; Nam, G.-H.; Sindoro, M.; Zhang, H., Recent Advances in Ultrathin Two-Dimensional Nanomaterials. *Chem. Rev.* **2017**, *117* (9), 6225–6331.
 18. Wang, Q.; O'Hare, D., Recent Advances in the Synthesis and Application of Layered Double Hydroxide (LDH) Nanosheets. *Chem. Rev.* **2012**, *112* (7), 4124–4155.
 19. Zhang, H., Ultrathin Two-Dimensional Nanomaterials. *ACS Nano* **2015**, *9* (10), 9451–9469.
 20. Deng, D.; Novoselov, K. S.; Fu, Q.; Zheng, N.; Tian, Z.; Bao, X., Catalysis with two-dimensional materials and their heterostructures - Nature Nanotechnology. *Nat. Nanotechnol.* **2016**, *11* (3), 218–230.
 21. Wang, Q. H.; Kalantar-Zadeh, K.; Kis, A.; Coleman, J. N.; Strano, M. S., Electronics and optoelectronics of two-dimensional transition metal dichalcogenides - Nature Nanotechnology. *Nat. Nanotechnol.* **2012**, *7* (11), 699–712.
 22. Tyagi, D.; Wang, H.; Huang, W.; Hu, L.; Tang, Y.; Guo, Z.; Ouyang, Z.; Zhang, H., Recent advances in two-dimensional-material-based sensing technology toward health and environmental monitoring applications. *Nanoscale* **2020**, *12* (6), 3535–3559.
 23. Rohaizad, N.; Mayorga-Martinez, C. C.; Fojtů, M.; Latiff, N. M.; Pumera, M., Two-dimensional materials in biomedical, biosensing and sensing applications. *Chem. Soc. Rev.* **2021**, *50* (1), 619–657.
 24. Rojaee, R.; Shahbazian-Yassar, R., Two-Dimensional Materials to Address the Lithium Battery Challenges. *ACS Nano* **2020**, *14* (3), 2628–2658.
 25. Osada, M.; Sasaki, T., Two-Dimensional Dielectric Nanosheets: Novel Nanoelectronics From Nanocrystal Building Blocks. *Adv. Mater.* **2012**, *24* (2), 210–228.

6 References

26. Elshof, J. E. t.; Yuan, H.; Rodriguez, P. G., Two-Dimensional Metal Oxide and Metal Hydroxide Nanosheets: Synthesis, Controlled Assembly and Applications in Energy Conversion and Storage. *Adv. Energy Mater.* **2016**, *6* (23), 1600355.
27. Mendoza-Sánchez, B.; Gogotsi, Y., Synthesis of Two-Dimensional Materials for Capacitive Energy Storage. *Adv. Mater.* **2016**, *28* (29), 6104–6135.
28. Zhang, Q.; Zhang, J.; Wan, S.; Wang, W.; Fu, L., Stimuli-Responsive 2D Materials Beyond Graphene. *Adv. Funct. Mater.* **2018**, *28* (45), 1802500.
29. Norrish, K., The swelling of montmorillonite. *Discuss. Faraday Soc.* **1954**, *18* (0), 120–134.
30. West, W. J., Size determinations of clay particles in water suspensions by use of low-angle x-ray diffraction. *J. Colloid Sci.* **1952**, *7* (3), 295–305.
31. Faustini, M.; Nicole, L.; Ruiz-Hitzky, E.; Sanchez, C., History of Organic–Inorganic Hybrid Materials: Prehistory, Art, Science, and Advanced Applications. *Adv. Funct. Mater.* **2018**, *28* (27), 1704158.
32. Hofmann, U.; Frenzel, A., Quellung von Graphit und die Bildung von Graphitsäure. *Ber. dtsh. Chem. Ges. A/B* **1930**, *63* (5), 1248–1262.
33. Walker, G. F.; Garrett, W. G., Chemical Exfoliation of Vermiculite and the Production of Colloidal Dispersions. *Science* **1967**, *156* (3773), 385–387.
34. Garrett, W. G.; Walker, G. F., Swelling of Some Vermiculite–Organic Complexes in Water. *Clays Clay Miner.* **1960**, *9* (1), 557–567.
35. Walker, G. F., Macroscopic Swelling of Vermiculite Crystals in Water - Nature. *Nature* **1960**, *187* (4734), 312–313.
36. Walker, G. F., Water Layers in Vermiculite. *Nature* **1949**, *163* (4149), 726–727.
37. Norrish, K., Crystalline Swelling of Montmorillonite: Manner of Swelling of Montmorillonite - Nature. *Nature* **1954**, *173* (4397), 256–257.
38. Rosenfeldt, S.; Stöter, M.; Schlenk, M.; Martin, T.; Albuquerque, R. Q.; Förster, S.; Breu, J., In-Depth Insights into the Key Steps of Delamination of Charged 2D Nanomaterials. *Langmuir* **2016**, *32* (41), 10582–10588.
39. Daab, M.; Eichstaedt, N. J.; Habel, C.; Rosenfeldt, S.; Kalo, H.; Schießling, H.; Förster, S.; Breu, J., Onset of Osmotic Swelling in Highly Charged Clay Minerals. *Langmuir* **2018**, *34* (28), 8215–8222.
40. Daab, M.; Eichstaedt, N. J.; Edenharter, A.; Rosenfeldt, S.; Breu, J., Layer charge robust delamination of organo-clays. *RSC Adv.* **2018**, *8* (50), 28797–28803.

6 References

41. Daab, M.; Rosenfeldt, S.; Kalo, H.; Stöter, M.; Bojer, B.; Siegel, R.; Förster, S.; Senker, J.; Breu, J., Two-Step Delamination of Highly Charged, Vermiculite-like Layered Silicates via Ordered Heterostructures. *Langmuir* **2017**, *33* (19), 4816–4822.
42. Miyamoto, N.; Nakato, T., Liquid Crystalline Inorganic Nanosheet Colloids Derived From Layered Materials. *Isr. J. Chem.* **2012**, *52* (10), 881–894.
43. Ma, R.; Sasaki, T., Nanosheets of Oxides and Hydroxides: Ultimate 2D Charge-Bearing Functional Crystallites. *Adv. Mater.* **2010**, *22* (45), 5082–5104.
44. Bizeto, M. A.; Shiguihara, A. L.; Constantino, V. R. L., Layered niobate nanosheets: building blocks for advanced materials assembly. *J. Mater. Chem.* **2009**, *19* (17), 2512–2525.
45. Ma, R.; Sasaki, T., Two-Dimensional Oxide and Hydroxide Nanosheets: Controllable High-Quality Exfoliation, Molecular Assembly, and Exploration of Functionality. *Acc. Chem. Res.* **2015**, *48* (1), 136–143.
46. Zhu, X.; Su, Z.; Wu, C.; Cong, H.; Ai, X.; Yang, H.; Qian, J., Exfoliation of MoS₂ Nanosheets Enabled by a Redox-Potential-Matched Chemical Lithiation Reaction. *Nano Lett.* **2022**, *22* (7), 2956–2963.
47. Ottmers, D. M.; Rase, H. F., Potassium graphites prepared by mixed-reaction technique. *Carbon* **1966**, *4* (1), 125–127.
48. Meunier, A., Why are clay minerals small? *Clay Miner.* **2006**, *41* (2), 551–566.
49. Pérez-Rodríguez, J. L.; Carrera, F.; Poyato, J.; Pérez-Maqueda, L. A., Sonication as a tool for preparing nanometric. *Nanotechnology* **2002**, *13* (3), 382–387.
50. Addison, J., Vermiculite: A Review of the Mineralogy and Health Effects of Vermiculite Exploitation. *Regul. Toxicol. Pharm.* **1995**, *21* (3), 397–405.
51. Skipper, N. T.; Soper, A. K.; McConnell, J. D. C., The structure of interlayer water in vermiculite. *J. Chem. Phys.* **1991**, *94* (8), 5751–5760.
52. Stöter, M.; Kunz, D. A.; Schmidt, M.; Hirsemann, D.; Kalo, H.; Putz, B.; Senker, J.; Breu, J., Nanoplatelets of Sodium Hectorite Showing Aspect Ratios of $\approx 20\,000$ and Superior Purity. *Langmuir* **2013**, *29* (4), 1280–1285.
53. Breu, J.; Seidl, W.; Stoll, A. J.; Lange, K. G.; Probst, T. U., Charge Homogeneity in Synthetic Fluorohectorite. *Chem. Mater.* **2001**, *13* (11), 4213–4220.
54. Nicolosi, V.; Chhowalla, M.; Kanatzidis, M. G.; Strano, M. S.; Coleman, J. N., Liquid Exfoliation of Layered Materials. *Science* **2013**.
55. Geim, A. K.; Grigorieva, I. V., Van der Waals heterostructures - Nature. *Nature* **2013**, *499* (7459), 419–425.

6 References

56. Dudko, V.; Khoruzhenko, O.; Weiß, S.; Daab, M.; Loch, P.; Schwieger, W.; Brey, J., Repulsive Osmotic Delamination: 1D Dissolution of 2D Materials. *Adv. Mater. Technol.* **2023**, *8* (3), 2200553.
57. Möller, M. W.; Lunkenbein, T.; Kalo, H.; Schieder, M.; Kunz, D. A.; Brey, J., Barrier Properties of Synthetic Clay with a Kilo-Aspect Ratio. *Adv. Mater.* **2010**, *22* (46), 5245–5249.
58. Möller, M. W.; Handge, U. A.; Kunz, D. A.; Lunkenbein, T.; Altstädt, V.; Brey, J., Tailoring Shear-Stiff, Mica-like Nanoplatelets. *ACS Nano* **2010**, *4* (2), 717–724.
59. Backes, C., Fragile nanosheets stripped from crystals. *Nature* **2022**, *602*, 582–583.
60. Gardolinski, J. E. F. C.; Lagaly, G., Grafted organic derivatives of kaolinite: II. Intercalation of primary n-alkylamines and delamination. *Clay Miner.* **2005**, *40* (4), 547–556.
61. Ciesielski, A.; Samori, P., Graphene via sonication assisted liquid-phase exfoliation. *Chem. Soc. Rev.* **2013**, *43* (1), 381–398.
62. Backes, C.; Higgins, T. M.; Kelly, A.; Boland, C.; Harvey, A.; Hanlon, D.; Coleman, J. N., Guidelines for Exfoliation, Characterization and Processing of Layered Materials Produced by Liquid Exfoliation. *Chem. Mater.* **2017**, *29* (1), 243–255.
63. Niu, L.; Coleman, J. N.; Zhang, H.; Shin, H.; Chhowalla, M.; Zheng, Z., Production of Two-Dimensional Nanomaterials via Liquid-Based Direct Exfoliation. *Small* **2016**, *12* (3), 272–293.
64. Wiewióra, A.; Pérez-Rodríguez, J. L.; Pérez-Maqueda, L. A.; Drapała, J., Particle size distribution in sonicated high- and low-charge vermiculites. *Appl. Clay Sci.* **2003**, *24* (1), 51–58.
65. Bracamonte, M. V.; Lacconi, G. I.; Urreta, S. E.; Foa Torres, L. E. F., On the Nature of Defects in Liquid-Phase Exfoliated Graphene. *J. Phys. Chem. C* **2014**, *118* (28), 15455–15459.
66. Li, Z.; Young, R. J.; Backes, C.; Zhao, W.; Zhang, X.; Zhukov, A. A.; Tillotson, E.; Conlan, A. P.; Ding, F.; Haigh, S. J.; Novoselov, K. S.; Coleman, J. N., Mechanisms of Liquid-Phase Exfoliation for the Production of Graphene. *ACS Nano* **2020**, *14* (9), 10976–10985.
67. Coleman, J. N.; Lotya, M.; O'Neill, A.; Bergin, S. D.; King, P. J.; Khan, U.; Young, K.; Gaucher, A.; De, S.; Smith, R. J.; Shvets, I. V.; Arora, S. K.; Stanton, G.; Kim, H.-Y.; Lee, K.; Kim, G. T.; Duesberg, G. S.; Hallam, T.; Boland, J. J.; Wang, J. J.; Donegan, J. F.; Grunlan, J. C.; Moriarty, G.; Shmeliov, A.; Nicholls, R. J.; Perkins, J. M.; Grievson, E. M.; Theuwissen, K.; McComb, D. W.; Nellist, P. D.; Nicolosi, V., Two-Dimensional Nanosheets Produced by Liquid Exfoliation of Layered Materials. *Science* **2011**.
68. Zheng, W.; Lee, L. Y. S., Beyond sonication: Advanced exfoliation methods for scalable production of 2D materials. *Matter* **2022**, *5* (2), 515–545.

6 References

69. Yu, P.; Lowe, S. E.; Simon, G. P.; Zhong, Y. L., Electrochemical exfoliation of graphite and production of functional graphene. *Curr. Opin. Colloid Interface Sci.* **2015**, *20* (5), 329–338.
70. Lerf, A., Storylines in intercalation chemistry. *Dalton Trans.* **2014**, *43* (27), 10276–10291.
71. Norrish, K., Crystalline Swelling of Montmorillonite: Manner of Swelling of Montmorillonite. *Nature* **1954**, *173* (4397), 256–257.
72. Hansen, E. L.; Hemmen, H.; Fonseca, D. M.; Coutant, C.; Knudsen, K. D.; Plivelic, T. S.; Bonn, D.; Fossum, J. O., Swelling transition of a clay induced by heating. *Sci. Rep.* **2012**, *2* (618), 1–4.
73. Hofmann, U.; Klemen, R., Verlust der Austauschfähigkeit von Lithiumionen an Bentonit durch Erhitzung. *Z. Anorg. Chem.* **1950**, *262* (1-5), 95–99.
74. Herling, M. M.; Kalo, H.; Seibt, S.; Schobert, R.; Breu, J., Tailoring the Pore Sizes of Microporous Pillared Interlayered Clays through Layer Charge Reduction. *Langmuir* **2012**, *28* (41), 14713–14719.
75. Maluangnont, T.; Matsuba, K.; Geng, F.; Ma, R.; Yamauchi, Y.; Sasaki, T., Osmotic Swelling of Layered Compounds as a Route to Producing High-Quality Two-Dimensional Materials. A Comparative Study of Tetramethylammonium versus Tetrabutylammonium Cation in a Lepidocrocite-type Titanate. *Chem. Mater.* **2013**, *25* (15), 3137–3146.
76. Geng, F.; Ma, R.; Nakamura, A.; Akatsuka, K.; Ebina, Y.; Yamauchi, Y.; Miyamoto, N.; Tateyama, Y.; Sasaki, T., Unusually stable ~100-fold reversible and instantaneous swelling of inorganic layered materials. *Nat Commun* **2013**, *4*, 1632.
77. Sasaki, T.; Watanabe, M., Osmotic Swelling to Exfoliation. Exceptionally High Degrees of Hydration of a Layered Titanate. *J. Am. Chem. Soc.* **1998**, *120* (19), 4682–4689.
78. Dudko, V.; Ottermann, K.; Rosenfeldt, S.; Papastavrou, G.; Breu, J., Osmotic Delamination: A Forceless Alternative for the Production of Nanosheets Now in Highly Polar and Aprotic Solvents. *Langmuir* **2021**, *37* (1), 461–468.
79. Sasaki, T.; Watanabe, M.; Hashizume, H.; Yamada, H.; Nakazawa, H., Macromolecule-like Aspects for a Colloidal Suspension of an Exfoliated Titanate. Pairwise Association of Nanosheets and Dynamic Reassembling Process Initiated from It. *J. Am. Chem. Soc.* **1996**, *118* (35), 8329–8335.
80. Geng, F.; Ma, R.; Nakamura, A.; Akatsuka, K.; Ebina, Y.; Yamauchi, Y.; Miyamoto, N.; Tateyama, Y.; Sasaki, T., Unusually stable ~100-fold reversible and instantaneous swelling of inorganic layered materials - Nature Communications. *Nat. Commun.* **2013**, *4* (1632), 1–7.

6 References

81. Omomo, Y.; Sasaki, T.; Wang; Watanabe, M., Redoxable Nanosheet Crystallites of MnO₂ Derived via Delamination of a Layered Manganese Oxide. *J. Am. Chem. Soc.* **2003**, *125* (12), 3568-3575.
82. Gaillot, A.-C.; Lanson, B.; Drits, V. A., Structure of Birnessite Obtained from Decomposition of Permanganate under Soft Hydrothermal Conditions. 1. Chemical and Structural Evolution as a Function of Temperature. *Chem. Mater.* **2005**, *17* (11), 2959-2975.
83. Song, Y.; Iyi, N.; Hoshida, T.; Ozawa, T. C.; Ebina, Y.; Ma, R.; Yamamoto, S.; Miyamoto, N.; Sasaki, T., Massive hydration-driven swelling of layered perovskite niobate crystals in aqueous solutions of organo-ammonium bases. *Dalton Transactions* **2018**, *47* (9), 3022-3028.
84. Fukuoka, H.; Isami, T.; Yamanaka, S., Crystal Structure of a Layered Perovskite Niobate KCa₂Nb₃O₁₀. *Journal of Solid State Chemistry* **2000**, *151* (1), 40-45.
85. Sasaki, T.; Kooli, F.; Iida, M.; Michiue, Y.; Takenouchi, S.; Yajima, Y.; Izumi, F.; Chakoumakos, B. C.; Watanabe, M., A Mixed Alkali Metal Titanate with the Lepidocrocite-like Layered Structure. Preparation, Crystal Structure, Protonic Form, and Acid/Base Intercalation Properties. *Chem. Mater.* **1998**, *10* (12), 4123-4128.
86. Kim, H.-N.; Keller, S. W.; Mallouk, T. E.; Schmitt, J.; Decher, G., Characterization of Zirconium Phosphate/Polycation Thin Films Grown by Sequential Adsorption Reactions. *Chem. Mater.* **1997**, *9* (6), 1414-1421.
87. Clearfield, A.; Smith, G. D., Crystallography and structure of .alpha.-zirconium bis(monohydrogen orthophosphate) monohydrate. *Inorganic Chemistry* **1969**, *8* (3), 431-436.
88. Mathieson, A. M.; Walker, G. F., Crystal Structure of Magnesium-Vermiculite. *Amer. Min* **1954**, *39* (3), 231-255.
89. Walker, G. F., Macroscopic Swelling of Vermiculite Crystals in Water. *Nature* **1960**, *187* (4734), 312-313.
90. McCarney, J.; Smalley, M. V., Electron Microscopy Study of n-Butylammonium Vermiculite Swelling. *Clay Miner.* **1995**, *30*, 187-194.
91. Yamaguchi, D.; Miyamoto, N.; Koizumi, S.; Nakato, T.; Hashimoto, T., Hierarchical structure of niobate nanosheets in aqueous solution. *J. Appl. Crystallogr.* **2007**, *40* (s1), s101-s105.
92. Gasperin, M.; Le Bihan, M. T., Mecanisme d'hydratation des niobates alcalins lamellaires de formule A₄Nb₄O₁₇ (A = K, Rb, Cs). *Journal of Solid State Chemistry* **1982**, *43* (3), 346-353.

6 References

93. Roth, W. J.; Sasaki, T.; Wolski, K.; Song, Y.; Tang, D.-M.; Ebina, Y.; Ma, R.; Grzybek, J.; Kalahurska, K.; Gil, B.; Mazur, M.; Zapotoczny, S.; Cejka, J., Liquid dispersions of zeolite monolayers with high catalytic activity prepared by soft-chemical exfoliation. *Sci. Adv.* **2020**, *6* (12), eaay8163.
94. Chemicalize - Instant Cheminformatics Solutions. 2022.
95. Selvam, T.; Inayat, A.; Schwieger, W., Reactivity and applications of layered silicates and layered double hydroxides. *Dalton Trans.* **2014**, *43* (27), 10365–10387.
96. Vortmann, S.; Rius, J.; Siegmann, S.; Gies, H., Ab Initio Structure Solution from X-ray Powder Data at Moderate Resolution: Crystal Structure of a Microporous Layer Silicate. *J. Phys. Chem. B* **1997**, *101* (8), 1292–1297.
97. Stöter, M.; Rosenfeldt, S.; Breu, J., Tunable Exfoliation of Synthetic Clays. *Annu. Rev. Mater. Res.* **2015**, *45* (1), 129–151.
98. Mayr, L.; Amschler, S.; Edenharter, A.; Dudko, V.; Kunz, R.; Rosenfeldt, S.; Breu, J., Osmotic Swelling of Sodium Hectorite in Ternary Solvent Mixtures: Nematic Liquid Crystals in Hydrophobic Media. *Langmuir* **2020**, *36* (14), 3814–3820.
99. Kunz, R.; Amschler, S.; Edenharter, A.; Mayr, L.; Herlitz, S.; Rosenfeldt, S.; Breu, J., GIANT MULTISTEP CRYSTALLINE VS. OSMOTIC SWELLING OF SYNTHETIC HECTORITE IN AQUEOUS ACETONITRILE. *Clays Clay Miner.* **2019**, *67* (6), 481–487.
100. Dudko, V.; Rosenfeldt, S.; Siegel, R.; Senker, J.; Matejdes, M.; Breu, J., Delamination by Repulsive Osmotic Swelling of Synthetic Na-Hectorite with Variable Charge in Binary Dimethyl Sulfoxide–Water Mixtures. *Langmuir* **2022**, 2022.

7 Osmotic delamination: Forceless alternative for the production of nanosheets now in highly polar and aprotic solvents

7 Osmotic delamination: Forceless alternative for the production of nanosheets now in highly polar and aprotic solvents

Volodymyr Dudko, Katharina Ottermann, Sabine Rosenfeldt, Georg Papastavrou and Josef Breu

This work was published in *Langmuir* 37, 461 (2021). *Reprinted with permission from V. Dudko et al.: Langmuir* 37, 461 (2021). Copyright 2021 American Chemical Society.

Osmotic Delamination: A Forceless Alternative for the Production of Nanosheets Now in Highly Polar and Aprotic Solvents

Volodymyr Dudko, Katharina Ottermann, Sabine Rosenfeldt, Georg Papastavrou, and Josef Breu*

Cite This: *Langmuir* 2021, 37, 461–468

Read Online

ACCESS |

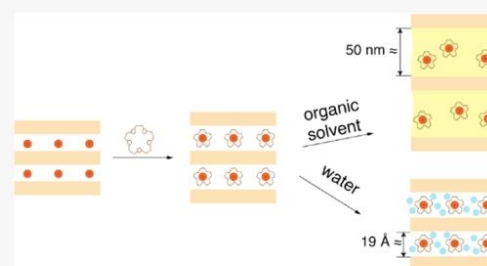
Metrics & More

Article Recommendations

Supporting Information

Downloaded via UNIV BAYREUTH on April 4, 2023 at 10:13:14 (UTC).
See <https://pubs.acs.org/sharingguidelines> for options on how to legitimately share published articles.

ABSTRACT: Repulsive osmotic delamination is thermodynamically allowed “dissolution” of two-dimensional (2D) materials and therefore represents an attractive alternative to liquid-phase exfoliation to obtain strictly monolayered nanosheets with an appreciable aspect ratio with quantitative yield. However, osmotic delamination was so far restricted to aqueous media, severely limiting the range of accessible 2D materials. Alkali-metal intercalation compounds of MoS₂ or graphite are excluded because they cannot tolerate even traces of water. We now succeeded in extending osmotic delamination to polar and aprotic organic solvents. Upon complexation of interlayer cations of synthetic hectorite clay by crown ethers, either 15-crown-5 or 18-crown-6, steric pressure is exerted, which helps in reaching the threshold separation required to trigger osmotic delamination based on translational entropy. This way, complete delamination in water-free solvents like aprotic ethylene and propylene carbonate, *N*-methylformamide, *N*-methylacetamide, and glycerol carbonate was achieved.



INTRODUCTION

A conventional, well-established method to produce mono- or few-layer nanosheets is liquid-phase exfoliation,¹ where the anisotropy in the mechanical strength of layered materials is taken advantage of to produce thinner stacks by introducing large shear forces. Limited to a handful of ionic layered compounds like lepidocrocite-type titanates,² layered antimony phosphates,^{3,4} graphene oxide,⁵ and layered zeolites,⁶ the long-known⁷ but rare phenomenon of osmotic swelling⁸ represents an appealing alternative to achieve delamination into monolayers with quantitative yield. While for these materials, delamination is complete and nematic liquid crystalline phases are spontaneously formed even at low concentrations, for graphite, delamination was reported⁹ but with a low 4% yield of graphene. Osmotic delamination is limited to one-dimensional (1D) ionic crystals meaning that the layers carry a charge that is compensated by counterions residing between the layers. Osmotic swelling is a thermodynamically allowed process that consequently does not require any mechanical force. Being repulsive^{10,11} in nature, it allows for utter and most gentle delamination (for the definition of delamination versus exfoliation, see ref 12) In this line, delamination is comparable to the dissolution of salts; however, it is limited to 1D dissolution in the sense mentioned above due to layered compounds' anisotropic nature. Consequently, osmotic swelling preserves the aspect ratio (diameter/thickness ratio) inherent in the platelet diameter of the nondelaminated layered starting material.

All of the above examples are not redox-active, can be handled in air, and delaminate osmoically in water. Extending the osmotic delamination to more attractive but highly reducing two-dimensional (2D) compounds like Li-MoS₂ or K-graphite will require two major steps. The suspension medium's redox stability window needs to be large enough to be inert in redox reactions while still showing sufficient swelling capacity. On top of that, all handling has to be done strictly in an inert atmosphere. To avoid the latter restriction and allow for easier and faster screening of variables while allowing a quick check via visual inspection by birefringence, we here tackle the first step by applying a synthetic clay, sodium fluorohectorite (Na-Hec, [Na_{0.5}]^{inter}[Mg_{2.5}Li_{0.5}]^{oct}[Si₄]^{tet}O₁₀F₂) that is synthesized as large crystals.¹³ Rotation of these high aspect ratio nanosheets (20 000 nm diameter and 1 nm thickness; Figure 1A) in suspension is sterically hindered. Even very dilute suspensions of Na-Hec (<1 vol %), therefore are caught in the nematic liquid crystalline state (Figure 1C left);¹⁴ at higher concentrations, gels are obtained. In dilute aqueous dis-

Received: October 26, 2020

Revised: December 16, 2020

Published: December 28, 2020



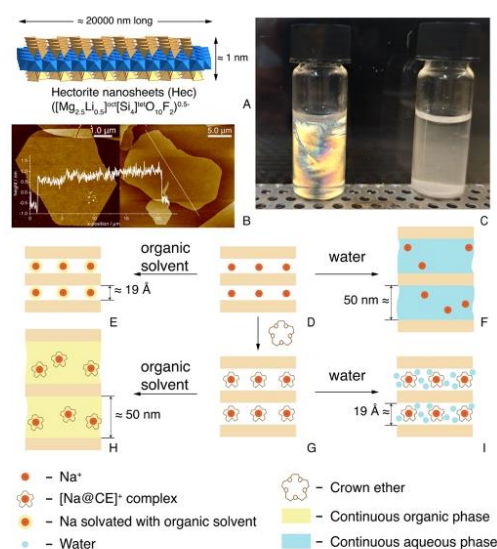


Figure 1. (A) Schematic illustration of the structure of negatively charged unilamellar hectorite nanosheets. (B) Topographic AFM image of a unilamellar Na-Hec nanosheet. (C) (left) Birefringent suspension of osmotically swollen CE-modified Na-Hec in NMF and (right) crystalline swollen CE-modified Na-Hec in water. (D) Pristine Na-Hec with negatively charged layers held together by cations. (E) Crystalline swelling of Na-Hec in organic solvents. (F) Spontaneous delamination by osmotic swelling of pristine Na-Hec in water. (G) Na-Hec intercalated with the crown ethers (CEs) forming the $[\text{Na}@\text{CE}]^+$ complex. (H) CE-modified Na-Hec spontaneously delaminates by osmotic swelling in organic solvents. (I) CE-modified Na-Hec no longer osmotically delaminates in water.

persions, as also reported for titanate nanosheets,¹⁵ like-charged nanosheets adopt a cofacial arrangement due to strong electrostatic repulsion and exhibit structural colors. While being easier to handle, hectorite perfectly mimics Li-MoS₂ or K-graphite as negatively charged nanosheets that are held together by interlayer cations, which can be solvated.

Besides the more fundamental aspect of extending osmotic delamination into organic media, these high aspect ratio nanosheets are already applied as fillers in polymer nanocomposites¹⁶ where they improve mechanical properties,^{17,18} decrease gas permeability,^{19,20} and significantly enhance flame retardancy²¹ and thermal conductivity.²² In particular for highly filled nanocomposites, solution blending offers the best^{23,24} control over homogeneity—even 1D crystalline Bragg stacks of strictly alternating polymer/filler arrangements may be obtained.²⁵ Solution blending requires both filler and polymer to be dissolved/dispersed in the same solvent. Since osmotic swelling till now could only be achieved in aqueous media (water,¹³ binary,²⁶ and ternary mixtures²⁷ of water with organic solvents), this severely restricts the choice of polymers. Osmotic delamination in water-free media will significantly widen the range of polymers for nanocomposite applications to more hydrophobic matrices like biodegradable polyesters. Besides, with such a system, it would be possible to work with moisture-sensitive precursors (e.g., isocyanates) and to try

potential applications of nanosheet gels, for instance, “superionic”^{28,29} battery electrolytes.

Here, we describe the successful transfer of repulsive osmotic delamination of Na-Hec to (aprotic) water-free organic solvents. This will allow in the future to extend the range of nanosheets accessible through osmotic swelling to the redox-active intercalation compounds.

EXPERIMENTAL SECTION

Synthesis of Sodium Hectorite. Sodium hectorite ($[\text{Na}_{0.5}]^{\text{inter}}[\text{Mg}_{2.5}\text{Li}_{0.5}]^{\text{oct}}[\text{Si}_4]^{\text{tet}}\text{O}_{10}\text{F}_2$, Na-Hec) was obtained by melt synthesis followed by long-term annealing according to a published procedure.¹³ The material featured a cation exchange capacity (CEC) of 1.27 mmol/g and a density of 2.73 g/cm³.

Swelling Experiments. Na-Hec was dried at 110 °C under vacuum for 24 h. Solvents were carefully dried by standard procedures suggested by Armarego³⁰ before the addition of Na-Hec. Ethylene carbonate (EC, 99%, Alfa Aesar) and propylene carbonate (PC, anhydrous, 99.7%, Merck) were purified with molecular sieves (VWR of sieves, 5 Å, dried at 350 °C for 3 h under a stream of argon), followed by distillation under vacuum. Glycerol carbonate (GC, 90% abcr) was purified with molecular sieves (VWR of sieves, 5 Å, dried at 350 °C for 3 h under a stream of argon) and was stored over molecular sieves. This solvent was freshly prepared before use. Formamide (FA, 99%, Merck), *N*-methylformamide (NMF, 99%, Merck), *N*-methylacetamide (NMA, 99%, Merck), *N,N*-dimethylformamide (DMF, 99.8%, anhydrous, Merck), and *N,N*-dimethylacetamide (DMA, 99.8%, anhydrous, Merck) were purified with molecular sieves (VWR of sieves, 4 Å, dried at 350 °C for 3 h under a stream of argon), followed by distillation under vacuum.

Typically, 30–60 mg of Na-Hec was added to 1 mL of the solvent corresponding to 2.5–5 wt % (1–2 vol %) of clay. Then, the crown ethers were added in amounts corresponding to 200% of CEC (around 0.15 mmol for 60 mg of Na-Hec).

All samples were equilibrated in an overhead shaker for 5 days at room temperature except for EC and NMA, which were equilibrated at 40 °C to prevent solvent solidification.

Small Angle X-Ray Scattering (SAXS). SAXS data were collected with “Double Ganesha AIR” system (SAXSLAB, Denmark). In this laboratory-based system, a microfocussed X-ray beam is provided by a rotating copper anode (MicoMax 007HF, Rigaku Corporation, Japan). A position-sensitive detector (PILATUS 300 K, Dectris) was used in different positions to cover the range of the scattering vector $q = 0.004\text{--}0.6 \text{ \AA}^{-1}$. Before the measurement, the clay suspensions were filled in 1 mm glass capillaries (Hilgenberg, code 4007610). The circularly averaged data were normalized to the incident beam, sample thickness, and measurement time.

Complexation of Interlayer Na⁺ by Crown Ethers. For comparison with suspensions, Na-Hec was modified with crown ethers in a solvent that did not trigger delamination. Na-Hec powder was immersed into the solutions of 12-crown-4 (12CE4, 99%, Merck), 15-crown-5 (15CE5, 99%, Merck), and 18-crown-6 (18CE6, 99%, Merck) in 5 mL of methanol (VWR, p.a.) with concentrations corresponding to a >25-fold excess of the CEC (approximately 1.5 mmol of crown ether). All samples were allowed to intercalate in an overhead shaker for 5 days at room temperature. Samples were dried under vacuum (2 mbar) at 110 °C.

X-Ray Diffraction (XRD). Measurement of XRD patterns of dispersions was performed in transmission mode on a STOE STADI P powder diffractometer (Cu $K\alpha_1$ radiation, GE monochromator, linear position-sensitive detector). Before the measurement, the clay suspensions were filled in 1 mm glass capillaries (Hilgenberg, code 4007610) and sealed. Crown ether-modified Na-Hec samples were transferred to 0.5 mm glass capillaries (Hilgenberg, code 4007605) and sealed. The same samples as for the SAXS measurements were used to measure the Na-Hec gel XRD pattern.

Atomic Force Microscopy (AFM). The surface topography was determined by atomic force microscopic measurements. The images were acquired with a Dimension Icon (Bruker Nano Inc.) in

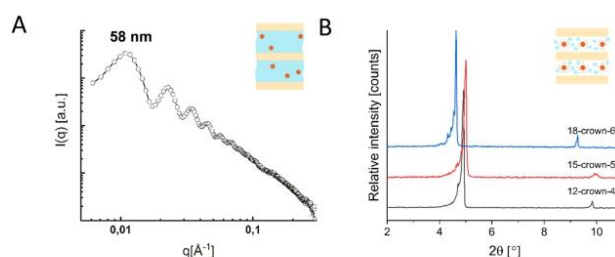


Figure 2. (A) SAXS pattern of osmotically swollen Na-Hec (1.17 vol %) in pure water. (B) XRD patterns of crystalline swollen, aqueous suspensions of Na-Hec in a water solution containing 12CE4, 15CE5, and 18CE6. The schematic structure indicates the swelling state of the Na-Hec (B) crystalline and (A) osmotic.

PeakForce tapping mode in air. A ScanAsyst Air cantilever (Bruker Nano Inc.) with a typical spring constant of 0.4 N/m and a resonant frequency of 70 kHz was used. The PeakForce amplitude was 60 nm and the PeakForce frequency was 2 kHz.

The AFM images were processed with NanoScope Analysis 1.80 (Bruker Nano Inc.). The topography was flattened by subtracting the first-order polynomial background using a threshold to exclude platelets from flattening. Platelet heights were determined by means of "step tool" in NanoScope Analysis software. The samples were prepared by slow evaporation of a few drops of a diluted suspension (0.02 g/L) on a Si wafer under ambient conditions.

RESULTS AND DISCUSSION

Swelling in Water in the Presence of Crown Ethers.

Generally, for clay minerals, two swelling regimes exist: crystalline³¹ and osmotic swelling.³² In the crystalline swelling regime, the interlayer space is solvated, involving a defined stoichiometry of solvent molecules and thus a distinct *d*-spacing. In this regime, swelling refers to phase transitions where layer charge,³³ water activity,³⁴ temperature and pressure,³⁵ and solvation enthalpy of interlayer cation³⁶ determine the equilibrium. For instance, Na-Hec incorporates one or two water layers at relative humidities of 43 and 93%, corresponding to *d*-spacings of 12.4 and 15.5 Å, respectively.¹³ Upon crystalline swelling, adhesion between adjacent layers is weakened but remains attractive. Exfoliation thus requires massive shear input.³⁶ Contrary to crystalline swelling, the separation of adjacent layers in liquid crystalline phases produced by osmotic swelling is defined solely by the volume content of clay.¹⁴ When osmotic swelling is observed, adjacent layers repel each other, and the suspensions are considered utterly delaminated. Osmotic swelling is a spontaneous, thermodynamically allowed process, and consequently, this route for obtaining nanosheets requires no mechanical agitation whatsoever. When casting a diluted suspension on a glass substrate, individual delaminated unilamellar hectorite nanosheets are observed by atomic force microscopy (Figure 1B).

To expand the interlayer space beyond the specific threshold, we previously used an ion-exchange reaction. However, it would be easier if the complexation of the interlayer cation governed the interlayer space expansion. As published by others before,³⁷ crown ethers were found to form stable complexes with interlayer Na⁺ cations,³⁸ expanding the interlayer space of Na-Hec.³⁹ (Figure S1). Without the addition of crown ethers, Na-Hec spontaneously delaminates in an aqueous suspension (Figures 1F and 2A), separating the adjacent nanosheets to 58 nm at 1.17 vol %, while in the

presence of crown ethers, repulsive osmotic delamination is no longer observed (Figures 1E,C (right) and 2B). Swelling is instead limited to the crystalline swelling regime with *d*-spacings of 18.0, 17.6, and 19.1 Å for 12-crown-4 (12CE4), 15-crown-5 (15CE5), and 18-crown-6 (18CE6), respectively. We hypothesize that crown ethers replace water in the coordination sphere of Na⁺ rendering it more hydrophobic,⁴⁰ and thus limiting swelling to crystalline swelling.

As previously suggested,¹¹ the interaction between adjacent layers becomes repulsive above a certain separation threshold where the translational entropic contribution of interlayer species (counter cations and solvent molecules) is outweighing the electrostatic attraction between the positive counterions and the negatively charged nanosheet surface. For Na-Hec in water, solely the hydration enthalpy is sufficient to achieve this threshold separation,¹⁴ while for the crown ether complexes, it appears to be no longer adequate (Figure 1I).

Osmotic Swelling in Organic Solvents in the Presence of Crown Ethers. Swelling behavior varies drastically upon changing the solvent environment. Based on the similarity of chemical structures, two groups of solvents were chosen for the investigation of swelling behavior: cyclic carbonates containing ethylene carbonate (EC), propylene carbonate (PC), and glycerol carbonate (GC) and amides containing formamide (FA), *N*-methylformamide (NMF), *N*-methylacetamide (NMA), *N,N*-dimethylformamide (DMF), and *N,N*-dimethylacetamide (DMA). All of these solvents possess a high dipole moment, and the dielectric constant varies within each group, while the Hansen H-bond parameter systematically varies within the cyclic carbonates. The chemical formulas of the solvents are given in Table 1.

Given the large diameter of Na-Hec of $\approx 20 \mu\text{m}$, the concentrations were chosen to yield nematic liquid crystalline phases¹⁴ if delamination by osmotic swelling was successful. The suspensions were first examined visually. Sediment (Figure 1C right) indicated that swelling was limited to the crystalline regime, which was further verified by the XRD of the dispersion. If birefringence under polarized light was observed (Figure 1C left) and the dispersion's viscosity was significantly higher than that of the applied solvent, the sample was characterized by SAXS.

Because of the 2D shape of dispersed colloids, SAXS curves scale with q^{-2} at low and intermediate q values.⁴¹ In addition, the separation distance of alike charged nanosheets adopting a cofacial arrangement in the nematic phase can be deduced from the interference peaks observed on the q^{-2} background. Finally, if delamination happens not to be complete, a peak at a

7 Osmotic delamination: Forceless alternative for the production of nanosheets now in highly polar and aprotic solvents

high q value will be observed corresponding to the d -spacing of crystalline swollen Na-Hec, which can also be observed on the XRD done on the swollen Na-Hec gel in FA with 15CES (Figure S2).

Opposite to the swelling behavior in water, for pure cyclic carbonates, swelling of Na-Hec was limited to the crystalline regime (Figure 3A). Comparing with dry Na-Hec (9.6 Å)

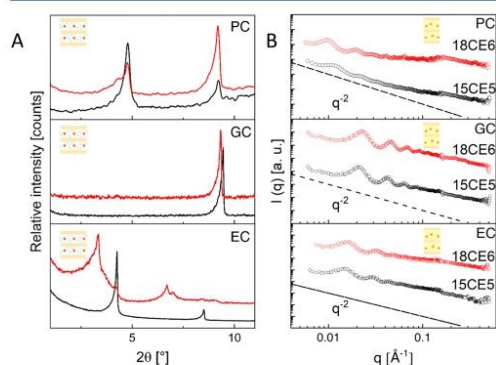


Figure 3. (A) XRD pattern of crystalline swollen Na-Hec in pure solvents (PC, GC, and EC) and in the presence of 12CE4. (B) SAXS curves of osmotically swollen Na-Hec in PC, GC, and EC containing 15CES or 18CE6. The scaling of q for the low q -range is indicated by a dashed line. The intensities of the 18CE6 sample are shifted to avoid overlap. The schematic structure indicates the swelling state of the Na-Hec (A) crystalline and (B) osmotic.

samples, only moderate increases of the interlayer space by 9.8 and 11.2 Å (d -spacing of 18.4 and 20.8 Å) were observed for EC and PC, respectively, while for GC, no increase at all was observed, suggesting that GC could not access the interlayer space.

With the addition of 12CE4, the swelling was also at best limited to crystalline swelling. For GC, neither 12CE4 nor solvent was intercalated; for PC, only the solvent was intercalated, while for EC, a d -spacing (26.0 Å) larger than that of dry Na@12CE4-Hec (17.2 Å) was observed, indicating that both crown ether and the solvent were entering the interlayer space but limited to a certain extent.

Dispersions of Na-Hec in GC, EC, and PC in the presence of 15CES and 18CE6 showed, however, a significantly increased viscosity, and no sediment could be spotted. Moreover, birefringence was observed in cross-polarized light (Figure 1C left) for translucent suspensions. SAXS patterns (Figure 3B) suggested repulsive osmotic swelling to monophasic gels (Figure 1H) with a uniform separation of adjacent nanosheets to 55.0 nm ($q = 0.011 \text{ \AA}^{-1}$) and 63 nm ($q = 0.01 \text{ \AA}^{-1}$) in PC in the presence of 15CES (4 wt % or 1.81 vol %) and 18CE6 (3.6 wt % or 1.59 vol %), respectively. With GC as a solvent, the separation was 31 nm ($q = 0.0201 \text{ \AA}^{-1}$) for 15CES (6.1 wt % or 3.2 vol %) and 28 nm ($q = 0.0222 \text{ \AA}^{-1}$) for 18CE6 (6.8 wt % or 3.5 vol %). In EC, the separation was 42.1 nm ($q = 0.0149 \text{ \AA}^{-1}$) for 15CES (4.9 wt % or 2.4 vol %) and 40 nm ($q = 0.0157 \text{ \AA}^{-1}$) for 18CE6 (5.1 wt % or 2.5 vol %).

No peaks were observed at high q values or low 2θ values on the XRD pattern of the swollen gel (Figures S3 and 3B), suggesting complete delamination of Na-Hec down to

monolayers in all three solvents upon addition of 15CES or 18CE6. As expected for nanosheets, intermediate q values scale with q^{-2} . In addition, the dependence of the nanosheet separation as $d = \delta/\Phi$, where δ is the nanosheet thickness and Φ is the volume fraction of the clay, gives the value of the nanosheet thickness in the range of 0.7–1 nm, which is in agreement with previous reports,²⁷ and the thickness of the single clay sheets based on X-ray diffraction.¹³ This corroborates complete delamination.

For the complete amide group, comprising DMF, DMA, NMF, NMA, and FA, swelling of Na-Hec in pure solvents was also limited to the crystalline regime with d -spacings of 21.7, 20.9, 17.4, 18.0, and 17.6 Å, respectively (Figures S4–S6 and 4A).

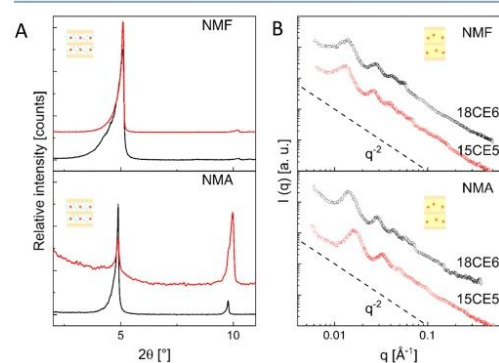


Figure 4. (A) XRD patterns of crystalline swollen Na-Hec in pure solvents (black curve) (NMF and NMA) and in the presence of 12CE4 (red curve). (B) SAXS curves of osmotically swollen Na-Hec in NMF and NMA containing 15CES or 18CE6. The scaling of q for the low q -range is indicated by a dashed line. The intensities of the 18CE6 sample are shifted to avoid overlap. The schematic structure indicates the swelling state of the Na-Hec (A) crystalline and (B) osmotic.

For DMA, DMF, and FA, the limitation to crystalline swelling was not lifted upon the addition of any of the three crown ethers (Figures S4–S6), neither could swelling be pushed beyond the crystalline regime upon addition of 12CE4 in NMA and NMF with no changes of d -spacings observed (Figure 4A) compared to the samples suspended in the pure solvent.

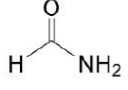
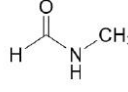
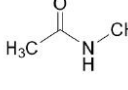
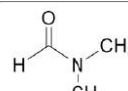
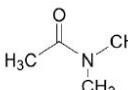
Dispersion of Na-Hec in NMF and NMA in the presence of 15CES and 18CE6, however, triggered osmotic swelling (Figure 4B) similar to what was observed for the cyclic carbonates. In NMF, the separation was 43.7 nm ($q = 0.0144 \text{ \AA}^{-1}$) for 15CES (4 wt % or 1.47 vol %) and 47.2 nm ($q = 0.0133 \text{ \AA}^{-1}$) for 18CE6 (3.5 wt % or 1.28 vol %). In NMA, the separation was 45.2 nm ($q = 0.0139 \text{ \AA}^{-1}$) for 15CES (3.8 wt % or 1.39 vol %) and 39.5 nm ($q = 0.0159 \text{ \AA}^{-1}$) for 18CE6 (4.6 wt % or 1.68 vol %).

As with cyclic carbonates, no peaks were observed at high q values or low 2θ values on the XRD pattern of the swollen gel (Figure S7), suggesting complete delamination of Na-Hec in both these two solvents upon addition of 15CES or 18CE6. As expected for nanosheets, intermediate q values scale with q^{-2} .

Why are 15CES and 18CE6 Game Changers? The crown ethers drastically change the swelling behavior, altering

7 Osmotic delamination: Forceless alternative for the production of nanosheets now in highly polar and aprotic solvents

Table 1. Dipole Moment, Relative Permittivity, a Product of Dipole Moment and Dielectric Constant, and H-Bond Donor Parameter of the Used Solvents^{46–48}

	Dipole moment [D]	Relative permittivity [ϵ], (at 20°C)	D* ϵ	Hansen H bond parameter [MPa ^{1/2}] ⁴⁶	Chemical Formula
Propylene carbonate (PC)	5.36 ⁴⁷	66.6 ⁴⁷	357	5.1	
Glycerol carbonate (GC)	5.05 ⁴⁷	111.5 ⁴⁷	563	17.4	
Ethylene carbonate (EC)	4.81 ⁴⁷	90.5 (40°C) ⁴⁷	435	4.1	
Formamide (FA)	3.73 ⁴⁸	110.0 ⁴⁸	410	19	
Methyl Formamide (NMF)	3.83 ⁴⁸	189.0 ⁴⁸	723	15.9	
Methyl acetamide (NMA)	4.3 ⁴⁸	179.0 ⁴⁸	769	13	
Dimethyl formamide (DMF)	3.82 ⁴⁸	38.3 ⁴⁸	146	11.3	
Dimethyl acetamide (DMA)	3.7 ⁴⁸	38.9 ⁴⁸	144	9.4	

it from the crystalline swelling to the osmotic swelling, leading to delamination down to monolayers. Upon coordination of the interlayer Na⁺ by crown ethers, two factors are changed, which are decisive for the swelling energetics. First, the

solvation enthalpies of naked Na⁺ and the crown ether complexes⁴⁰ are quite different. While the naked cation is electrophilic (Figure 1D), the complex cation surface is nucleophilic (Figure 1G).⁴² The solvation enthalpy of crown

ethers is generally higher for organic solvents than water,⁴³ suggesting that the interlayer becomes more hydrophobic upon complexation. Second, the area occupied by the interlayer cation increases. For instance, the area³⁹ occupied by the sodium-15-crown-5 complex $[\text{Na}@15\text{C}5]^+$ amounts to 80 \AA^2 , much larger than the equivalent area of Na-Hec (48 \AA^2 per charge¹¹). Consequently, the disc-shaped $[\text{Na}@15\text{C}5]^+$ or $[\text{Na}@18\text{C}6]^+$ cannot arrange in a flat orientation in the interlayer space but instead has to be inclined to achieve a packing density sufficient for charge balance. Accordingly, the complexation of interlayer Na^+ by the larger crown ethers will generate steric pressure that will assist the solvation enthalpy in expanding the interlayer space beyond the threshold, which is required for rendering the interaction between adjacent layers in the stack repulsive by translational entropy (Figure 11). The decisive role of such steric assistance was previously demonstrated for highly charged vermiculites where osmotic delamination in water could be triggered by ion exchange with bulky, hydrophilic organocations.^{10,11} Note, crown ethers form complexes with a handful of ions including Li^+ , NH_4^+ , K^+ , etc., making it possible to use them with numerous intercalation compounds of various 2D materials.⁴⁴ The complexation of interlayer sodium with 12CE4 and formation of 2 to 1 complex with sodium do not lead to delamination. We assume that the 2 to 1 complex hinders the interaction of the solvent with sodium, which is still partially accessible in the case of 1 to 1 complexes of 18CE6 and 15C5E, which might have a decisive impact on the energetics of delamination.

In the course of osmotic delamination, solvent properties will have an impact in several ways: while still being in the attractive crystalline swelling regime, the solvation enthalpy should be crucial and will be dominated by the dipolar interaction with the interlayer cation and the nanosheet surface, which in turn is related to solvation energy⁴⁵ and the solvent–solvent interaction in the second solvation shell. Additionally, polar solvent molecules will screen the charge and thus weaken the electrostatic interaction between the interlayer cation and the nanosheet surface. Obviously, the dipole moment and the dielectric constant should, therefore, be highly relevant solvent parameters. Indeed, we previously found that the dipole moment is strongly correlated with the phenomenon of osmotic swelling in ternary mixtures of water and two organic solvents.²⁷ In crown ether-induced swelling, the strong correlation with the dipole moment holds too (Table 1) but is not decisive on its own. Solvents like tetrahydrofuran (THF), acetone, ethanol, methanol, and many others were tested, and they did not trigger osmotic swelling in the presence of crown ethers.

For the amide group, the dielectric constant increases in the order $\text{DMF} = \text{DMA} < \text{FA} < \text{NMF} < \text{NMA}$, and the dielectric constant was found to correlate with osmotic swelling. Only the two solvents with the highest dielectric constant are capable of triggering osmotic swelling. Norrish already put forward the connection of dipole moment/solvation energy and the dielectric constant with osmotic swelling,⁴⁹ suggesting that the swelling potential is proportional to $U \epsilon / \nu^2$, where U is the solvation energy, ϵ is the dielectric constant of the interlayer solvent, and ν is the charge of the interlayer cation. We propose instead to use the product of the dipole moment and the dielectric constant to predict whether a specific solvent will trigger osmotic swelling. This product has a high value for all successful solvents. FA is, however, an outlier based on that criterion, as it should induce osmotic swelling while it could

not be observed experimentally. Nevertheless, this criterion was successfully applied to identify and include NMF and NMA into the study, two solvents that indeed triggered osmotic swelling. Please note that the colloidal suspension of nanosheets is stable in humid air atmosphere.

Contrary to graphene oxide,⁵⁰ hydrogen bonding does not seem to play a significant role, since within the cyclic carbonate group, the Hansen hydrogen bonding parameter varies over a wide range, while the solvents showed similar swelling behavior. Additionally, the fact that two out of five solvents capable of osmotically delaminating Na-Hec in the presence of crown ethers are aprotic indicates that hydrogen bonding is not crucial for osmotic swelling and delamination.

CONCLUSIONS

Gentle and utter delamination down to monolayers by thermodynamically allowed osmotic swelling clearly is not restricted to aqueous media but can be extended to water-free and aprotic solvents. This is the first and probably most crucial methodological step toward extending osmotic delamination to more technically interesting materials like graphite and MoS_2 intercalation compounds. To sum up the approach, whenever the ionic layered solid is suspended in appropriate solvent media (it should possess high dipole moment and high dielectric constant and have high interaction energy with the interlayer ionic species) and the interlayer space is expanded to the specific threshold, the crystalline swelling is switched to the osmotic delamination regime, yielding quantitative delamination. In this regime, the nanosheets could be processed with great ease.

Furthermore, the nematic suspensions in water-free organic solvents will allow for an extended range of polymer matrices possible for fabricating ordered nanocomposites via solution blending. This will give access to composites of uniformly dispersed nanosheets within hydrophobic polymer systems, including isocyanate-based polyurethanes. In addition, since cyclic carbonates, which are popular solvents in the battery technology field, are among the successful candidates, inorganic gel electrolytes may be probed as superionic conductors.

ASSOCIATED CONTENT

Supporting Information

The Supporting Information is available free of charge at <https://pubs.acs.org/doi/10.1021/acs.langmuir.0c03113>.

XRD patterns of crown ether intercalated Na-Hec nondelaminated dispersions; XRD patterns of the osmotically delaminated gel; and table with solvent parameters (PDF)

AUTHOR INFORMATION

Corresponding Author

Josef Breu – Department of Inorganic Chemistry I, Bavarian Polymer Institute, University of Bayreuth, 95440 Bayreuth, Germany; orcid.org/0000-0002-2547-3950; Email: josef.breu@uni-bayreuth.de

Authors

Volodymyr Dudko – Department of Inorganic Chemistry I, Bavarian Polymer Institute, University of Bayreuth, 95440 Bayreuth, Germany

Katharina Ottermann – Department of Physical Chemistry II, Bavarian Polymer Institute, University of Bayreuth, 95440 Bayreuth, Germany

Sabine Rosenfeldt – Department of Physical Chemistry I, Bavarian Polymer Institute, University of Bayreuth, 95440 Bayreuth, Germany

Georg Papastavrou – Department of Physical Chemistry II, Bavarian Polymer Institute, University of Bayreuth, 95440 Bayreuth, Germany; orcid.org/0000-0002-5870-6693

Complete contact information is available at:
<https://pubs.acs.org/10.1021/acs.langmuir.0c03113>

Author Contributions

The manuscript was written through contributions of V.D. and J.B. S.R. conducted SAXS measurements and helped with data analysis and K.O. and G.P. conducted AFM measurements and helped with data analysis. All authors have given approval to the final version of the manuscript.

Notes

The authors declare no competing financial interest.

ACKNOWLEDGMENTS

The authors thank F. Puchtlar for producing the synthetic hectorite. The authors also thank O. Khoruzhenko and S. Weiss for the graphic design. The authors thank R. Timmins for English proofreading. This work was supported by the Deutsche Forschungsgemeinschaft (SFB 1357 (B2 and C2)).

REFERENCES

- Coleman, J. N.; Lotya, M.; O'Neill, A.; Bergin, S. D.; King, P. J.; Khan, U.; Young, K.; Gaucher, A.; De, S.; Smith, R. J.; Shvets, I. V.; Arora, S. K.; Stanton, G.; Kim, H.-Y.; Lee, K.; Kim, G. T.; Duesberg, G. S.; Hallam, T.; Boland, J. J.; Wang, J. J.; Donegan, J. F.; Grunlan, J. C.; Moriarty, G.; Shmeliov, A.; Nicholls, R. J.; Perkins, J. M.; Grieveson, E. M.; Theuwissen, K.; McComb, D. W.; Nellist, P. D.; Nicolosi, V. Two-Dimensional Nanosheets Produced by Liquid Exfoliation of Layered Materials. *Science* **2011**, *331*, 568–571.
- Wang, L.; Sasaki, T. Titanium Oxide Nanosheets: Graphene Analogues with Versatile Functionalities. *Chem. Rev.* **2014**, *114*, 9455–9486.
- Davidson, P.; Penisson, C.; Constantin, D.; Gabriel, J.-C. P. Isotropic, nematic, and lamellar phases in colloidal suspensions of nanosheets. *Proc. Natl. Acad. Sci. U.S.A.* **2018**, *115*, 6662–6667.
- Gabriel, J.-C. P.; Camerel, F.; Lemaire, B. J.; Desvaux, H.; Davidson, P.; Batail, P. Swollen liquid-crystalline lamellar phase based on extended solid-like sheets. *Nature* **2001**, *413*, 504–508.
- Liu, R.; Gong, T.; Zhang, K.; Lee, C. Graphene oxide papers with high water adsorption capacity for air dehumidification. *Sci. Rep.* **2017**, *7*, No. 9761.
- Roth, W. J.; Sasaki, T.; Wolski, K.; Song, Y.; Tang, D.-M.; Ebina, Y.; Ma, R.; Grzybek, J.; Kalahurska, K.; Gil, B.; Mazur, M.; Zapotoczny, S.; Cejka, J. Liquid dispersions of zeolite monolayers with high catalytic activity prepared by soft-chemical exfoliation. *Sci. Adv.* **2020**, *6*, No. eaay8163.
- Lerf, A. Storylines in intercalation chemistry. *Dalton Trans.* **2014**, *43*, 10276–10291.
- Michot, L. J.; Bihannic, I.; Maddi, S.; Funari, S. S.; Baravian, C.; Levitz, P.; Davidson, P. Liquid–crystalline aqueous clay suspensions. *Proc. Natl. Acad. Sci. U.S.A.* **2006**, *103*, 16101–16104.
- Bepete, G.; Anglaret, E.; Ortolani, L.; Morandi, V.; Huang, K.; Pénicaud, A.; Drummond, C. Surfactant-free single-layer graphene in water. *Nat. Chem.* **2017**, *9*, 347–352.
- Daab, M.; Eichstaedt, N. J.; Edenharter, A.; Rosenfeldt, S.; Breu, J. Layer charge robust delamination of organo-clays. *RSC Adv.* **2018**, *8*, 28797–28803.
- Daab, M.; Eichstaedt, N. J.; Habel, C.; Rosenfeldt, S.; Kalo, H.; Schießling, H.; Förster, S.; Breu, J. Onset of Osmotic Swelling in Highly Charged Clay Minerals. *Langmuir* **2018**, *34*, 8215–8222.
- Gardolinski, J. E. F. C.; Lagaly, G. Grafted organic derivatives of kaolinite: II. Intercalation of primary n-alkylamines and delamination. *Clay Miner.* **2005**, *40*, 547–556.
- Stöter, M.; Kunz, D. A.; Schmidt, M.; Hirsemann, D.; Kalo, H.; Putz, B.; Senker, J.; Breu, J. Nanoplatelets of Sodium Hectorite Showing Aspect Ratios of $\approx 20\,000$ and Superior Purity. *Langmuir* **2013**, *29*, 1280–1285.
- Rosenfeldt, S.; Stöter, M.; Schlenk, M.; Martin, T.; Albuquerque, R. Q.; Förster, S.; Breu, J. In-Depth Insights into the Key Steps of Delamination of Charged 2D Nanomaterials. *Langmuir* **2016**, *32*, 10582–10588.
- Sano, K.; Kim, Y. S.; Ishida, Y.; Ebina, Y.; Sasaki, T.; Hikima, T.; Aida, T. Photonic water dynamically responsive to external stimuli. *Nat. Commun.* **2016**, *7*, No. 12559.
- Alexandre, M.; Dubois, P. Polymer-layered silicate nanocomposites: preparation, properties and uses of a new class of materials. *Mater. Sci. Eng., R* **2000**, *28*, 1–63.
- Zhao, C.; Zhang, P.; Zhou, J.; Qi, S.; Yamauchi, Y.; Shi, R.; Fang, R.; Ishida, Y.; Wang, S.; Tomsia, A. P.; Liu, M.; Jiang, L. Layered nanocomposites by shear-flow-induced alignment of nanosheets. *Nature* **2020**, *580*, 210–215.
- Ziadeh, M.; Fischer, B.; Schmid, J.; Altstädt, V.; Breu, J. On the importance of specific interface area in clay nanocomposites of PMMA filled with synthetic nano-mica. *Polymer* **2014**, *55*, 3770–3781.
- Habel, C.; Tsurko, E. S.; Timmins, R. L.; Hutschreuther, J.; Kunz, R.; Schuchardt, D. D.; Rosenfeldt, S.; Altstädt, V.; Breu, J. Lightweight Ultra-High-Barrier Liners for Helium and Hydrogen. *ACS Nano* **2020**, *14*, 7018–7024.
- Kunz, D. A.; Schmid, J.; Feicht, P.; Erath, J.; Fery, A.; Breu, J. Clay-Based Nanocomposite Coating for Flexible Optoelectronics Applying Commercial Polymers. *ACS Nano* **2013**, *7*, 4275–4280.
- Das, P.; Thomas, H.; Moeller, M.; Walther, A. Large-scale, thick, self-assembled, nacre-mimetic brick-walls as fire barrier coatings on textiles. *Sci. Rep.* **2017**, *7*, No. 39910.
- Chen, J.; Huang, X.; Sun, B.; Jiang, P. Highly Thermally Conductive Yet Electrically Insulating Polymer/Boron Nitride Nanosheets Nanocomposite Films for Improved Thermal Management Capability. *ACS Nano* **2019**, *13*, 337–345.
- Eckert, A.; Abbasi, M.; Mang, T.; Saalwächter, K.; Walther, A. Structure, Mechanical Properties, and Dynamics of Polyethylenoxide/Nanoclay Nacre-Mimetic Nanocomposites. *Macromolecules* **2020**, *53*, 1716–1725.
- Habel, C.; Maiz, J.; Olmedo-Martínez, J. L.; López, J. V.; Breu, J.; Müller, A. J. Competition between nucleation and confinement in the crystallization of poly(ethylene glycol)/large aspect ratio hectorite nanocomposites. *Polymer* **2020**, *202*, No. 122734.
- Wang, Z.; Rolle, K.; Schilling, T.; Hummel, P.; Philipp, A.; Kopera, B. A. F.; Lechner, A. M.; Retsch, M.; Breu, J.; Fytas, G. Tunable Thermoelastic Anisotropy in Hybrid Bragg Stacks with Extreme Polymer Confinement. *Angew. Chem., Int. Ed.* **2020**, *59*, 1286–1294.
- Kunz, R.; Amschler, S.; Edenharter, A.; Mayr, L.; Herlitz, S.; Rosenfeldt, S.; Breu, J. Giant Multistep Crystalline vs. Osmotic Swelling Of Synthetic Hectorite In Aqueous Acetonitrile. *Clays Clay Miner.* **2019**, *67*, 481–487.
- Mayr, L.; Amschler, S.; Edenharter, A.; Dudko, V.; Kunz, R.; Rosenfeldt, S.; Breu, J. Osmotic Swelling of Sodium Hectorite in Ternary Solvent Mixtures: Nematic Liquid Crystals in Hydrophobic Media. *Langmuir* **2020**, *36*, 3814–3820.
- Sun, P.; Ma, R.; Sasaki, T. Recent progress on exploring exceptionally high and anisotropic H⁺/OH⁻ ion conduction in two-dimensional materials. *Chem. Sci.* **2018**, *9*, 33–43.
- Hiebl, C.; Loch, P.; Brinek, M.; Gombotz, M.; Gadermaier, B.; Heitjans, P.; Breu, J.; Wilkening, H. M. R. Rapid Low-Dimensional Li

7 Osmotic delamination: Forceless alternative for the production of nanosheets now in highly polar and aprotic solvents

- + Ion Hopping Processes in Synthetic Hectorite-Type $\text{Li}_0.5\text{[Mg}_2\text{Si}_4\text{O}_{10}\text{F}_2]$. *Chem. Mater.* **2020**, *32*, 7445–7457.
- (30) Armarego, W. L. F. *Purification of Laboratory Chemicals*; Butterworth-Heinemann, 2017.
- (31) Norrish, K. Crystalline Swelling of Montmorillonite: Manner of Swelling of Montmorillonite. *Nature* **1954**, *173*, 256–257.
- (32) Paineau, E.; Bihannic, I.; Baravian, C.; Philippe, A.-M.; Davidson, P.; Levitz, P.; Funari, S. S.; Rochas, C.; Michot, L. J. Aqueous Suspensions of Natural Swelling Clay Minerals. I. Structure and Electrostatic Interactions. *Langmuir* **2011**, *27*, 5562–5573.
- (33) Daab, M.; Rosenfeldt, S.; Kalo, H.; Stöter, M.; Bojer, B.; Siegel, R.; Förster, S.; Senker, J.; Breu, J. Two-Step Delamination of Highly Charged, Vermiculite-like Layered Silicates via Ordered Heterostructures. *Langmuir* **2017**, *33*, 4816–4822.
- (34) Stöter, M.; Rosenfeldt, S.; Breu, J. Tunable Exfoliation of Synthetic Clays. *Annu. Rev. Mater. Res.* **2015**, *45*, 129–151.
- (35) You, S.; Kunz, D.; Stöter, M.; Kalo, H.; Putz, B.; Breu, J.; Talyzin, A. V. Pressure-Induced Water Insertion in Synthetic Clays. *Angew. Chem., Int. Ed.* **2013**, *52*, 3891–3895.
- (36) Möller, M. W.; Handge, U. A.; Kunz, D. A.; Lunkenbein, T.; Altstädt, V.; Breu, J. Tailoring Shear-Stiff, Mica-like Nanoplatelets. *ACS Nano* **2010**, *4*, 717–724.
- (37) Ruiz-Hitzky, E.; Casal, B. Crown ether intercalations with phyllosilicates. *Nature* **1978**, *276*, 596–597.
- (38) Aranda, P.; Casal, B.; Fripiat, J. J.; Ruiz-Hitzky, E. Intercalation of Macrocyclic Compounds (Crown Ethers and Cryptands) into 2:1 Phyllosilicates. Stability and Calorimetric Study. *Langmuir* **1994**, *10*, 1207–1212.
- (39) Casal, B.; Aranda, P.; Sanz, J.; Ruiz-Hitzky, E. Interlayer Adsorption of Macrocyclic Compounds (Crown-Ethers and Cryptands) in 2:1 Phyllosilicates: II. Structural Features. *Clay Miner.* **1994**, *29*, 191–203.
- (40) Solov'ev, V. P.; Strakhova, N. N.; Raevsky, O. A.; Rüdiger, V.; Schneider, H.-J. Solvent Effects on Crown Ether Complexations. *J. Org. Chem.* **1996**, *61*, 5221–5226.
- (41) Boldon, L.; Laliberte, F.; Liu, L. Review of the fundamental theories behind small angle X-ray scattering, molecular dynamics simulations, and relevant integrated application. *Nano Rev.* **2015**, *6*, No. 25661.
- (42) Sam, D. J.; Simmons, H. E. Crown ether chemistry. Substitution reactions of potassium halide and potassium hydroxide complexes of dicyclohexyl-18-crown-6. *J. Am. Chem. Soc.* **1974**, *96*, 2252–2253.
- (43) Józwiak, M. The effect of properties of water–organic solvent mixtures on the solvation enthalpy of 12-crown-4, 15-crown-5, 18-crown-6 and benzo-15-crown-5 ethers at 298.15 K. *Thermochim. Acta* **2004**, *417*, 31–41.
- (44) Wan, J.; Lacey, S. D.; Dai, J.; Bao, W.; Fuhrer, M. S.; Hu, L. Tuning two-dimensional nanomaterials by intercalation: materials, properties and applications. *Chem. Soc. Rev.* **2016**, *45*, 6742–6765.
- (45) Bissada, K. K.; Johns, W. D.; Cheng, F. S. Cation-dipole interactions in clay organic complexes. *Clay Miner.* **1967**, *7*, 155–166.
- (46) Hansen, C. M. *Hansen Solubility Parameters*; CRC Press, 2007.
- (47) Chernyak, Y. Dielectric Constant, Dipole Moment, and Solubility Parameters of Some Cyclic Acid Esters. *J. Chem. Eng. Data* **2006**, *51*, 416–418.
- (48) Haynes, W. M. *CRC Handbook of Chemistry and Physics*; CRC Press, 2011.
- (49) Norrish, K. The swelling of montmorillonite. *Discuss. Faraday Soc.* **1954**, *18*, 120–134.
- (50) Jalili, R.; Aboutalebi, S. H.; Esrafilzadeh, D.; Konstantinov, K.; Moulton, S. E.; Razal, J. M.; Wallace, G. G. Organic Solvent-Based Graphene Oxide Liquid Crystals: A Facile Route toward the Next Generation of Self-Assembled Layer-by-Layer Multifunctional 3D Architectures. *ACS Nano* **2013**, *7*, 3981–3990.

Supporting Information

Osmotic delamination: Forceless alternative for the production of nanosheets now in highly polar and aprotic solvents

*Volodymyr Dudko*¹, *Katharina Ottermann*², *Sabine Rosenfeldt*³, *Georg Papastavrou*² and *Josef Breu*^{1*}

¹Department of Inorganic Chemistry I and Bavarian Polymer Institute, University of Bayreuth, Universitätsstr. 30, 95440 Bayreuth, Germany.

²Department of Physical Chemistry II and Bavarian Polymer Institute, University of Bayreuth, Universitätsstr. 30, 95440, Bayreuth, Germany.

³Department of Physical Chemistry I and Bavarian Polymer Institute, University of Bayreuth, Universitätsstr. 30, 95440, Bayreuth, Germany.

*Correspondence to J. Breu (josef.breu@uni-bayreuth.de)

Number of pages:5

Number of figures:7

7 Osmotic delamination: Forceless alternative for the production of nanosheets now in highly polar and aprotic solvents

Additional Data

Na-Hec intercalated with crown ethers

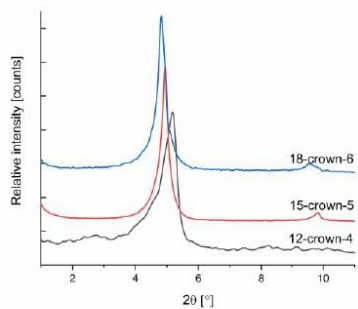


Figure S1. XRD patterns of crown-ether intercalated Na-Hec containing 12CE4, 15CE5, 18CE6. D-spacing of 17.2 Å, 17.8 Å, 18.3 Å, respectively.

Na-Hec gel swollen in FA with 15CE5 featuring partial delamination

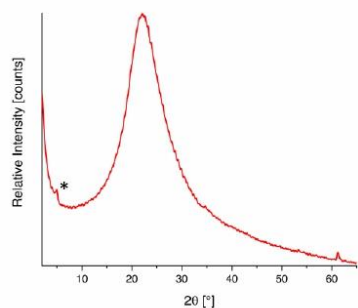


Figure S2. XRD pattern of Na-Hec gel swollen in FA with 15CE5 featuring not fully delaminated domains as indicated by the peak at $4.91^\circ 2\theta$ (marked by an asterisk) corresponding to the 001 reflection of the crystalline swollen phase. The most intense broad peak originates from the solvent.

7 Osmotic delamination: Forceless alternative for the production of nanosheets now in highly polar and aprotic solvents

Osmotically swollen crown-ether modified Na-Hec gel in PC, GC and EC featuring full delamination down to monolayers

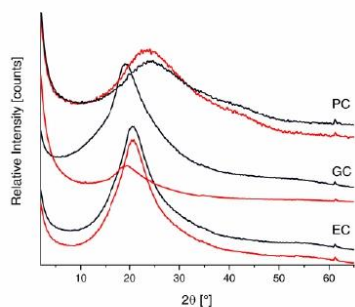


Figure S3. XRD patterns of crown-ether modified Na-Hec gel containing 15CE5 (red curve), 18CE6 (black curve) in PC, GC and EC. The absence of a low angle peak indicates fully delaminated nanosheets while the clearly observable 060 band at 61.2° 2θ peak indicates nanosheets concentrations being sufficiently high to observe a signal. The intense broad peak originates from the solvent.

7 Osmotic delamination: Forceless alternative for the production of nanosheets now in highly polar and aprotic solvents

Crystalline swelling of crown-ether modified Na-Hec in FA, DMF, DMA

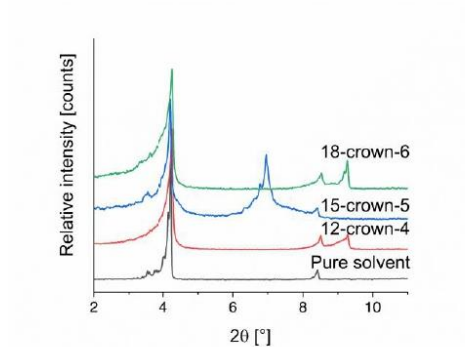


Figure S4. XRD patterns of crystalline swollen Na-Hec in pure DMA and in the presence of 12CE4, 15CE5, 18CE6.

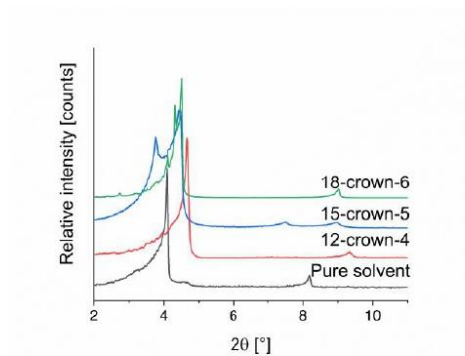


Figure S5. XRD patterns of crystalline swollen Na-Hec in pure DMF and in the presence of 12CE4, 15CE5, 18CE6.

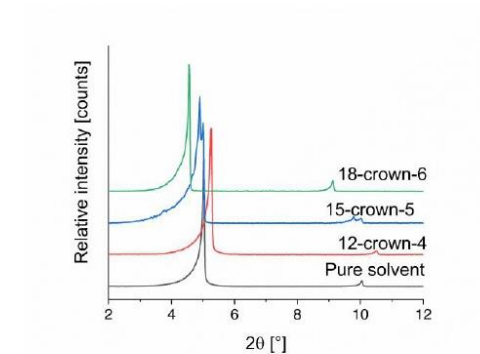


Figure S6. XRD patterns of crystalline swollen Na-Hec in pure FA and in the presence of 12CE4, 15CE5, 18CE6.

7 Osmotic delamination: Forceless alternative for the production of nanosheets now in highly polar and aprotic solvents

Osmotically swollen crown-ether modified Na-Hec gel in NMA and NMF featuring full delamination down to monolayers

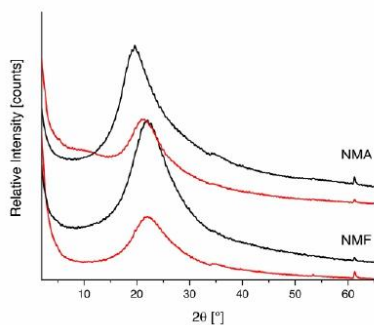


Figure S7. XRD patterns of crown-ether modified Na-Hec gel containing 15CE5 (red curve), 18CE6 (black curve) in NMA and NMF. The absence of a low angle peak indicates fully delaminated nanosheets while the clearly observable 060 band at 61.2° 2θ peak indicates nanosheets concentrations being sufficiently high to observe a signal. The intense broad peak originates from the solvent.

8 Delamination by repulsive osmotic swelling of synthetic Na-hectorite with variable charge in binary DMSO-water mixtures

8 Delamination by repulsive osmotic swelling of synthetic Na-hectorite with variable charge in binary DMSO-water mixtures

Volodymyr Dudko, Sabine Rosenfeldt, Renée Siegel, Jürgen Senker, Marian Matejdes and Josef Breu

This work was published in *Langmuir* 38, 10781 (2022). *Reprinted with permission from V. V. Dudko et al.: Langmuir 38, 10781 (2022). Copyright 2022 American Chemical Society.*

Delamination by Repulsive Osmotic Swelling of Synthetic Na-Hectorite with Variable Charge in Binary Dimethyl Sulfoxide–Water Mixtures

Volodymyr Dudko, Sabine Rosenfeldt, Renée Siegel, Jürgen Senker, Marian Matejdes,* and Josef Breu*

Cite This: *Langmuir* 2022, 38, 10781–10790

Read Online

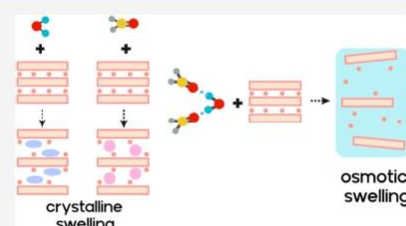
ACCESS |

Metrics & More

Article Recommendations

Supporting Information

ABSTRACT: Swelling of clays is hampered by increasing layer charge. With vermiculite-type layer charge densities, crystalline swelling is limited to the two-layer hydrate, while osmotic swelling requires ion exchange with bulky and hydrophilic organic molecules or with Li^+ cations to trigger repulsive osmotic swelling. Here, we report on surprising and counterintuitive osmotic swelling behavior of a vermiculite-type synthetic clay $[\text{Na}_{0.7}]^{\text{inter}}[\text{Mg}_{2.3}\text{Li}_{0.7}]^{\text{oct}}[\text{Si}_4]^{\text{tet}}\text{O}_{10}\text{F}_2$ in mixtures of water and dimethyl sulfoxide (DMSO). Although swelling in pure water is restricted to crystalline swelling, with the addition of DMSO, osmotic swelling sets in at some threshold composition. Finally, when the DMSO concentration is increased further to 75 vol %, swelling is restricted again to crystalline swelling as expected. Repulsive osmotic swelling thus is observed in a narrow composition range of the binary water–DMSO mixture, where a freezing point suppression is observed. This suppression is related to DMSO and water molecules exhibiting strong interactions leading to stable molecular clusters. Based on this phenomenological observation, we hypothesize that the unexpected swelling behavior might be related to the formation of different complexes of interlayer cations being formed at different compositions. Powder X-ray diffraction and ^{23}Na magic angle spinning-NMR evidence is presented that supports this hypothesis. We propose that the synergistic solvation of the interlayer sodium at favorable compositions exerts a steric pressure by the complexes formed in the interlayer. Concomitantly, the basal spacing is increased to a level, where entropic contributions of interlayer species lead to a spontaneous thermodynamically allowed one-dimensional dissolution of the clay stack.



INTRODUCTION

Repulsive osmotic swelling,¹ which resembles a one-dimensional dissolution of layered materials, is an appealing alternative to the conventional method of liquid-phase exfoliation² to produce 2D nanosheets. It is a thermodynamically allowed and thus spontaneous process that does not require any mechanical force. Unfortunately, it has only been observed for a handful of ionic layered compounds like lepidocrocite-type titanates,³ layered antimony phosphates,^{4,5} graphene oxide,⁶ some layered zeolites,⁷ and layered silicates.⁸ Being repulsive^{9,10} in nature assures utter and most gentle delamination. Contrary to exfoliation, delamination means complete separation of the nanosheets into the single layers (for a more extended definition of delamination vs exfoliation, see Gardolinski and Lagaly).¹¹ Consequently, repulsive osmotic swelling preserves the diameter of the non-delaminated pristine platy crystals in the nanosheets obtained by delamination and thus maximizes the aspect ratio (diameter/thickness ratio). This is crucial for mechanical¹² and barrier properties.¹³

Swelling of the highly charged silicates, in particular, beyond crystalline swelling is getting progressively challenging, if not impossible, due to the strong electrostatic interactions between

counter cations and anionic nanosheets. In the case of vermiculite-type 2:1 layered silicates, first, a complete cation exchange is required with a bulky and hydrophilic organic cation or with monovalent cations of high hydration enthalpy like Li^+ to trigger osmotic swelling.^{14–19} These observations highlight the complexity of the interactions accompanying repulsive osmotic swelling. Generally, swelling of clay minerals in suspensions goes through two distinct phases: crystalline²⁰ and osmotic.^{21–23} During crystalline swelling, basal planes and interlayer cations are solvated, and the process is controlled by layer charge,²⁴ solvent activity,^{25,26} and solvation enthalpy.^{27–29} Crystalline swelling corresponds to phase transitions, and the individual steps correspond to distinct *d*-spacings, corresponding to different but defined solvation shells of interlayer cations.^{30–32}

Received: April 16, 2022

Revised: July 10, 2022

Published: July 21, 2022



Downloaded via UNIV BAYREUTH on April 4, 2023 at 10:26:41 (UTC). See https://pubs.acs.org/sharingguidelines for options on how to legitimately share published articles.

8 Delamination by repulsive osmotic swelling of synthetic Na-hectorite with variable charge in binary DMSO-water mixtures

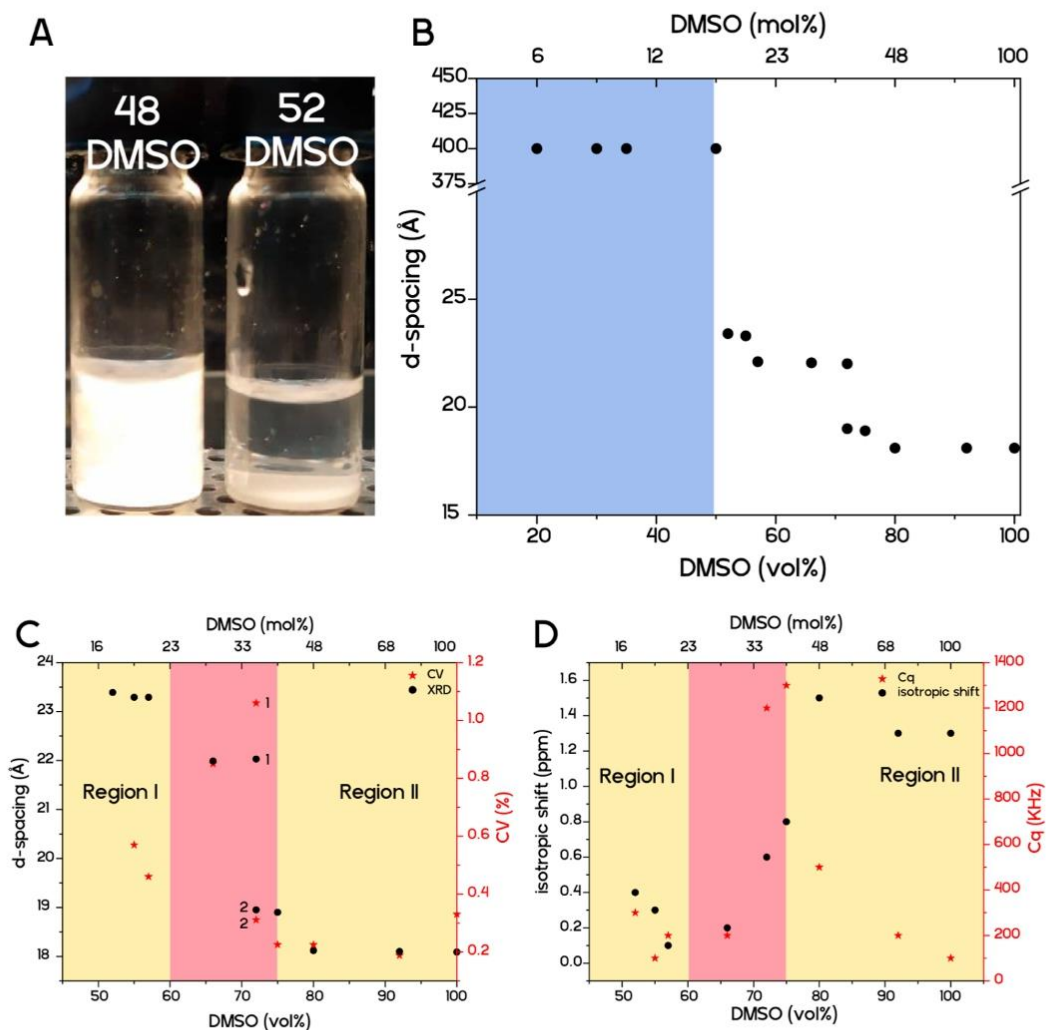


Figure 1. Swelling behavior of 0.5 Hec in water–DMSO mixtures. (A) Photo in cross-polarized light of the suspension of 0.5 Hec at 48 and 52 vol % of DMSO featuring osmotic (48 vol %) and crystalline (52 vol %) swelling. (B) Drastic change of *d*-spacing when going from the nematic liquid crystalline suspension obtained by osmotic swelling (left) to discretely crystalline swollen states. The blue area indicates water–DMSO compositions triggering osmotic swelling (the *d*-spacing corresponds to around 2.8 ± 0.1 vol %). (C) *d*-values and the CV in the crystalline swollen regime as a function of water–DMSO composition. The two yellow areas mark rational *d*-values observed for distinct solvates as indicated by CV values <0.75, while the red area refers to the transition zone between the two where both distinct swelling states coexist in a random interstratification as indicated by CV values >0.75 (for PXRD patterns, see Figure S1, and for tabulated data, see Table S1). (D) Diagram of ²³Na MAS-NMR features (isotopic shift and quadrupole coupling constant, C_q) as a function of water–DMSO composition. Region I is characterized by a small isotopic shift in combination with small C_q values. This difference indicates differing interlayer coordination spheres. The two regions are separated again by a transition zone (for tabulated data and NMR spectra, see Table S2 and Figure S2).

Natural 2:1 layered silicates (smectites and vermiculites) suffer from compositional inhomogeneity that is reflected by local variations of the intracrystalline reactivity. Together with random interstratifications involved, this masks swelling behavior and renders interpretation of observed basal spacing difficult. We therefore prefer to study swelling applying layered silicates synthesized from the melt and defined model

compound, which are characterized by phase purity and charge homogeneity and which are accessible with a wide range of layer charges spanning from smectites to vermiculite-type.^{3,3–3,5} Here, we apply 0.5 Hec ([Na_{0.5}]^{inter}[Mg_{2.5}Li_{0.5}]^{oct}[Si₄]^{tet}O₁₀F₂) and 0.7 Hec ([Na_{0.7}]^{inter}[Mg_{2.3}Li_{0.7}]^{oct}[Si₄]^{tet}O₁₀F₂). Due to superb charge homogeneity, these synthetic clay minerals show sharp

transitions between crystalline swelling steps and from crystalline to osmotic swelling. We previously studied a swelling of 0.5 Hec in binary³⁶ and ternary³⁷ water–organic solvent mixtures and in pure organic solvents.³⁸ The aspect ratio is of prime importance in various applications, in particular, in nanocomposite barrier liners,^{39,40} and as the diameter of the pristine clay minerals tends to increase with charge density,⁴¹ we here extend studying repulsive osmotic swelling to 0.7 Hec. Needless to say, the decrease in equivalent area (area per 1 charge) from 48 to 34 Å²/charge when going from 0.5 Hec to 0.7 Hec not only increases the Coulombic cohesion but also has a significant influence on the packaging of even modestly bulky cations and complexes^{42,43} in the interlayer space. For instance, formation of J- versus H-aggregates of dyes intercalated in the interlayer space can be controlled via variation of the layer charge density, which, in turn, greatly alters emission spectra, while neither the host material nor the nature of the guest molecules is changed.^{44,45}

Here, we show that by simply varying the composition of the dispersion medium, different interlayer complexes may form that, in turn, lead to a significant alteration of the swelling behavior. In particular, in a mixture of water and dimethyl sulfoxide (DMSO), repulsive osmotic swelling is triggered, while in both pure water and pure DMSO, swelling is restricted to crystalline swelling. Osmotic swelling is observed in a specific composition range, where water and DMSO are known to strongly interact as indicated by a freezing point suppression.^{46–48} Therefore, we attribute the onset of osmotic swelling to changes in the first and second coordination/solvation sphere as indicated by significant changes in the ²³Na magic angle spinning (MAS)-NMR spectra.

RESULTS AND DISCUSSION

Swelling Behavior of Low-Charged Hectorite (0.5 Hec)

To emphasize the unique swelling behavior of 0.7 Hec, we first look at the conventional swelling behavior of 0.5 Hec, which shows the expected transition from crystalline swelling to the osmotic swelling upon decreasing the DMSO content (Figure 1A,B). In the binary mixture, the transition was observed around 50 vol % (18 mol %) of DMSO, which resembles the transition found for montmorillonite (60 vol % or 28 mol %).³⁰ We notice that this seems to be a general trend for binary mixtures of water with organic solvents.³⁶ Upon increasing the water content, at a particular mixture, osmotic swelling sets in.

Crystalline swelling encompasses particular thermodynamically favorable interlayer compositions of water and a solvent, which differ from the composition of the surrounding dispersion medium.³⁶ This most likely implies distinct coordination spheres around the interlayer cations, which, in turn, might vary with the composition and the activities of water and the organic solvent going along with it. Although the various crystalline swollen states are at thermodynamic equilibrium, the coordination in the interlayer space is nevertheless expected to be highly dynamic, and we only can observe time-averaged structural information. As the compounds suffer from turbostratic disorder, structural information can only be derived from interlayer heights derived from *d*-spacing supplemented by local information extracted from ²³Na MAS-NMR features. For both analytical methods, sediment wet powders were applied with the excess solvent adsorbed to external surfaces, which we assume assures preservation of the state of solvation found in the suspension.

²³Na NMR was used to study glasses and silicates including montmorillonite.^{49–52} Being a nucleus with the spin 3/2, ²³Na is strongly sensitive to the local environment.^{53,54} In particular, the second-order quadrupolar interactions⁵⁵ are advantageous to studying the coordination sphere of solvated interlayer Na. Fitting of spectra, including the spinning sideband pattern, allows us to extract a quadrupolar coupling constant (*C_q*) and an isotropic chemical shift (δ_{iso}), which provide unique information about the local coordination environment of the quadrupolar nuclei. These features are correlated to distances and symmetry of the ²³Na environment and thus help spot differences in the solvation behavior as a function of solvent composition. Although it remains impossible to derive decisive structural models by following the evolution of the features, it is therefore still highly informative in sensing changes with solvent composition.

As suggested by X-ray diffraction (XRD) and MAS-NMR data, aside from the osmotically swollen phase (Figure 1A,B), two regions can be identified in the crystalline swollen regime (Figure 1C,D): region I from 50 to around 60 vol %, the transition region from 60 to 75 vol %, and region II from 75 to 100 vol %. Please note that the transition is not sharp but rather steady; thus, the colors on figures are used as a guide for the eye and indication of a high coefficient of variation.

In region I, the basal spacing is 23.2 Å, and it has a low coefficient of variation (CV)⁵⁶ (more information in the Supporting Information), indicating a well-defined and uniform *d*-spacing with no or little interstratification. The MAS-NMR spectra in this region show an isotropic shift of 0.2 ± 0.1 ppm in combination with a low *C_q* indicating a high coordination symmetry of interlayer sodium. In region II of crystalline swelling, the *d*-value is 18.8 Å, and it again shows a low CV indicating a well-defined solvation state. This second solvation state is now characterized by a larger isotropic shift of 1.4 ± 0.1 ppm, in combination with a small *C_q* around 0.3 MHz. The different NMR features clearly indicate a different first solvation shell/coordination of the interlayer cation as compared to region I.

The transition between the two crystalline swollen regions is characterized by a large CV value indicating a random interstratification of the two solvation states. As NMR is a local method, it is insensitive to the crystallographic disorder encountered in the random interstratification, and consequently, the NMR features observed represent a superposition of the features of the two individual bordering solvation states.

In terms of the interlayer structure, the indirect experimental evidence may be rationalized as follows: The isotropic shift correlates with the number and the distance of oxygen atoms in the coordination sphere of sodium.⁵⁷ As has been shown in previous NMR studies of NaCl in water or DMSO,⁵⁴ the isotropic shift differs insignificantly in the two solvents. In mixtures, we indeed observed only a slight drift of the isotropic shift with composition (Figure S3, Table S3). As we see very similar isotropic shifts, we attribute this to a similar number of oxygen atoms being coordinated to sodium at a similar distance in both region I and region II. The isotropic shift thus does not allow us to spot a change in the number of DMSO and/or water molecules in the first solvation shell of interlayer sodium. Nevertheless, the *C_q* value is significantly different in region I and region II, which can only be attributed to the ratio of oxygen atoms donated to sodium from water and DMSO. As the DMSO activity is higher in region II, the larger *C_q* value

8 Delamination by repulsive osmotic swelling of synthetic Na-hectorite with variable charge in binary DMSO-water mixtures

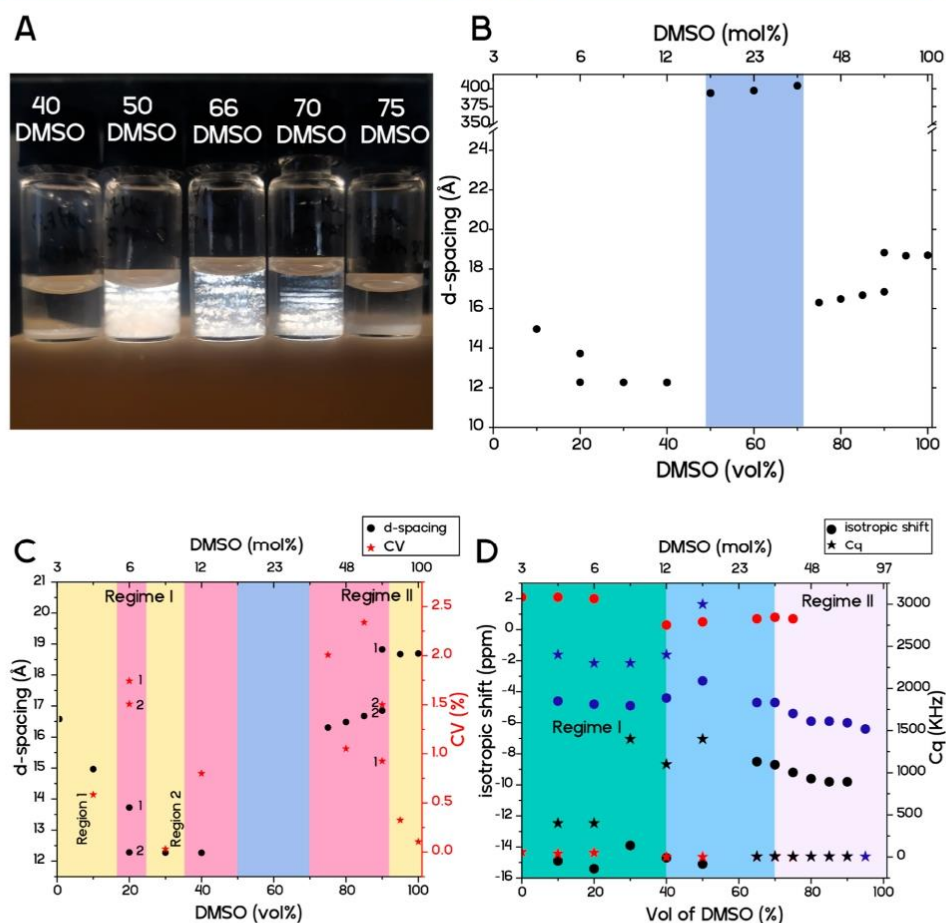


Figure 2. Swelling behavior of 0.7 Hec in water–DMSO mixtures. (A) Photo in cross-polarized light of the suspension of 0.7 Hec in the region of 40 vol % to 75 vol % of DMSO featuring the transition from crystalline (40 vol %) to osmotic (50–70 vol %) (the *d*-spacing corresponds to around 2.8 ± 0.1 vol %) and back to crystalline (75 vol %) swelling. (B) Drastic change of *d*-spacing when going from crystalline swelling regime I to the nematic liquid crystalline suspension and back to crystalline swelling regime II. The blue area indicates the water–DMSO composition range in which osmotic swelling is triggered. (C) *d*-values and the CV in crystalline swollen regime I and regime II as a function of water–DMSO composition. The areas mark rational *d*-values observed for distinct solvates as indicated by CV values <0.7, while the red area refers to the transition zone where both different swelling states coexist in a random interstratification as indicated by CV values >0.7 (for PXRD patterns, see Figure S6, and for tabulated data, see Table S5). (D) Diagram of ^{23}Na MAS-NMR features as a function of water–DMSO composition. Two crystalline swelling regimes I and II (green and purple) and the osmotically swelling regime (blue). Filled circles indicate the position of the isotropic shift, and the star of the respective color indicates the quadrupole coupling constant, C_q .

might go along with a higher number of oxygen atoms of DMSO in the coordination environment of interlayer sodium.

In any case, we can safely conclude that while both powder XRD (PXRD) and ^{23}Na MAS-NMR spectroscopy identify similar regions in the phase diagram, the latter additionally gives valuable qualitative information on the local environment of the interlayer sodium, in particular, via the quadrupolar coupling constant. This advantage will turn out to be even more beneficial when we turn to the swelling behavior of 0.7 Hec.

Swelling Behavior with Vermiculite-Type Charge Density (0.7 Hec). Contrary to 0.5 Hec, the swelling behavior

of 0.7 Hec in water–DMSO mixtures was found to be puzzling and quite counterintuitive (Figure 2). On both ends of the phase diagram, swelling is limited to the crystalline regime (Figure 2B,C). This is in line with previous reports for montmorillonite in DMSO,³⁰ Na-vermiculite,^{15,17,22} and Na-0.7 Hec.^{9,10} For the latter two, the restriction of swelling to the crystalline swollen regime was rationalized by the higher Coulomb attraction as compared to 0.5 Hec, which spontaneously delaminates by osmotic swelling when immersed into water. As seen for the 0.5 Hec, one of crystalline swelling-comprised regimes comprises two regions with distinct basal spacing and thus different solvated structures.

8 Delamination by repulsive osmotic swelling of synthetic Na-hectorite with variable charge in binary DMSO-water mixtures

However, quite unexpected in a certain range of mixed compositions, spontaneous delamination into birefringent (Figure 2A) nematic phases by osmotic swelling was observed (Figure 2B). As to the nature of the liquid crystalline phase obtained in the osmotic swelling regime, it appears to be nematic at first glance, as no discrete diffraction spots could be seen that would indicate smectic, accordion-type volumes in the suspensions. Small-angle X-ray scattering (SAXS) data suggest complete delamination with a separation of 42 ± 1 nm, which is in good agreement with expected separations based on the thickness of the nanosheets as ≈ 1 nm and a concentration of the suspension of 2.8 ± 1 vol % (Figure S8). In the following, we try to derive a tentative explanation by extracting indirect structural information on the two crystalline swelling regimes bordering the osmotically swollen regime by XRD and ^{23}Na MAS-NMR data.

As ^{23}Na MAS-NMR spectra of the 0.7 Hec for solvent mixtures generally look complex (Figure 3), first spectra were

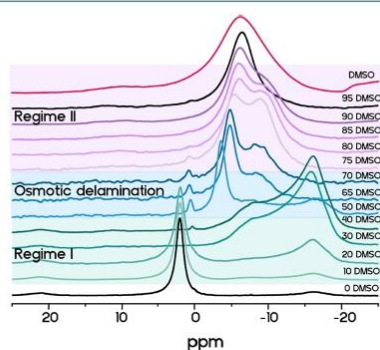


Figure 3. Overview of ^{23}Na MAS-NMR spectra of 0.7 Hec in varying water–DMSO mixtures showing three different types of spectra in the two crystalline swelling regimes I and II (green and purple) and the osmotically swelling regime (blue).

recorded for samples in pure water and for pure DMSO (Figures 3, S4 and Table S4), where the coordination sphere of sodium in the crystalline swollen phases is known for water³³ and is fixed to pure DMSO in the other limiting case.

As indicated by a basal spacing of 15.1 Å, 0.7 Hec swells to the two-layer hydrate (2WL) when immersed into water (Figure S5). Single crystal structure refinements had shown that in 2WL of 0.7 Hec, interlayer Na^+ is octahedrally coordinated by water molecules, while the voids between these $[\text{Na}(\text{H}_2\text{O})_6]^+$ complexes are filled with additional uncoordinated interlayer water.³³ As previously reported, when lowering the water activity to 43 RH %, the basal spacing collapses to 12.4 Å, which represents the 1WL, where interlayer Na^+ is coordinated by six oxygen molecules of the tetrahedral layer on one side and three water molecules on the other side.³³

The isotropic chemical shift (as obtained by fitting Figure S4) moves to the higher field upon increase in the number of water molecules in the solvation environment—5.1 ppm for 1WL to +2.1 ppm for 2WL (Figure S4 and Table S4). These results are in good agreement with the previously published result of Na-montmorillonite hydrates.^{58,59} Noticeably, the 2WL (Figure S4) exhibits a much smaller quadrupolar coupling constant (60 kHz) than the 1WL (Figure S4), indicating a more symmetrical solvation environment as

expected for octahedral $[\text{Na}(\text{H}_2\text{O})_6]^+$. The less symmetric coordination in 1WL leads to a large C_q of 2 MHz.

The solvated crystalline swollen state of 0.7 Hec in pure DMSO (Figure S6) showed a basal spacing of 18.8 Å, and the isotropic ^{23}Na shift is significantly larger (−6.4 ppm) (Figures 3 and S4) than that for the 2WL. Although the low C_q (5 kHz) suggests a similarly symmetric sodium environment, the difference in the shift might indicate a lower coordination number, for instance, tetrahedral coordination.⁵⁷ Without firm crystallographic data, this of course remains hypothetical.

Both the crystalline swelling and the osmotically swelling regime of 0.7 Hec identified by XRD (Figure 2B,C) can also be clearly distinguished in the ^{23}Na MAS-NMR spectra (Figures 2D and 3). According to the PXRD data, crystalline swelling regimes comprise two regions in regime I and one in regime II with a distinct solvation environment of the interlayer sodium, separated by a transition zone characterized by larger CV values (Figure 2C, red areas). The d -spacing (15.1 Å) observed in region 1 of regime I (Figures 2C and 4A) indicates a 2WL, and the NMR signature also resembles the one of the 2WL. With the increasing DMSO content above 20 vol %, this signal vanishes, and a new signal emerges (Figure 4A, green area). This new signal is characterized by a main signal with an isotropic shift of −15 ppm and a C_q of 1 MHz and a trace component with a shift of −5 ppm and a C_q of 2.4 MHz. The latter is similar to what is observed for the 1WL. Additionally, two d -spacings are observed in this solvent mixture: 12.3 and 13.7 Å, both having a high CV. This indicates that two phases coexist and that these phases both have random interstratifications of two different basal spacings. Most likely, the same two basal spacings are randomly stacked in the different phases, and the phases differ in the ratio of the two different d -spacings, most likely for kinetic reasons. Interestingly, the basal spacing in region 2 of regime I has collapsed to 12.3 Å. Although this basal spacing is very similar to the value observed for 1WL, the decently different NMR features would suggest that some DMSO might have been coordinated with interlayer sodium in this solvation state. At the DMSO-rich border of region 2 of regime I, an NMR feature appears at an isotropic shift of 0.3 ppm, which is similar to the signal attributed to Na^+ in NaCl solution (Figure S3 and Table S3). This rather narrow peak without any signs of quadrupolar interaction, which can be explained by averaging the interaction by fast motion, indicates a highly mobile, liquid like Na-species,⁵³ which will be encountered again in the osmotically swollen regime (Figure 4B).

In 70 to 90 vol % of DMSO-rich crystalline swelling regime II (Figure 2C), we observed two main NMRs (Figure 4C). In addition to these, at the border of this region to the osmotically swollen regime at 75 vol % DMSO, a trace of the highly mobile Na^+ species at 0.7 ppm was again visible. The two main NMRs in this regime have an isotropic shift of -10 ± 1 ppm and a low C_q of 6 kHz (Figure 4C purple region) and of -6 ± 1 ppm and a low C_q of 5 kHz (Figure 4C pink area) and the first decreases in intensity with the increasing content of DMSO until it is no longer visible in 95 vol % DMSO. The latter peak at -6 ± 1 ppm is the only peak visible in 95 vol % of regime II and goes along with a basal spacing of 18.7 Å resembling the value observed for 0.7 Hec swollen in pure DMSO. Therefore, we assign this peak to interlayer sodium, being coordinated solely by DMSO.

It is not clear why two solvated phases coexist in 70 to 90 vol % of regime II. Moreover, while the NMR data give clear

8 Delamination by repulsive osmotic swelling of synthetic Na-hectorite with variable charge in binary DMSO-water mixtures

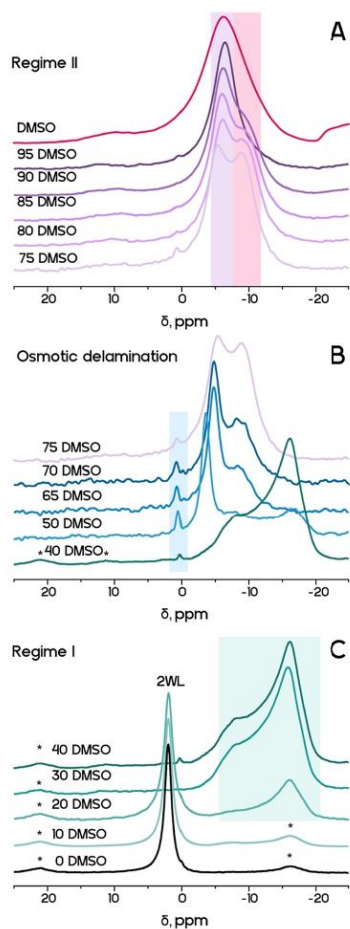


Figure 4. ^{23}Na MAS-NMR spectra of 0.7 Hec in varying water–DMSO mixtures. (A) Zoom of regime I where a significant increase in the signal in the -20 to -5 ppm range (green area) upon increase in the DMSO content (* indicates spinning sidebands) is seen. (B) Zoom of the osmotically swelling regime (from 40 to 75 vol % of DMSO) where the signal attributed to liquid-like, highly mobile Na^+ in the diffuse double layer (blue area) is most intense in the middle of the regime. The rest of the signals resemble the NMR signals observed in the bordering crystalline swelling regimes. (C) Zoom of regime II where the signal attributed to Na^+ with the mixed water–DMSO coordination sphere (pink area) is steadily increasing at the expense of the intensity of the signal attributed to a pure DMSO coordination environment of Na^+ (purple area) with the decreasing DMSO content. (For detailed fitting, see Figure S7.)

evidence for the -6 ± 1 ppm species to be present, the XRD data show only one basal spacing, significantly lower than 18.7 Å. This is because NMR looks at the local length scale, while XRD averages over the coherence length of the X-ray beam. This means that NMR remains sensitive to the very few interlayers that have the -6 ± 1 ppm signature. These few

layers, however, hardly show up in the diffraction experiment, which averages over some 10 interlayers, most of them being of the -10 ± 1 ppm signature. As indicated by a comparably high CV and a gradual increase in the virtual d -spacing from 16.3 to 16.8 Å, the two phases most probably coexist as random interstratification. The significantly different d -spacing together with the distinct NMR features suggests some DMSO in the coordination sphere of sodium to be replaced by water in the 10 ± 1 ppm solvation phase. In summary, both crystalline swollen phases bordering the osmotic swelling regime have a different coordination environment of the interlayer sodium, this might suggest that the first solvation shell is not decisive for osmotic swelling to be triggered. At the phase transition from crystalline swollen phases to osmotically swollen nematic liquid crystalline phases of nanosheets, the interaction of the solvated interlayer cation with excess dispersion medium in order to form higher solvation shells has to be exergonic. Thus, most likely, the transition to osmotic swelling is decided by solvent–solvent interactions. Therefore, we turn to the water–DMSO phase diagram at this point in order to rationalize the puzzling swelling behavior and the fact that osmotic swelling is only triggered in a selected range of solvent mixtures for 0.7 Hec.

We believe that the counterintuitive swelling behavior is related to the physical and structural properties of water–DMSO mixtures, where the two constituents have experimentally been shown to strongly interact and to cluster just in the same composition range, where we observe osmotic swelling.^{46–48} Depending on the composition of the mixture, different solvent clusters exist in solution and contribute differently to the population fraction (Figure 5). In the

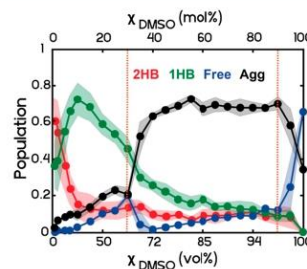


Figure 5. Schematic representation of the HB ensemble populations as a function of the DMSO mole fraction. The shaded regions represent the standard deviations from the fits as described in the Supporting Information. The approximate boundaries of the three interaction regions are shown above the plot. Figures adapted with permission from ref 47. Copyright 2017 Wiley.

composition range of interest (30 to 72 vol % or 10 mol % to 40 mol % DMSO), three main species are present: non-self-interacting DMSO species (free), H_2O :DMSO cluster single-hydrogen-bonded (1HB), and aggregated self-interacting DMSO molecules (Agg), whereas 1HB is the dominant species. In the range of 30 to 63 vol % (10 to 30 mol %), almost 70% of the DMSO molecules are bound in the 1HB state. Below and above this range, the concentration of the 1HB state quickly vanishes. The composition range with high

1HB concentrations correlates with a strong free point suppression. The coincidence of compositions with high concentrations of the 1HB cluster and osmotic swelling to be observed might suggest that it is this cluster that triggers and/or drives the phase transition to the osmotically swollen nematic liquid crystalline phase. Based on this hypothesis, we propose the following model to explain the peculiar swelling behavior of 0.7 Hec.

In both crystalline swelling regions bordering the osmotically swelling regime, we have mixed solvent coordination of the interlayer sodium, which in respect to composition resembles the 1HB cluster found at high concentrations in solvent mixtures of that composition range (Figure 6A,C). Because of

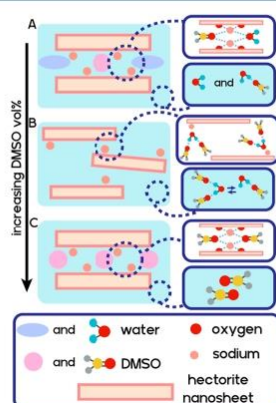


Figure 6. Schematic representation of the swelling behavior of 0.7 Hec in water–DMSO mixtures. (A) Regime I, (B) osmotically swelling region, and (C) Regime II.

the compositional and structural similarity, the solvation energy of the interlayer complexes with 1HB clusters is high, fostering an exergonic formation of higher solvation shells against the electrostatic attraction of the one-dimensional salt formed by cationic interlayer species and negative clay nanosheets (Figure 6B). Similar to what has been reported for 0.5 Hec immersed into pure water, the solvation energy therefore drives the system beyond a threshold separation where the one-dimensional dissolution becomes thermodynamically favorable, and the clay tactoids delaminate by osmotic swelling. At first glance, the different swelling behavior of the two materials with different charge densities might appear puzzling as the two differ only in the content of same interlayer cations. As pointed out in the Introduction, we have, however, previously shown for organo-clays that the threshold separation required to kick off thermodynamically driven osmotic swelling may be achieved by two different contributions: solvation of interlayer cations and a steric contribution once interlayer cations have equivalent areas larger than the underlying charge density of the clay. Therefore, the charge density is actually expected to play a major role. The first contribution clearly is the highest with aqueous Na complexation. The latter is more likely with coordination with bulkier DMSO molecules. Moreover, the higher coordination shells will contribute significantly to the total energy at higher separations beyond the crystalline regime. As the DMSO/water system is far from being ideal,

this contribution is substantial and depends on composition in a nonlinear way. Although this rather qualitative scenario is fully consistent with all experimental data, we are fully aware that a quantitative detailed balance is beyond reach because of the lack of hard structural data due to the disorder inherent in layered materials. To nail down the mechanism, structural models are needed. We hope to address this in future work applying total scattering or grand canonical MD simulations.

CONCLUSIONS

We studied the swelling behavior in aqueous DMSO mixtures of synthetic hectorite with layer charges in the group of smectites and vermiculites (0.5 and 0.7) using PXRD and ^{23}Na MAS-NMR. We are reporting for the first time repulsive osmotic delamination of the sodium form of the vermiculite-type synthetic hectorite, which was previously considered impossible due to the strong electrostatic interactions. Delamination via repulsive osmotic swelling occurs only within a narrow range of 50 to 70 vol % DMSO in the binary water–DMSO mixture. This composition range is also known to show unusual non-ideal behavior like freeze point depression due to strong intermolecular interactions. We therefore propose a mechanism of synergistic solvation of the first solvation shell of interlayer cations, which resembles the dominant 1HB cluster present in solvent mixtures of the particular composition range. Due to structural similarities, the solvation energy of the solvation shell is exergonic, leading to the thermodynamically favored formation of the second solvation shell in the interlayer space, which, in turn, overrules the strong electrostatic attraction between anionic nanosheets and interlayer cations. This is fostered by strong intermolecular interaction between water and DMSO molecules, which, however, becomes weaker again with the increasing DMSO content, eventually leading to the substitution of the water molecules in the first solvation shell and a concomitant collapse of osmotic swelling to ordinary crystalline swelling. This paper is of interest not only from the point of gaining a fundamental understanding of spontaneous, repulsive osmotic swelling but also from the point of opening new venues that take advantage of high-aspect ratio nanosheets in nanocomposites, super-ion conductors, and hybrid organic–inorganic functional structures.

MATERIALS AND METHODS

Synthesis of Sodium Hectorite. Sodium hectorite ($[\text{Na}_{0.5}]^{\text{int}}[\text{Mg}_{2.5}\text{Li}_{0.5}]^{\text{oct}}[\text{Si}_4]^{\text{tet}}\text{O}_{10}\text{F}_2$ and $[\text{Na}_{0.7}]^{\text{int}}[\text{Mg}_{2.3}\text{Li}_{0.5}]^{\text{oct}}[\text{Si}_4]^{\text{tet}}\text{O}_{10}\text{F}_2$) was obtained by melt synthesis followed by long-term annealing according to a published procedure.³⁴ The material featured a density of 2.73 g/cm³.

Swelling Experiments. Both Hecs were dried at 110 °C under vacuum for 24 h. DMSO was carefully dried by standard procedures suggested by W.L.F. Armarego⁶⁰ before the addition of Hec. DMSO (anhydrous, $\geq 99.9\%$, Sigma-Aldrich) was purified with molecular sieves (VWR of sieves, 4 Å, dried at 350 °C for 3 h under a stream of argon), followed by distillation under vacuum. Typically, 150 mg of Hec was added to 2 mL of the solvent blend which corresponds to around 7–7.5 wt % (2.7–2.9 vol %) of clay in the suspension.

X-ray Diffraction. Measurement of XRD patterns of dispersions was performed in the transmission mode on a STOE STADI P powder diffractometer (Cu $K\alpha 1$ radiation, GE monochromator, linear position sensitive detector). Before the measurement, the clay suspensions were filled in 1 mm glass capillaries (Hilgenberg, code 4007610) and sealed. The same samples as for the SAXS measurements were used to measure the Hec gel XRD pattern.

Small-Angle X-ray Scattering. SAXS data were collected with a “Double Ganesha AIR” (SAXSLAB, Denmark). In this laboratory-

based system, a micro-focused X-ray beam is provided by a rotating copper anode (MicoMax 007HF, Rigaku Corporation, Japan). A position-sensitive detector (PILATUS 300 K, Dectris) was used in different positions to cover the range of the scattering vector $q = 0.004\text{--}0.6 \text{ \AA}^{-1}$. Before the measurement, the clay suspensions were filled in 1 mm glass capillaries (Hilgenberg, code 4007610). The circularly averaged data were normalized to the incident beam, sample thickness, and measurement time.

Solid-State NMR. All ^{23}Na solid-state NMR experiments were performed on a Bruker Avance-III HD operating in a B_0 field of 14.1 T using a 3.2 mm HFXQ quadrupole-resonance probe. ^{23}Na (158.7 MHz) MAS spectra were acquired with a spinning speed of 3.0–15.0 kHz after a 10° flip angle pulse of 1.0 μs and recycle delays of 1.0–60 s. The reference was set using a solution of NaCl. Fitting was performed using Bruker TopSpin ver.4.1.1 with the Fit Solids NMR model (sola). The model used is QUAD all and CSA options of Haebleren. Goodness of the fit was judged on the parameter of best overlap (%).

■ ASSOCIATED CONTENT

SI Supporting Information

The Supporting Information is available free of charge at <https://pubs.acs.org/doi/10.1021/acs.langmuir.2c00965>.

XRD of the 0.5 Hec and 0.7 Hec powder solvated with different water–DMSO mixtures; table of data; ^{23}Na MAS-NMR spectrum of the 0.5 Hec powder in different water–DMSO mixtures; ^{23}Na NMR spectrum of NaCl in different water–DMSO mixtures; ^{23}Na MAS-NMR of the OWL, 1WL, 2WL, and DMSO spectrum of 0.7 Hec; PXRD of the (0.7 Hec) synthetic hectorite with OWL, 1WL, and 2WL; and ^{23}Na MAS-NMR spectrum of the 0.7 Hec powder in different DMSO–water mixtures and SAXS of the osmotically swelled 0.7 Hec nanosheet (PDF)

■ AUTHOR INFORMATION

Corresponding Authors

Marian Matejdes – Department of Inorganic Materials, Faculty of Chemical and Food Technology, Slovak University of Technology, Bratislava 812 37, Slovakia; Institute of Inorganic Chemistry, Slovak Academy of Sciences, Bratislava 845 36, Slovakia; Email: marian.matejdes@savba.sk

Josef Breu – Department of Chemistry and Bavarian Polymer Institute, University of Bayreuth, Bayreuth 95440, Germany; orcid.org/0000-0002-2547-3950; Email: josef.breu@uni-bayreuth.de

Authors

Volodymyr Dudko – Department of Chemistry and Bavarian Polymer Institute, University of Bayreuth, Bayreuth 95440, Germany

Sabine Rosenfeldt – Department of Chemistry and Bavarian Polymer Institute, University of Bayreuth, Bayreuth 95440, Germany

Renée Siegel – Department of Chemistry and Bavarian Polymer Institute, University of Bayreuth, Bayreuth 95440, Germany

Jürgen Senker – Department of Chemistry and Bavarian Polymer Institute, University of Bayreuth, Bayreuth 95440, Germany; orcid.org/0000-0002-7278-7952

Complete contact information is available at: <https://pubs.acs.org/doi/10.1021/acs.langmuir.2c00965>

Author Contributions

The manuscript was written through contributions of V.D., J.B., and M.M. R.S. and J.S. assisted with NMR measurements. S.R. assisted with the XRD and SAXS measurements. All authors have given approval to the final version of the manuscript.

Notes

The authors declare no competing financial interest.

■ ACKNOWLEDGMENTS

The authors thank F. Puchtl for producing the synthetic hectorite, Michael Thelen for AFM measurements, and Beate Bojer for recording NMR data. We also thank O. Khoruzhenko for the graphic design. This work was supported by the Deutsche Forschungsgemeinschaft [SFB 1357 (B2 and C2)]. V.D. thanks the Elite Network of Bavaria for support.

■ REFERENCES

- (1) Michot, L. J.; Bihannic, I.; Maddi, S.; Funari, S. S.; Baravian, C.; Levitz, P.; Davidson, P. Liquid-crystalline aqueous clay suspensions. *Proc. Natl. Acad. Sci. U.S.A.* **2006**, *103*, 16101–16104.
- (2) Coleman, J. N.; Lotya, M.; O'Neill, A.; Bergin, S. D.; King, P. J.; Khan, U.; Young, K.; Gaucher, A.; De, S.; Smith, R. J.; Shvets, I. V.; Arora, S. K.; Stanton, G.; Kim, H.-Y.; Lee, K.; Kim, G. T.; Duesberg, G. S.; Hallam, T.; Boland, J. J.; Wang, J. J.; Donegan, J. F.; Grunlan, J. C.; Moriarty, G.; Shmeliov, A.; Nicholls, R. J.; Perkins, J. M.; Grievson, E. M.; Theuwissen, K.; McComb, D. W.; Nellist, P. D.; Nicolosi, V. Two-Dimensional Nanosheets Produced by Liquid Exfoliation of Layered Materials. *Science* **2011**, *331*, 568–571.
- (3) Wang, L.; Sasaki, T. Titanium Oxide Nanosheets: Graphene Analogues with Versatile Functionalities. *Chem. Rev.* **2014**, *114*, 9455–9486.
- (4) Davidson, P.; Penisson, C.; Constantin, D.; Gabriel, J.-C. P. Isotropic, nematic, and lamellar phases in colloidal suspensions of nanosheets. *Proc. Natl. Acad. Sci. U.S.A.* **2018**, *115*, 6662–6667.
- (5) Gabriel, J.-C. P.; Camerel, F.; Lemaire, B. J.; Desvieux, H.; Davidson, P.; Batail, P. Swollen liquid-crystalline lamellar phase based on extended solid-like sheets. *Nature* **2001**, *413*, 504–508.
- (6) Liu, R.; Gong, T.; Zhang, K.; Lee, C. Graphene oxide papers with high water adsorption capacity for air dehumidification. *Sci. Rep.* **2017**, *7*, 9761.
- (7) Roth, W. J.; Sasaki, T.; Wolski, K.; Song, Y.; Tang, D.-M.; Ebina, Y.; Ma, R.; Grzybek, J.; Kalahurska, K.; Gil, B.; Mazur, M.; Zapotoczny, S.; Cejka, J. Liquid dispersions of zeolite monolayers with high catalytic activity prepared by soft-chemical exfoliation. *Sci. Adv.* **2020**, *6*, No. eaay8163.
- (8) Lorf, A. Storylines in intercalation chemistry. *Dalton Trans.* **2014**, *43*, 10276–10291.
- (9) Daab, M.; Eichstaedt, N. J.; Edenharter, A.; Rosenfeldt, S.; Breu, J. Layer charge robust delamination of organo-clays. *RSC Adv.* **2018**, *8*, 28797–28803.
- (10) Daab, M.; Eichstaedt, N. J.; Habel, C.; Rosenfeldt, S.; Kalo, H.; Schießling, H.; Förster, S.; Breu, J. Onset of Osmotic Swelling in Highly Charged Clay Minerals. *Langmuir* **2018**, *34*, 8215–8222.
- (11) Gardolinski, J. E. F. C.; Lagaly, G. Grafted organic derivatives of kaolinite: II. Intercalation of primary n-alkylamines and delamination. *Clay Miner.* **2005**, *40*, 547–556.
- (12) Das, P.; Malho, J.-M.; Rahimi, K.; Schacher, F. H.; Wang, B.; Demco, D. E.; Walther, A. Nacre-mimetics with synthetic nanoclays up to ultrahigh aspect ratios. *Nat. Commun.* **2015**, *6*, 5967.
- (13) Möller, M. W.; Lunkenbein, T.; Kalo, H.; Schieder, M.; Kunz, D. A.; Breu, J. Barrier Properties of Synthetic Clay with a Kilo-Aspect Ratio. *Adv. Mater.* **2010**, *22*, 5245–5249.
- (14) Braganza, L. F.; Crawford, R. J.; Smalley, M. V.; Thomas, R. K. Swelling of n-Butylammonium Vermiculite in Water. *Clays Clay Miner.* **1990**, *38*, 90–96.

- (15) Garrett, W. G.; Walker, G. F. Swelling of Some Vermiculite-Organic Complexes in Water. *Clays Clay Miner.* **1960**, *9*, 557–567.
- (16) Rausell-Colom, J. A.; Saez-Auñón, J.; Pons, C. H. Vermiculite gelation: structural and textural evolution. *Clay Miner.* **1989**, *24*, 459–478.
- (17) Rausell-Colom, J. A.; Salvador, P. S. Complexes vermiculite-aminoacidos. *Clay Miner.* **1971**, *9*, 139–149.
- (18) Smalley, M. V. Electrical Theory of Clay Swelling. *Langmuir* **1994**, *10*, 2884–2891.
- (19) Smalley, M. V.; Thomas, R. K.; Braganza, L. F.; Matsuo, T. Effect of Hydrostatic Pressure on the Swelling of n-Butylammonium Vermiculite. *Clays Clay Miner.* **1989**, *37*, 474–478.
- (20) Norrish, K. Crystalline Swelling of Montmorillonite: Manner of Swelling of Montmorillonite. *Nature* **1954**, *173*, 256–257.
- (21) Paineau, E.; Bihannic, I.; Baravian, C.; Philippe, A.-M.; Davidson, P.; Levitz, P.; Funari, S. S.; Rochas, C.; Michot, L. J. Aqueous Suspensions of Natural Swelling Clay Minerals. I. Structure and Electrostatic Interactions. *Langmuir* **2011**, *27*, 5562–5573.
- (22) Madsen, F. T.; Müller-Vonmoos, M. The swelling behaviour of clays. *Appl. Clay Sci.* **1989**, *4*, 143–156.
- (23) Rosenfeldt, S.; Stöter, M.; Schlenk, M.; Martin, T.; Albuquerque, R. Q.; Förster, S.; Breu, J. In-Depth Insights into the Key Steps of Delamination of Charged 2D Nanomaterials. *Langmuir* **2016**, *32*, 10582–10588.
- (24) Daab, M.; Rosenfeldt, S.; Kalo, H.; Stöter, M.; Bojer, B.; Siegel, R.; Förster, S.; Senker, J.; Breu, J. Two-Step Delamination of Highly Charged, Vermiculite-like Layered Silicates via Ordered Heterostructures. *Langmuir* **2017**, *33*, 4816–4822.
- (25) Stöter, M.; Rosenfeldt, S.; Breu, J. Tunable Exfoliation of Synthetic Clays. *Annu. Rev. Mater. Res.* **2015**, *45*, 129–151.
- (26) Mooney, R. W.; Keenan, A. G.; Wood, L. A. Adsorption of Water Vapor by Montmorillonite. I. Heat of Desorption and Application of BET Theory. *J. Am. Chem. Soc.* **1952**, *74*, 1367–1371.
- (27) Möller, M. W.; Handge, U. A.; Kunz, D. A.; Lunkenbein, T.; Altstädt, V.; Breu, J. Tailoring Shear-Stiff, Mica-like Nanoplatelets. *ACS Nano* **2010**, *4*, 717–724.
- (28) Bissada, K. K.; Johns, W. D.; Cheng, F. S. Cation-dipole interactions in clay organic complexes. *Clay Miner.* **1967**, *7*, 155–166.
- (29) Mooney, R. W.; Keenan, A. G.; Wood, L. A. Adsorption of Water Vapor by Montmorillonite. II. Effect of Exchangeable Ions and Lattice Swelling as Measured by X-Ray Diffraction. *J. Am. Chem. Soc.* **1952**, *74*, 1371–1374.
- (30) Brindley, G. W. Intracrystalline Swelling of Montmorillonites in Water-Dimethylsulfoxide Systems. *Clays Clay Miner.* **1980**, *28*, 369–372.
- (31) Olejnik, S.; Posner, A. M.; Quirk, J. P. Swelling of Montmorillonite in Polar Organic Liquids. *Clays Clay Miner.* **1974**, *22*, 361–365.
- (32) Norrish, K. The swelling of montmorillonite. *Discuss. Faraday Soc.* **1954**, *18*, 120–134.
- (33) Kalo, H.; Milius, W.; Breu, J. Single crystal structure refinement of one- and two-layer hydrates of sodium fluorohectorite. *RSC Adv.* **2012**, *2*, 8452–8459.
- (34) Stöter, M.; Kunz, D. A.; Schmidt, M.; Hirsemann, D.; Kalo, H.; Putz, B.; Senker, J.; Breu, J. Nanoplatelets of sodium hectorite showing aspect ratios of $\approx 20,000$ and superior purity. *Langmuir* **2013**, *29*, 1280–1285.
- (35) Stöter, M.; Biersack, B.; Reimer, N.; Herling, M.; Stock, N.; Schobert, R.; Breu, J. Ordered Heterostructures of Two Strictly Alternating Types of Nanoreactors. *Chem. Mater.* **2014**, *26*, 5412–5419.
- (36) Kunz, R.; Amschler, S.; Edenharter, A.; Mayr, L.; Herlitz, S.; Rosenfeldt, S.; Breu, J. GIANT MULTISTEP CRYSTALLINE VS. OSMOTIC SWELLING OF SYNTHETIC HECTORITE IN AQUEOUS ACETONITRILE. *Clays Clay Miner.* **2019**, *67*, 481–487.
- (37) Mayr, L.; Amschler, S.; Edenharter, A.; Dudko, V.; Kunz, R.; Rosenfeldt, S.; Breu, J. Osmotic Swelling of Sodium Hectorite in Ternary Solvent Mixtures: Nematic Liquid Crystals in Hydrophobic Media. *Langmuir* **2020**, *36*, 3814–3820.
- (38) Dudko, V.; Ottermann, K.; Rosenfeldt, S.; Papastavrou, G.; Breu, J. Osmotic Delamination: A Forceless Alternative for the Production of Nanosheets Now in Highly Polar and Aprotic Solvents. *Langmuir* **2021**, *37*, 461–468.
- (39) Kunz, D. A.; Schmid, J.; Feicht, P.; Erath, J.; Fery, A.; Breu, J. Clay-Based Nanocomposite Coating for Flexible Optoelectronics Applying Commercial Polymers. *ACS Nano* **2013**, *7*, 4275–4280.
- (40) Möller, M. W.; Kunz, D. A.; Lunkenbein, T.; Sommer, S.; Nennemann, A.; Breu, J. UV-Cured, Flexible, and Transparent Nanocomposite Coating with Remarkable Oxygen Barrier. *Adv. Mater.* **2012**, *24*, 2142–2147.
- (41) Kalo, H.; Möller, M. W.; Kunz, D. A.; Breu, J. How to maximize the aspect ratio of clay nanoplatelets. *Nanoscale* **2012**, *4*, 5633–5639.
- (42) Stöter, M.; Biersack, B.; Rosenfeldt, S.; Leitl, M. J.; Kalo, H.; Schobert, R.; Yersin, H.; Ozin, G. A.; Förster, S.; Breu, J. Encapsulation of Functional Organic Compounds in Nanoglass for Optically Anisotropic Coatings. *Angew. Chem., Int. Ed.* **2015**, *54*, 4963–4967.
- (43) Faustini, M.; Nicole, L.; Ruiz-Hitzky, E.; Sanchez, C. History of Organic-Inorganic Hybrid Materials: Prehistory, Art, Science, and Advanced Applications. *Adv. Funct. Mater.* **2018**, *28*, 1704158.
- (44) Matejdes, M.; Himeno, D.; Suzuki, Y.; Kawamata, J. The effect of the negative charge density on switchable properties of pseudoisocyanine dye. *Appl. Clay Sci.* **2017**, *144*, 54–59.
- (45) Matejdes, M.; Himeno, D.; Suzuki, Y.; Kawamata, J. Controlled formation of pseudoisocyanine J-aggregates in the interlayer space of synthetic saponite. *Appl. Clay Sci.* **2017**, *140*, 119–123.
- (46) Kirchner, B.; Reiher, M. The Secret of Dimethyl Sulfoxide–Water Mixtures. A Quantum Chemical Study of 1DMSO–nWater Clusters. *J. Am. Chem. Soc.* **2002**, *124*, 6206–6215.
- (47) Oh, K.-I.; Rajesh, K.; Stanton, J. F.; Baiz, C. R. Quantifying Hydrogen-Bond Populations in Dimethyl Sulfoxide/Water Mixtures. *Angew. Chem., Int. Ed.* **2017**, *56*, 11375–11379.
- (48) Wong, D. B.; Sokolowsky, K. P.; El-Barghouthi, M. I.; Fenn, E. E.; Giammanco, C. H.; Sturlaugson, A. L.; Fayer, M. D. Water Dynamics in Water/DMSO Binary Mixtures. *J. Phys. Chem. B* **2012**, *116*, 5479–5490.
- (49) Ai, X.; Chen, L.; Dong, J.; Ye, C.; Deng, F. Variation of sodium coordination during the hydration processes of layered sodium disilicates as studied by ^{23}Na MQMAS and $1\text{H}\leftrightarrow^{23}\text{Na}$ CP/MAS NMR spectroscopy. Electronic supplementary information (ESI) available: XRD patterns of SKS-5 and SKS-6 samples after different hydration times, and $1\text{H}-1\text{H}$ NOESY spectra of SKS-5 and SKS-6 hydrated for six months. See <http://www.rsc.org/suppdata/jm/b2/b209578e/>. *J. Mater. Chem.* **2003**, *13*, 614–621.
- (50) Ai, X.; Deng, F.; Dong, J.; Chen, L.; Ye, C. Stability of Layered Sodium Disilicate during Hydration Process As Studied by Multi-nuclear Solid State NMR Spectroscopy. *J. Phys. Chem. B* **2002**, *106*, 9237–9244.
- (51) Xue, X.; Stebbins, J. F. ^{23}Na NMR chemical shifts and local Na coordination environments in silicate crystals, melts and glasses. *Phys. Chem. Miner.* **1993**, *20*, 297–307.
- (52) Stebbins, J. F. Cation sites in mixed-alkali oxide glasses: correlations of NMR chemical shift data with site size and bond distance. *Solid State Ionics* **1998**, *112*, 137–141.
- (53) Bloor, E. G.; Kidd, R. G. Solvation of sodium ions studied by ^{23}Na nuclear magnetic resonance. *Can. J. Chem.* **1968**, *46*, 3425–3430.
- (54) Ryoko, T.; Misako, A.; Hazime, S. A High-Resolution Solid-State ^{23}Na NMR Study of Sodium Complexes with Solvents, Small Ligand Molecules, and Ionophores. ^{23}Na Chemical Shifts as Means for Identification and Characterization of Ion–Ion, Ion–Solvent, and Ion–Ligand Interactions. *Bull. Chem. Soc. Jpn.* **1986**, *59*, 1957–1966.
- (55) Freude, D. Quadrupolar Nuclei in Solid-State Nuclear Magnetic Resonance. *Encyclopedia of Analytical Chemistry*; John Wiley & Sons, Ltd: Chichester, England, U.K., 2006; p 240.
- (56) Bailey, S. W. Nomenclature for regular interstratifications. *Clay Miner.* **1982**, *17*, 243–248.

8 Delamination by repulsive osmotic swelling of synthetic Na-hectorite with variable charge in binary DMSO-water mixtures

(57) Koller, H.; Engelhardt, G.; Kentgens, A. P. M.; Sauer, J. ²³Na NMR Spectroscopy of Solids: Interpretation of Quadrupole Interaction Parameters and Chemical Shifts. *J. Phys. Chem.* **1994**, *98*, 1544–1551.

(58) Hougardy, J.; Stone, W. E. E.; Fripiat, J. J. NMR study of adsorbed water. I. Molecular orientation and protonic motions in the two-layer hydrate of a Na vermiculite. *J. Chem. Phys.* **1976**, *64*, 3840–3851.

(59) Laperche, V.; Lambert, J. F.; Prost, R.; Fripiat, J. J. High-resolution solid-state NMR of exchangeable cations in the interlayer surface of a swelling mica: sodium-23, cadmium-111, and cesium-133 vermiculites. *J. Phys. Chem.* **1990**, *94*, 8821–8831.

(60) Armarego, W. L. F. *Purification of Laboratory Chemicals*; Butterworth-Heinemann, 2017.

Recommended by ACS

Do Aqueous Suspensions of Smectite Clays Form a Smectic Liquid-Crystalline Phase?

Karin El Rifaii, Patrick Davidson, *et al.*

NOVEMBER 17, 2022
LANGMUIR

READ 

Formation and Dynamic Behavior of Macroscopic Aluminum-Based Silica Gardens

Julian Rieder, Matthias Kellermeier, *et al.*

AUGUST 17, 2022
LANGMUIR

READ 

Evolution of Chemical Bonding and Crystalline Swelling–Shrinkage of Montmorillonite upon Temperature Changes Probed by *in Situ* Fourier Transform Infrared S...

Cunjun Li, Chunhui Zhou, *et al.*

NOVEMBER 02, 2022
LANGMUIR

READ 

Effects of the Layer Charge Location and Interlayer Cation on Hectorite Swelling Properties: Comparison between Molecular Dynamics Simulations and Experiments

Wei Zhang, Lijiao Luo, *et al.*

JUNE 01, 2022
THE JOURNAL OF PHYSICAL CHEMISTRY C

READ 

Get More Suggestions >

8 Delamination by repulsive osmotic swelling of synthetic Na-hectorite with variable charge in binary DMSO-water mixtures

Supplementary materials

Delamination by repulsive osmotic swelling of synthetic Na-hectorite with variable charge in binary DMSO-water mixtures

*Volodymyr Dudko*¹, *Sabine Rosenfeldt*¹, *Renée Siegel*¹, *Jürgen Senker*¹, *Marian Matejdes*^{2,3*}
and *Josef Breu*^{1*}

¹ Department of Chemistry and Bavarian Polymer Institute, University of Bayreuth, Universitätsstr. 30, 95440 Bayreuth, Germany.

² Department of Inorganic Materials, Faculty of Chemical and Food Technology, Slovak University of Technology, Radlinského 9, 812 37 Bratislava, Slovakia

³ Institute of Inorganic Chemistry, Slovak Academy of Sciences, Dúbravská cesta 9, 845 36 Bratislava, Slovakia

8 Delamination by repulsive osmotic swelling of synthetic Na-hectorite with variable charge in binary DMSO-water mixtures

PXRD of the 0.5 Hec powder solvated with different water-DMSO mixtures

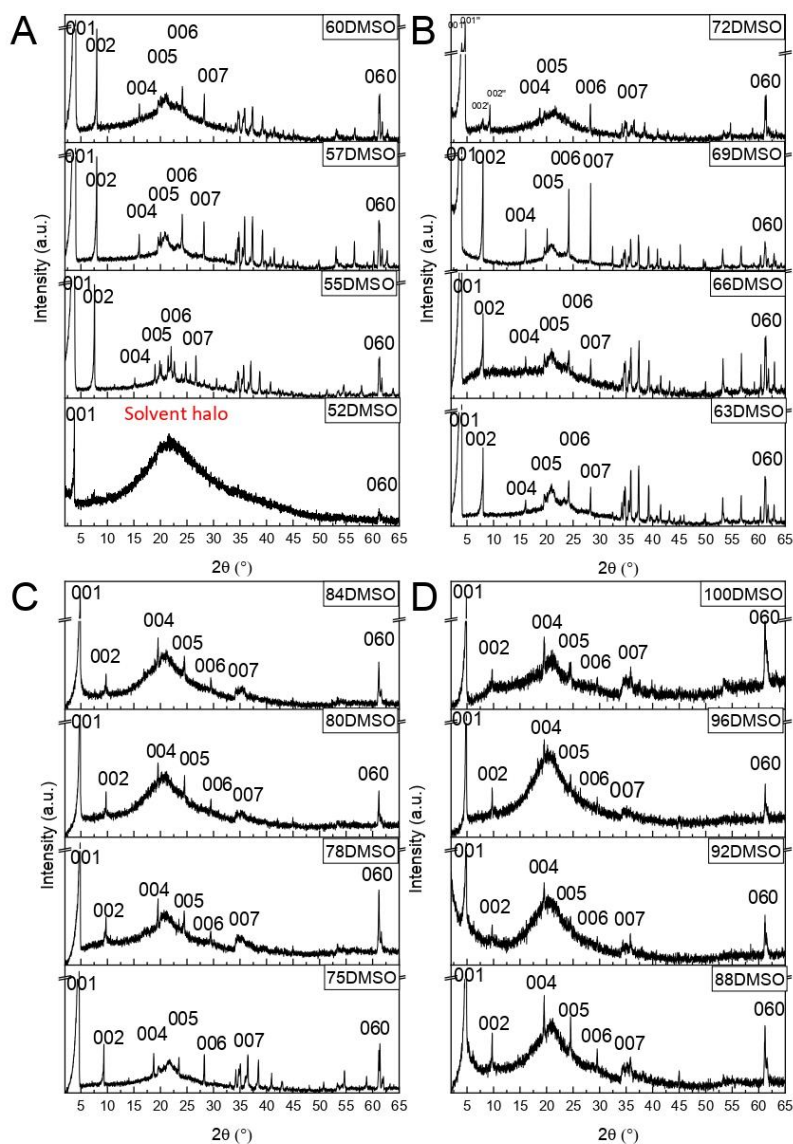


Figure S1: PXRD patterns of the crystalline swelled dispersions of 0.5 Hec in different water-DMSO mixture compositions. The broad peaks corresponds to the solvent scattering. A) PXRD of Composition from 52 to 60 vol% DMSO. B) PXRD of Composition from 63 to 72 vol% DMSO. C) PXRD of Composition from 75 to 84 vol% DMSO. D) PXRD of Composition from 88 to 100 vol% DMSO. Only most intense peaks were labeled to avoid overlapping of $00l$ labelling. For CV analysis more lines were used.

8 Delamination by repulsive osmotic swelling of synthetic Na-hectorite with variable charge in binary DMSO-water mixtures

Table S1: Data from Fig 1. Main text containing d-value and CV data

DMSO (vol%)	d-value, Å	CV (%)	Number of peaks used
52	23.4	N/A	
55	23.3	0.57	12
57	23.3	0.46	15
66	22.0	0.85	13
72	22.0	1.06	9
72	18.9	0.31	8
75	18.9	0.23	11
80	18.1	0.23	8
92	18.1	0.19	7
100	18.1	0.33	11

8 Delamination by repulsive osmotic swelling of synthetic Na-hectorite with variable charge in binary DMSO-water mixtures

^{23}Na MAS NMR spectrum of the 0.5 Hec powder in different water-DMSO mixtures

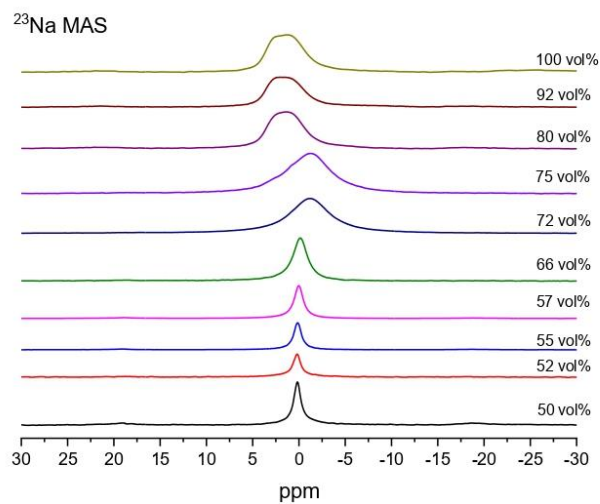


Figure S2: ^{23}Na MAS NMR of the solvated 0.5 Hec powder with different composition of water-

Table S2: The isotropic shift and quadrupole coupling for different DMSO-water mixture

Volume percent of DMSO in binary mixture, %	isotropic shift, ppm	Quadrupole coupling, Cq, kHz
52	0.4	300
55	0.3	100
57	0.1	200
66	0.2	200
72	0.6	1200
75	0.8	1300
80	1.5	500
92	1.3	200
100	1.3	100

8 Delamination by repulsive osmotic swelling of synthetic Na-hectorite with variable charge in binary DMSO-water mixtures

^{23}Na NMR spectrum of the NaCl in different water-DMSO mixtures

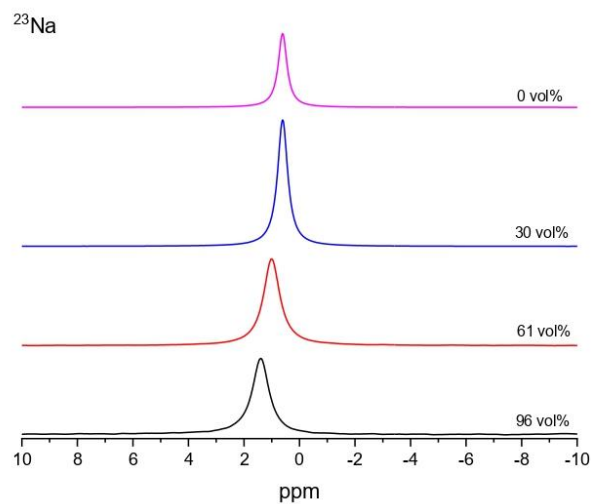


Figure S3: ^{23}Na NMR spectrum of NaCl with different composition of water-DMSO mixture. The labelling indicates the volume percent of DMSO.

Table S3: The isotropic shift of ^{23}Na for different water-DMSO mixture

Volume percent of DMSO in binary mixture, %	isotropic shift, ppm
0	0.59
30	0.62
61	1.01
96	1.38

8 Delamination by repulsive osmotic swelling of synthetic Na-hectorite with variable charge in binary DMSO-water mixtures

^{23}Na MAS NMR of 0WL, 1WL, 2WL and DMSO spectrum of 0.7 Hec

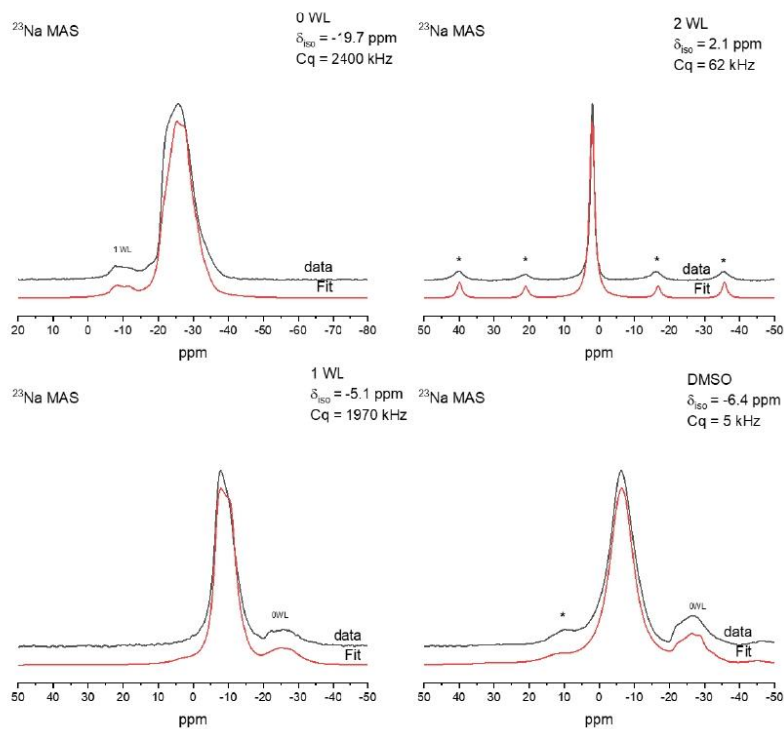


Figure S4: ^{23}Na MAS NMR spectrum of 0.7 Hec and the solid state NMR fit of different crystalline swelling regime with 0 WL, 1 WL 2 WL and DMSO. * indicate the spinning sidebands. In sample DMSO and 1WL, 0 WL peak is present and in sample 0 WL, 1 WL peak is present. These Na species were taken into account during the fitting.

8 Delamination by repulsive osmotic swelling of synthetic Na-hectorite with variable charge in binary DMSO-water mixtures

Table S4: The isotropic shift and quadrupole coupling for different 0.7 Hec crystalline swelling species

Crystalline swelling species	isotropic shift, ppm	Quadrupole coupling, Cq, kHz
0 WL	-19.7	2400
1WL	-5.1	1960
2WL	2.1	62
DMSO	-6.3	5

8 Delamination by repulsive osmotic swelling of synthetic Na-hectorite with variable charge in binary DMSO-water mixtures

PXRD of the 0.7 Hec with 0 WL, 1 WL and 2 WL

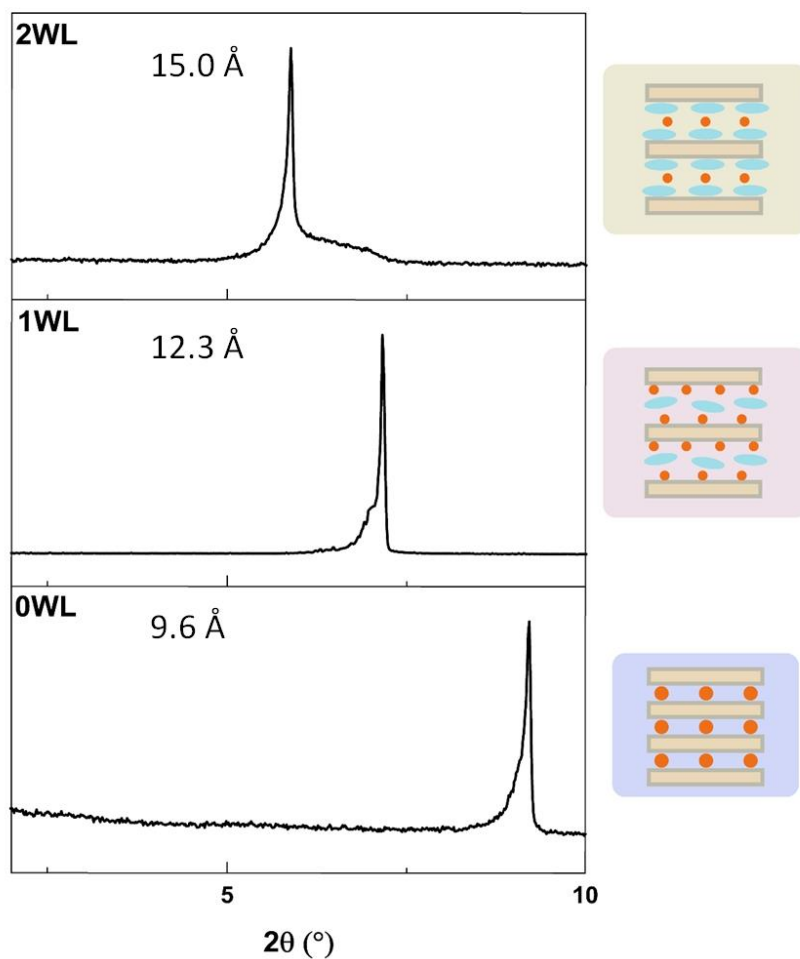


Figure S5: Different stages of water crystalline swelling of 0.7 Hec, featuring 0WL, 1WL and 2WL. Left is the schematic depiction of the water molecule arrangement. Orange circles are Na⁺ cation, blue ellipses are water molecules.

8 Delamination by repulsive osmotic swelling of synthetic Na-hectorite with variable charge in binary DMSO-water mixtures

PXRD of the 0.7 Hec dispersion in different water-DMSO mixtures

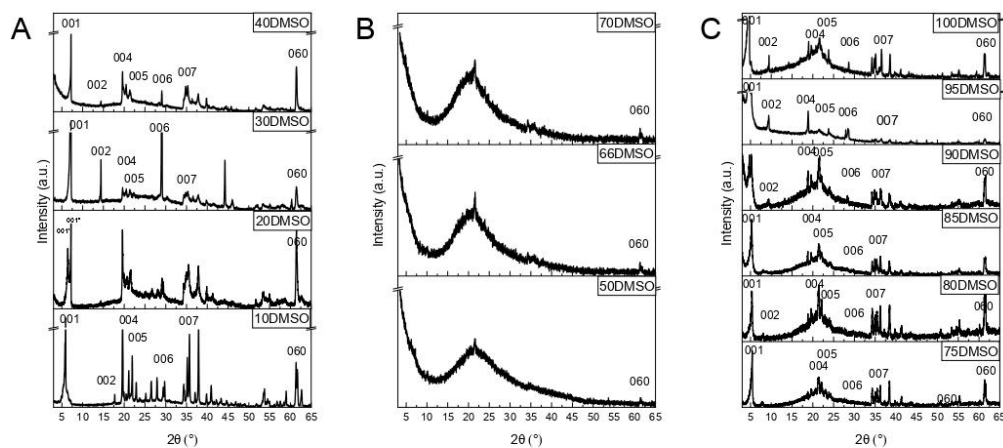


Figure S6: PXRD patterns of the crystalline swelled and osmotically swelled dispersions of 0.7 Hec in different water-DMSO mixture compositions. The broad peaks corresponds to the solvent scattering. A) PXRD of Composition from 10 to 40 vol% DMSO. B) PXRD of Composition from 50 to 70 vol% DMSO. C) PXRD of Composition from 75 to 100 vol% DMSO. Only most intense peaks were labeled to avoid overlapping of $00l$ labelling. For CV analysis more lines were used.

8 Delamination by repulsive osmotic swelling of synthetic Na-hectorite with variable charge in binary DMSO-water mixtures

Table S5: Data from Fig 2. main text containing d-value and CV data

DMSO (vol%)	d-value, Å	CV (%)	Number of peaks used
10	15.0	0.58	9
20	13.7	1.74	7
20	12.3	1.51	8
30	12.3	0.03	7
40	12.3	0.80	7
75	16.3	2.01	8
80	16.5	1.05	7
85	16.7	2.34	7
90	16.8	1.50	7
90	18.8	0.93	7
95	18.7	0.32	11
100	18.7	0.11	7

8 Delamination by repulsive osmotic swelling of synthetic Na-hectorite with variable charge in binary DMSO-water mixtures

^{23}Na MAS NMR spectrum of the 0.7 Hec powder in different DMSO-water mixtures

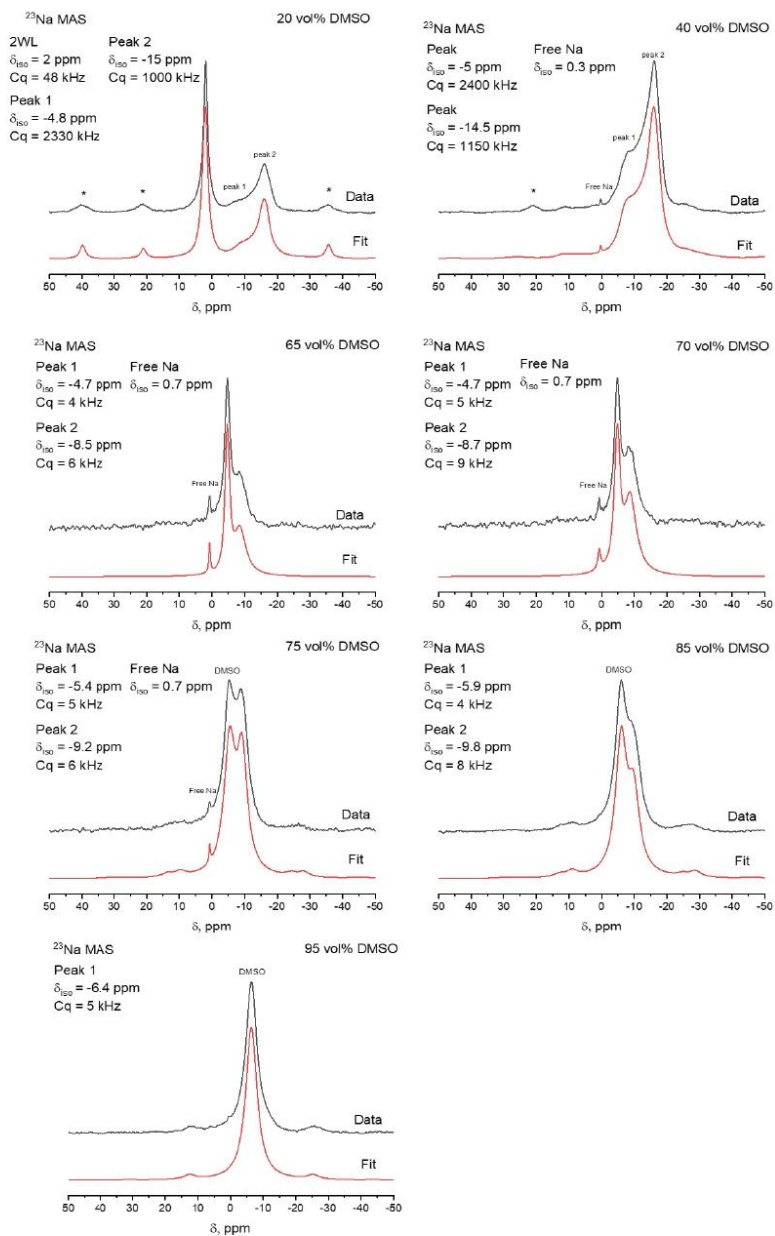


Figure S7: ^{23}Na MAS NMR spectrum of 0.7 Hec and the solid state NMR fit of solvent mixture of different compositions including (20, 40, 66, 70, 75, 85 and 95 vol% DMSO) * indicate the spinning sidebands.

8 Delamination by repulsive osmotic swelling of synthetic Na-hectorite with variable charge in binary DMSO-water mixtures

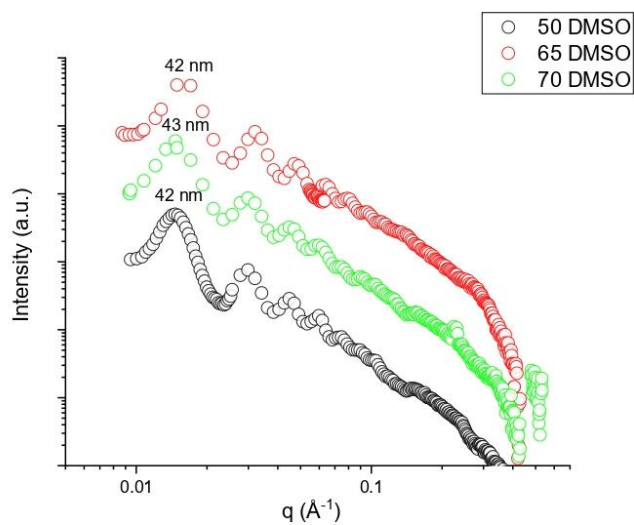


Figure S8: SAXS curves of the 0.7 Hec swelled in DMSO-water mixtures, where the number in legend indicate the vol% of DMSO in mixture. The number near the curve indicate the approximate separation between the nanosheets in solution. Curves are offset for the ease of read.

8 Delamination by repulsive osmotic swelling of synthetic Na-hectorite with variable charge in binary DMSO-water mixtures

Coefficient of variation (CV)

The coefficient of variation was calculated according to Bailey¹:

$$CV = \frac{100 * s}{X}$$

where s = standard deviation and X = mean of the observed 1 * d001 values. Due to overlap, we were only able to unambiguously determine the positions of the 001 and only reliable number of peaks are used, indicated in the tables as 'Number of peaks used'.

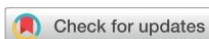
1. Bailey, S. W., Nomenclature for regular interstratifications. *Clay Miner.* **1982**, *17* (2), 243–248.

9 Spontaneous Delamination of Affordable Natural Vermiculite as a High Barrier Filler for Biodegradable Food Packaging

9 Spontaneous Delamination of Affordable Natural Vermiculite as a High Barrier Filler for Biodegradable Food Packaging

Volodymyr Dudko, Renee L. Timmins, Olena Khoruzhenko, Maximilian Röhl, Sabine Rosenfeldt, Tammelin Tekla, Seema Agarwal, Josef Breu

This work was published in *Mater. Adv.* 3, 9052 (2022). Reprinted with permission from V. Dudko et al.: *Mater. Adv.* 3, 9052 (2022). Copyright 2022 Royal Society of Chemistry.

Cite this: *Mater. Adv.*, 2022, 3, 9052

Spontaneous delamination of affordable natural vermiculite as a high barrier filler for biodegradable food packaging†

Volodymyr Dudko,^{‡a} Renee L. Timmins,^{‡a} Olena Khoruzhenko,^a Maximilian Röhrl,^a Christopher Greve,^{‡b,c} Sabine Rosenfeldt,^a Tekla Tammelin,^b Seema Agarwal,^a Eva M. Herzig,^{‡c} and Josef Breu^{‡*a}

Expensive biodegradable packaging as a preventative measure against continued accumulation of plastic waste in our environment is often in conflict with the need for high performing packaging materials that prevent food waste. Compounding with delaminated vermiculite nanosheets is a compelling concept to simultaneously improve barrier properties through creation of a 'tortuous path' while also decreasing the price of the system due to its natural abundance. However, an effective delamination process that captures the full barrier improvement potential of this natural filler has been lacking. Here, we present a superior protocol for vermiculite delamination based on reducing the intrinsic hydrophobicity due to interlayer Mg^{2+} cations and the transfer of this osmotically swollen, liquid crystalline state into organic solvents. Nanocomposite coatings of degradable polyesters on nanocellulose exhibited oxygen and water transmission rates of $130 \text{ cm}^3 \text{ m}^{-2} \text{ day}^{-1} \text{ atm}^{-1}$ and $1.74 \text{ g m}^{-2} \text{ day}^{-1}$, respectively, which competes with high-end, non-degradable poly(vinylidene dichloride) films.

Received 23rd June 2022,
Accepted 25th October 2022

DOI: 10.1039/d2ma00734g

rsc.li/materials-advances

Introduction

Innovative packaging plays a critical role in preventing loss of precious food products, yet presents a massive problem when considering their end-of-life scenarios. The United Nations Food and Agricultural Organisation estimates the global food wastage to be equivalent to 1.3 billion tons, which results in an unnecessary 3.3 billion tonnes of CO_2 equivalent of greenhouse gases being released into the atmosphere per year.¹ Materials like polyethylene, poly(vinylidene dichloride) (PVDC), and polyamide possess a high barrier to relevant permeants, including water vapour, carbon dioxide, and oxygen, which prevents food waste by protecting from contamination and preserving freshness, taste, and colour of the products. Despite these critical functions, the growing concerns and awareness of consumers towards plastic pollution and ubiquitous microplastic contamination was reflected in a major Ipsos poll conducted

in 2019, which found that 71% of global consumers believe that single use plastic products should be banned as soon as possible.² More recently, directives came from both the European Union and Canada to ban the use of certain single-use plastics,^{3,4} spearheading a growing movement to replace traditional plastics with biodegradable alternatives in the interest of environmental preservation and human health.^{5,6} Current coated and chemically treated paper alternatives only present an unrecyclable and non-compostable burden on waste management systems.⁷ There still lacks an environmentally friendly packaging option that provides the lightweight and convenient protection to which we have become accustomed.

Accordingly, one must consider the overall environmental impact of a packaged food product including the life cycle of the packaging material as well as the food. Implementation of bio-based and biodegradable packaging is an important step, but without high-performance properties that reduce food waste, the net environmental impact of the entire system is not improving.⁸ Moreover, most consumers are unwilling to pay a higher price for an item to have environmentally friendly packaging.⁹ A material substitution may become more attractive as the cost of certain biobased materials, *e.g.* cellulose and cellulose-based materials, decreases with increased production volumes while the rising price of petroleum threatens the rock-bottom price tag of conventional polymers.¹⁰ Practical and low cost solutions required to tackle the challenge of the poor and

^a Bavarian Polymer Institute and Department of Chemistry, University of Bayreuth, Universitätsstr. 30, 95440 Bayreuth, Germany. E-mail: Josef.Breu@uni-bayreuth.de

^b VTT Technical Research Centre of Finland Ltd, VTT, PO Box 1000, FI-02044 Espoo, Finland

^c Physikalisches Institut, Dynamik und Strukturbildung-Herzig Group, Universität Bayreuth, Universitätsstr. 30, 95447, Bayreuth, Germany

† Electronic supplementary information (ESI) available. See DOI: <https://doi.org/10.1039/d2ma00734g>

‡ Equal contribution.



moisture susceptible barrier properties of these bio-based and biodegradable materials are through multilayer strategies or surface hydrophobisation strategies.^{11–13} These methods indeed decrease moisture sensitivity of hydrophilic materials, but still fails to provide barrier levels acceptable for food packaging. Another such approach is by the application of a thin nanocomposite barrier coating using clay nanosheets. Nanocomposite foils have barrier performance improved by orders of magnitude compared to the neat substrate.^{14–16} The use of natural clays offers the additional benefit of being an inexpensive and sustainable filler that reduces the overall cost of the packaging.

As barrier improvement scales with the square of the platelet aspect ratio (diameter/thickness ratio) due to elongation of the diffusion path for permeates,¹⁷ the most commonly applied clay minerals, montmorillonite and LAPONITE[®]^{18,19} with an aspect ratio of <150 and 20, respectively, are insufficient. Particularly when considering the inherently poor barrier performance of biodegradable polymer matrixes,^{19,20} much larger aspect ratios are required. Layered fillers with promising diameters are synthetic hectorites²¹ or natural vermiculites. While efficient delamination protocols for the former have already been established (*i.e.*, osmotic swelling),²¹ the same cannot be said for the latter.

Osmotic swelling²² is an exceptionally effective method for the production of barrier nanosheets since it is a thermodynamically allowed process that does not require any mechanical force as opposed to ultrasound driven liquid-phase exfoliation methods. Being repulsive^{23,24} in nature allows for an utter and most gentle delamination into the thinnest possible nanosheets, while liquid phase exfoliation provides only nanosheets with a range of thicknesses (for a definition of delamination *versus* exfoliation, see: Gardolinsky and Lagay).²⁵ Consequently, only delamination *via* osmotic swelling preserves the aspect ratio inherent in the platelet diameter of the non-delaminated starting material.

Considering the polymer component of a nanocomposite coating, commercially produced biodegradable polymers like poly lactic acid (PLA), poly(butylene succinate-*co*-butylene adipate) (PBSA), and poly(butylene adipate terephthalate) (PBAT) are attractive options, but only soluble in organic solvents. Until recently, osmotic delamination was restricted to a very small number of layered compounds in water.^{26–30} Water soluble biodegradable polymers like poly(vinyl alcohol) (PVOH) are highly susceptible to swelling even under ambient conditions, significantly deteriorating the barrier performance.^{31,32} Fortunately, osmotic swelling of a synthetic hectorite could recently be extended into applicable organic solvents.³³

Natural vermiculites are 2:1 layered silicates are particularly appealing as a clay component in a nanocomposite barrier system, in contrast to a synthetic hectorite, because vermiculite deposits are abundant with global production at over 500 k tons per year³⁴ and cost around 20 ct per kg. Thermally expanded vermiculites are well-known in chemistry laboratories as the standard adsorbent for spilled organic solvents (Fig. 1a). Moreover, vermiculites have the same layer structure as the commonly applied

montmorillonite but with a much larger diameter, and hence a higher potential aspect ratio.^{35–37} Vermiculites unfortunately have a significantly higher charge density compared to montmorillonite, which renders osmotic swelling much more difficult.³⁸ Vermiculite swelling is not only impeded by the high charge density, but also by the dominant divalent interlayer cation Mg²⁺ that forms a strong and symmetrical electrostatic interaction with the adjacent nanosheets, pinning them together. Yet upon exchange with bulky organocations, vermiculite is known to swell osmotically in water.^{39–42} Due to the large diameter of nanosheets, gels obtained by swelling are not isotropic but rather viscous, liquid crystalline, nematic phases even at low concentrations of 1 vol%. It follows that in order to efficiently incorporate vermiculite into a biodegradable polymer matrix for use in sustainable food packaging, obtaining osmotic swelling in organic solvents is a critical hurdle. More specifically, for solution casting in a roll-to-roll production of nanocomposite coatings, osmotic swelling of vermiculite is required in a solvent that also dissolves biodegradable polyesters.

In this paper, we report a simple one-step ion exchange strategy for repulsive osmotic delamination of natural vermiculite in the organic solvent *N*-methyl formamide (NMF) and its mixtures that results in a high delamination yield (80 wt%) and preservation of the high aspect ratio of the nanosheets compared to ultrasonication-assisted methods.⁴³ Solution blending with biodegradable polymers like PLA becomes straightforward. Nanocomposite coatings obtained by the doctor blading of a polymer/clay suspension improved gas barrier performance of a natural, fully biodegradable,¹³ and highly hydroscopic wood-based nanocellulose paper substrate by 90.2% and 97.8%, respectively. The PLA-vermiculite coated nanocellulose system presents a biodegradable alternative to traditional high-performance food packaging with oxygen and water transmission rates of 1.30 cm³ m⁻² day⁻¹ atm⁻¹ and 1.74 g m⁻² day⁻¹, respectively. Moreover, our manufacturing strategy involves only facile and scalable unit operations positively contributing to the future implementation at a commercial scale.

Results and discussion

Repulsive osmotic delamination of natural vermiculites

Osmotic swelling of highly charged clays occurs when the interlayer cation is completely exchanged for select bulky and hydrophilic organocations.^{39–42} Cations are solvated by the solvent molecules, increasing the separation between nanosheets and boosting translational entropy within the interlayer space. Upon reaching a separation threshold, osmotic swelling sets in, allowing for a most gentle delamination process while preserving the aspect ratio inherent to the pristine platelet diameter.^{23,24,38,44}

Vermiculites are the weathering products of biotite, where the K⁺ cations are replaced by Mg²⁺ while at the same time the layer charge is reduced somewhat by oxidation of structural iron with oxygen in the air.⁴⁵ Due to the high hydration enthalpy of Mg²⁺, vermiculites are hydrated. Hydration of



9 Spontaneous Delamination of Affordable Natural Vermiculite as a High Barrier Filler for Biodegradable Food Packaging

Open Access Article. Published on 03 November 2022. Downloaded on 4/4/2023 11:29:52 AM.
This article is licensed under a Creative Commons Attribution 3.0 Unported Licence.

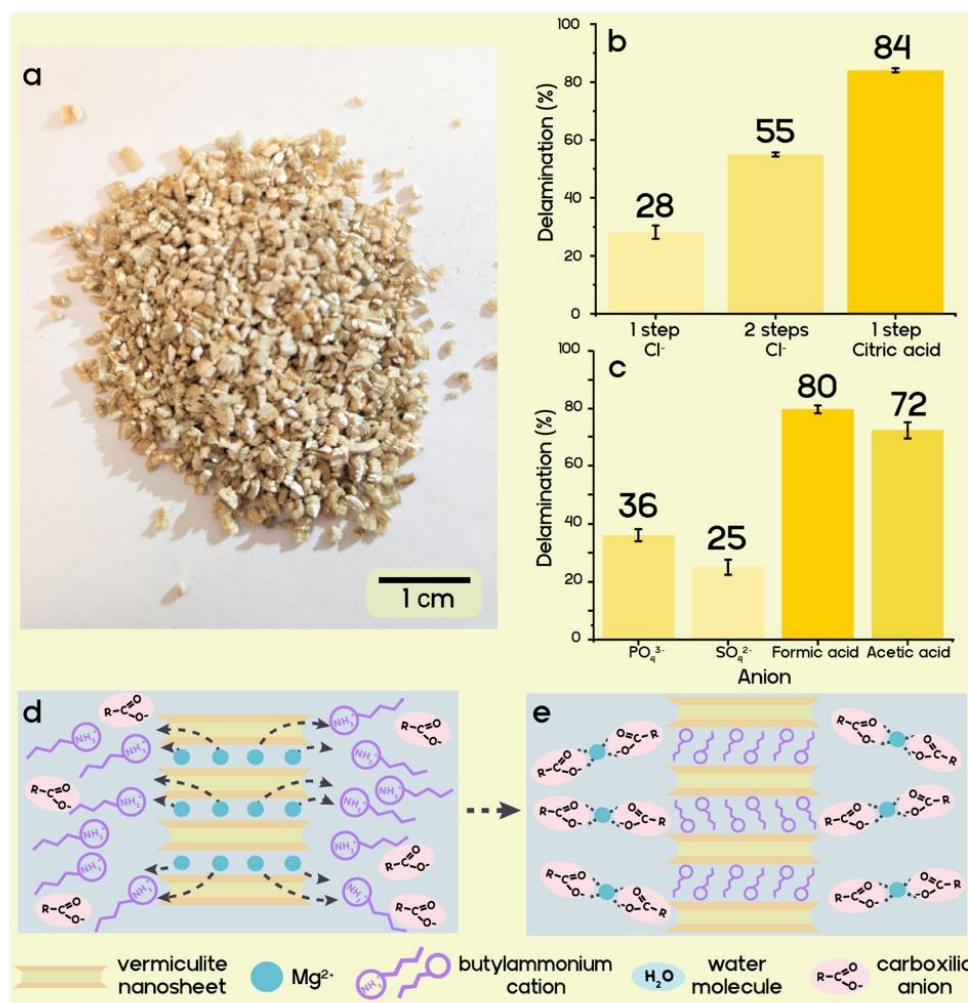


Fig. 1 Schematic representation of osmotic swelling of natural vermiculites. (a) Photo of thermally expanded natural vermiculite. (b) Delamination yield observed by a one-step ion exchange with butylammonium chloride or citrate as compared to a two-step ion exchange first to Na⁺ followed by butylammonium chloride. (c) Delamination yield observed by a one-step ion exchange with different inorganic and organic salts of butylammonium. (d) Schematic of ion exchange process in presence of carboxylic acid anions (e). The proposed process of ion exchange that leads to enhanced delamination yield. Magnesium cations form complexes with carboxylic acid anions, increasing the hydrophilicity and reducing the tendency to re-enter the interlayer space.

pristine vermiculites, however, is limited to a two-layer hydrate even when immersed into water because of the high charge density. Owing to the natural origins of such vermiculites, contamination with pristine biotite mica impurities (which have an inaccessible interlayer space and do not exhibit any swelling behaviour) is inevitable. We cannot expect to achieve a 100% yield of delaminated nanosheets from the raw mined material because of this remaining accessory mineral.

Divalent interlayer cations like Mg²⁺, as found in the pristine vermiculite, impede osmotic swelling. Complete exchange of

divalent interlayer cations with monovalent cations of higher hydration energy (*e.g.*, Li⁺)⁴⁶ or one capable of inducing steric pressure (*e.g.*, butylamine)³⁹ is essential for osmotic swelling to set in. The high selectivity in the interlayer space of vermiculite makes the direct and complete exchange of Mg²⁺ for Li⁺ or protonated butylamine difficult and time-consuming. According to Walker *et al.*, butylamine vermiculites that produce gels upon swelling have been obtained by repeated ion exchange of Mg²⁺ with Na⁺ over a period of one year.⁴⁰ Only then in a second step can Na⁺ be sufficiently replaced by butylammonium. Needless to

say, such a lengthy two-step ion exchange process is unsuitable for high-volume applications.³⁹

We hypothesise that by removing the Mg^{2+} cation from an exchange equilibrium through complexation, a high yield of ion-exchanged vermiculite in a single-step ion exchange is possible. Complexation is supplemented by the hydrophobicity of incoming organocations.⁴⁷ Carboxylic acids can be used for protonation of butylamine, while at the same time they can form stable complexes with Mg^{2+} , decreasing its activity to a level where butylammonium favourably enters the interlayer space. Vermiculite must first be activated for osmotic swelling by ion exchange in water. A series of ion exchanges were performed using butylamine in combination with one of several protonating acids to determine the most efficient pairing for maximizing the yield of the nematic phase consisting of delaminated nanosheets, and to compare with the published two-step ion exchange (Fig. 1b and c).⁴⁰ Direct ion exchange with butylammonium chloride gives only 28 wt% delamination yield, while the two-step method involving sequential exchange of Mg^{2+} for Na^+ , and then for butylammonium, provided a higher yield of 55 wt%. Butylammonium phosphate, sulfate, formate, and acetate produced yields of 36 wt%, 25 wt%, 80 wt%, and 72 wt%, respectively. The higher complex building constant for Mg^{2+} and the citrate anion compared to monodentate anions gives a superior yield of 84 wt% for butylammonium citrate (Fig. 1d and e).^{48,49} Moreover, it was found that the concentration of the butylamine solution can be decreased 10-fold without a dramatic reduction of the delamination yield (from 84% at 1 M to 75% at 0.1 M, Fig. S1, ESI†). As high ionic strength hampers repulsive osmotic swelling, the delamination yields were determined after washing in ethanol followed by redispersion into water. CHN analysis of butylammonium citrate exchanged vermiculite confirms the highest organic content out of all exchanged vermiculites, which corresponds to 91% of the cation exchange capacity, indicating a high degree of ion exchange (Table S1, ESI†).

Characterization of nematic phases and delaminated vermiculite nanosheets

Coarse-grained, non-delaminated mica may be removed through sedimentation by centrifugation, which also gives a concentrated gel of delaminated vermiculite in the supernatant. The small-angle X-ray scattering (SAXS) (Fig. 2a red dots) of gel in NMF confirms the separation to the single layers to 62.8 nm (corresponding to $q = 0.01 \text{ \AA}^{-1}$). Nematic ordering is confirmed by the presence of a rational $00l$ series and an absence of Bragg reflexes at high q values (Fig. 2a red line), which would correspond to the swollen intercalation compound of 1.4 nm.⁵⁰ The pattern can be modelled with the disk shape structure factor (Fig. 2a blue dotted line) having a diameter of 2000 nm and thickness of 1.8 nm.^{44,51,52}

Static light scattering (SLS) gave a mean particle size of about 4.9 μm (Fig. 2b), which corresponds to the hydrodynamic diameter of the nanosheets. Since SLS measurements were performed in aqueous dispersions, the particle size distribution is representative of the bulk material.⁵³ This value was cross-checked by assessing a large number of vermiculite

nanosheets with SEM micrographs (Fig. 2c), which gave a mean diameter of $4 \pm 1 \mu\text{m}$, in agreement with the SLS value.

While SAXS probes the bulk suspension, delamination of vermiculite may be confirmed at the level of individual nanosheets with atomic force microscopy (AFM). The average height of three nanosheets was $1.2 \pm 0.1 \text{ nm}$ (Fig. 2d and Fig. S2, ESI†). Since AFM images were recorded under ambient conditions, counter ions attached to the basal surface will be solvated, which adds to the true thickness of 1 nm for a 2:1 layered material.²¹ Taking this systematic error into account, it can safely be concluded that all imaged nanoplatelets are single layers because observed heights are significantly smaller than 2 nm.

Considering a nanosheet thickness of 1 nm and a 4 μm median lateral extension of the clay particles, delaminated natural vermiculite from Eucatex, Brazil offers a mean aspect ratio of 4000. This aspect ratio is more than an order of magnitude higher than the typical value for montmorillonite and is comparable to synthetic sodium tetrasilicic mica.⁵⁴ Such a high aspect ratio filler in a nanocomposite is expected to have a considerable impact on the barrier properties in combination with biodegradable polymers (Fig. S3 and eqn (S1), ESI†).

Nematic suspension of vermiculite in organic solvents

As most biodegradable polymers of commercial interest are non-water soluble polyesters (PLA, PBSA, PBAT, poly(ϵ -caprolactone)), the nematic aqueous vermiculite suspensions were freeze-dried before being re-suspended in organic solvents. Of the solvents tested, NMF proved to be capable of osmotic swelling butylammonium vermiculite yielding nematic suspensions. The greatest advantage of NMF over the other solvents is its exceptionally high dielectric constant ($\epsilon_r = 171$).⁵⁵ Unfortunately, NMF has been reported to considerably reduce the molecular weight of PLA during dissolution, which in turn ruins the mechanical integrity of PLA composites.¹⁶ Therefore, the suspension of vermiculite in NMF was concentrated by centrifugation to a gel with 9 wt% vermiculite. The gel is then diluted to 1 wt% with various other organic solvents yielding mixtures with less than 10 wt% NMF. Most low dielectric solvents instantly trigger flocculation. However, some moderately polar solvents that are used in the industrial coating preparation, including dimethylformamide (DMF), dimethylacetamide (DMAc), dimethyl sulfoxide (DMSO), *N*-methyl-2-pyrrolidone (NMP), ethanol, and γ -butyrolactone (γ -BL), preserve the nematic nature of the vermiculite suspension as indicated by birefringence under cross-polarised light (Fig. 2e).

Out of the various solvent parameters evaluated, only a high dielectric constant displays a correlation with the stability of the liquid crystal phase (Table S2, ESI†). The only clear outliers are acetonitrile and ethanol, where the former has a lower dielectric constant than expected, but still induces swelling. Assuming the wt% of NMF to be 10%, the threshold value for the dielectric constant of a co-solvent in a solvent mixture appears to be 36. The flocculated samples are shown in Fig. S4 (ESI†).

The solubility of biodegradable polymers may be estimated by applying the Hansen parameters⁵⁶ (Table S2, ESI†). Out of the listed solvents capable of osmotic swelling, γ -BL has Hansen



Open Access Article. Published on 03 November 2022. Downloaded on 4/4/2023 11:29:52 AM.
This article is licensed under a Creative Commons Attribution 3.0 Unported Licence.

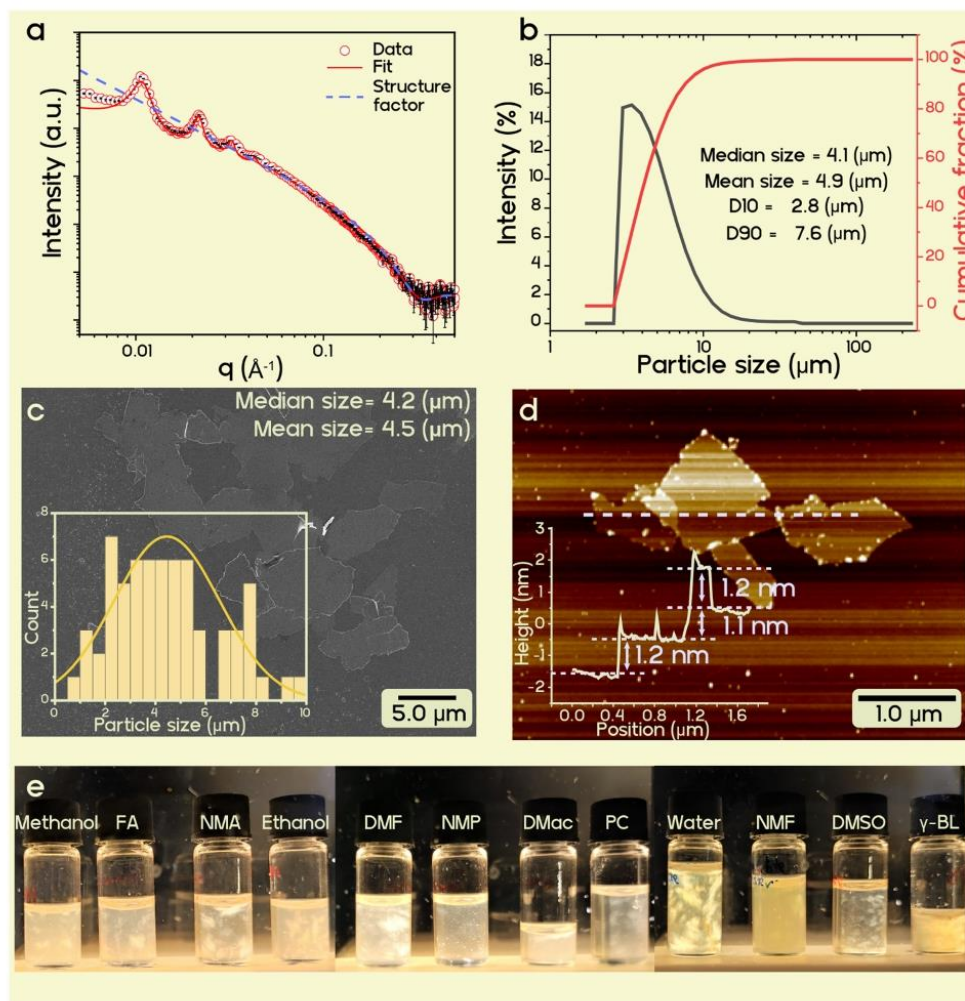


Fig. 2 Characterization of nematic suspensions and delaminated vermiculite nanosheets (a). SAXS intensity of vermiculite gel, indicating a liquid crystalline order in the nematic suspension in NMF. (b) Static light scattering number weighted size distribution indicating a mean size of 4.9 μm (c) SEM photo of vermiculite nanosheets on a Si wafer. Inset: Particle size distribution measured from the SEM image indicating a mean size of $4 \pm 1 \mu\text{m}$. (d) Topographic AFM image of vermiculite nanosheets and height profile from the single nanosheets indicating a height of $\sim 1.2 \text{ nm}$. (e) Photos of nematic suspensions of vermiculite in various solvents obtained by diluting a vermiculite/NMF gel, viewed under cross-polarized light, and reducing the tendency to re-enter the interlayer space.

parameters which indicate that it will also be capable of dissolving biodegradable polyesters (Hansen parameters for PLA are 18.9, 4.6 and 7.6 $\text{MPa}^{1/2}$ for δD , δP , and δH , respectively), as required for the preparation of high-performance, degradable nanocomposites via solution blending and roll-to-roll processing.

Fabrication of biodegradable food packaging foils

Cellulose nanofiber (CNF) paper has recently been established as an inexpensive, wood-based, sustainable, and completely

biodegradable substrate. Previous work has established the ability of this CNF substrate to degrade in compost within 4 weeks, which was comparable with other chemically unmodified cellulose variants.^{13,57,58} The CNF paper used, which was prepared from unmodified birch kraft pulp, was reported to show a pore size of approximately 5 nm and has even been applied for the purpose of organic solvent nanofiltration.⁵⁹ Physical characterizations of the film have been thoroughly studied in Lee *et al.* and others.^{13,60,61} Highly hydroscopic CNF

provides extremely poor barrier performance, especially in the presence of water vapour, making it alone unsuitable as a packaging material; therefore, we chose this substrate to demonstrate the barrier performance power of a vermiculite-filled nanocomposite. PLA was dissolved at 10 wt% in γ -BL. This solution was mixed with a 5 wt% suspension of vermiculite in the γ -BL/NMF mixture, obtained as described above, at a 50/50 weight ratio of PLA to vermiculite nanosheets. PLA addition does not compromise colloidal stability nor trigger flocculation as evidenced by no significant changes in the SAXS curves upon PLA addition (Fig. S5, ESI[†]). The nematic character of the mixture was confirmed by birefringence. The suspension with a total solid content (PLA + vermiculite) of 6.7 wt% was coated by doctor blading onto a CNF substrate. A wet coat thickness of 250 μm resulted in a $5 \pm 0.5 \mu\text{m}$ thick dry coating (PLA-verm/CNF) (Fig. S6, ESI[†]). Due to the porous nature of the CNF substrate, complete solvent removal could be achieved despite the high boiling point of NMF as solvent is allowed to permeate through the substrate while the larger clay particles and polymer chains are not. The area in which solvent molecules have to escape effectively doubles and prevents the trapping of solvent molecules within the coating as the wet layer dries from the outside inwards.

The dried nanocomposite coating resists cracking upon bending due to the highly flexible nanosheets, which is in agreement with previous work on coatings that employ high aspect ratio clay nanosheets.¹⁵ The coating also withstood scratching using a pencil of 2H hardness. For comparison, a CNF paper was coated with only PLA using the same procedure (PLA/CNF).

The oxygen transmission rate (OTR) of the PLA-verm/CNF foil was measured at 23 °C and an elevated 65% relative humidity (RH) and compared to the OTR of both the uncoated CNF paper (35 μm) and the PLA/CNF foil with a coating thickness of 10 μm . OTRs of the neat and the PLA/CNF foils were 13.3 and 13.2 $\text{cm}^3 \text{m}^{-2} \text{day}^{-1} \text{atm}^{-1}$, respectively. A coating layer of PLA on CNF paper has essentially zero effect on the oxygen barrier performance even as a thick coating, as expected, due to its exceptionally poor performance even as a bulk material (711 $\text{cm}^3 \text{m}^{-2} \text{day}^{-1} \text{atm}^{-1}$, 25 μm thickness). With or without a PLA coating, CNF oxygen barrier is not suitable for food packaging (Fig. 3a).⁶² The use of a PLA-vermiculite nanocomposite coating on CNF is a game-changer in this regard. A dramatic drop in the oxygen transmission rate for the PLA-verm/CNF foil to a value of 1.30 $\text{cm}^3 \text{m}^{-2} \text{day}^{-1} \text{atm}^{-1}$ was observed, equating to a barrier improvement factor of 3,484 (eqn (S2), ESI[†]) and a reduction in oxygen transmission by 90.2% as compared to the neat cellulose paper. This coating brings the oxygen barrier of a paper material (PLA-verm/CNF) into competition with non-degradable and high-performance materials like PVDC and metallized polyethylene terephthalate/polyethylene (PET/Met/PE) laminates, which reports OTR values in the range of 1–2 $\text{cm}^3 \text{m}^{-2} \text{day}^{-1} \text{atm}^{-1}$ ^{63,64} (Fig. 3b). Even more impressive was the drop in the water vapour transmission rate (WVTR) due to the PLA-vermiculite nanocomposite coating. CNF paper, being a hydroscopic substrate, naturally has a poor barrier to water

vapour, especially at an elevated 75% RH, which is well beyond what would be needed for swelling to set in and further deteriorate barrier performance.⁶⁵ The neat CNF paper reports a WVTR of 79.6 $\text{g m}^{-2} \text{day}^{-1}$, which is slightly improved by the addition of a PLA coating (40.1 $\text{g m}^{-2} \text{day}^{-1}$) due to its hydrophobicity, but nevertheless remains unsuitable for demanding food packaging applications. The PLA-verm/CNF foil recorded a dramatically reduced WVTR of 1.74 $\text{g m}^{-2} \text{day}^{-1}$, corresponding to a barrier improvement of 91 and a reduction in the CNF transmission rate by 97.8%. Other water soluble, high-barrier polymers like PVOH struggle to maintain WVTR values below 2 $\text{g m}^{-2} \text{day}^{-1}$ at RH above 50%.³¹ With a single degradable coating layer, our PLA-verm/CNF foil again outperforms PET/PE laminates having conventional barrier layers of ethylene vinyl alcohol (EVOH) or PVDC, and rather approaches a WVTR comparable to PET/Met/PE laminates⁶⁴ (Fig. 3b). The overall barrier performance of our PLA-verm/CNF foil sits well within the range expected for demanding applications like instant coffee packaging.

The nanocomposite coating imparts such dramatic barrier improvements due to the formation of a 'tortuous path' by impermeable clay nanosheets. The exceptional improvement observed for this vermiculite nanocomposite can be attributed to the preservation of a high aspect ratio during repulsive osmotic delamination and the high degree of orientation of the clay nanosheets that is promoted through solvent casting of osmotically swollen suspensions. These attributes increase the diffusion path of gas molecules, leading to enhanced barrier properties. In addition, the XRD pattern of the nanocomposite coating (Fig. S7, ESI[†]) indicates the intercalation of the PLA chains within the interlayer space of vermiculite, reflected by the increase in d -spacing from approximately 1.3 nm for butylamine vermiculite to 2.8 nm for the PLA nanocomposite. Previously we have demonstrated that the intercalation of polymer chains can improve the barrier properties of nanocomposite coatings and positively influence the barrier behaviour under increased relative humidity conditions.^{32,66} Previous attempts for a CNF nanocomposite film using montmorillonite could not achieve the high performing barrier values that we observed here. Despite a non-biodegradable cross-linked PVOH and poly(acrylic acid) polymer matrix that inherently has better barrier properties than PLA, without the use of a completely delaminated and high aspect ratio filler, the range of achievable barrier performance is limited.⁶⁷

Our method for vermiculite nanocomposites makes bio-based and sustainable materials like cellulose paper a viable option for even ambitious food packaging applications like crispy snacks or instant coffee packaging. While other platy fillers of synthetic origin are expensive and not environmentally benign, vermiculite is provided in bulk by nature for an appealing low price, rendering it attractive for high-volume applications such as food packaging. The coated foil also fulfills consumer preference for transparent packaging (Fig. 3c). The haze and clarity of the coated CNF is improved relative to the uncoated CNF substrate, although transparency decreases slightly from 91.7% to 85.1% for the PLA-verm/CNF foil (Fig. S7, ESI[†]).



Open Access Article. Published on 03 November 2022. Downloaded on 4/4/2023 11:29:52 AM.
This article is licensed under a Creative Commons Attribution 3.0 Unported Licence.

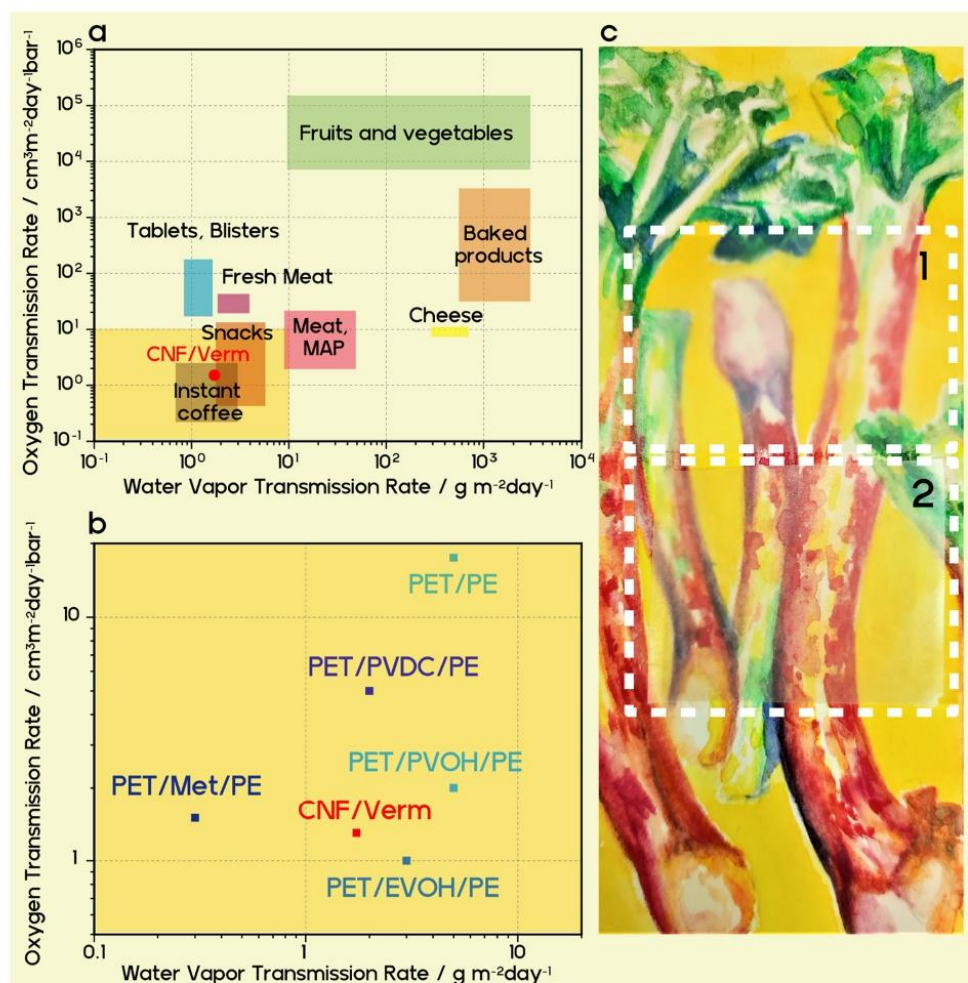


Fig. 3 Barrier properties of nanocomposites. (a) Barrier requirements for packaging of selected foods according to [62], and the barrier properties of PLA-verm/CNF foil. (b) OTR and WTR of commercial non-biodegradable high-performance multilayer packaging according to [64] in comparison with our PLA-verm/CNF foil. (c) Painting covered with the CNF substrate foil (1) and the PLA-verm/CNF foil (2).

High-performance food packaging plays a role in reducing food waste by extending the shelf life of packaged items. To explore the real life consequences of water transmission rate values, we can consider 500 g of a powdered food item (e.g. flour) that has a density of 1 g cm⁻³ and initial moisture content of 2 wt% with a critical moisture content of 8 wt% at which the food is regarded spoiled. This food item is packaged in a 3 cm × 15 cm × 10 cm rectangular plastic film pack that is exposed to 75% RH at 23 °C. If the film pack were to be made of neat CNF, the corresponding shelf life would be only 9 days. With a neat 10 μm PLA coating on CNF, the shelf life would be 18 days, making it only suitable for short-term use. Our PLA-verm/CNF foil has the shelf life of an outstanding 416 days,

opening up opportunities for long-term packaging applications (detailed calculation provided in ESI†).^{68,69} Such a shelf life extension has dramatic implications on the ability of biodegradable materials to not only reduce the amount of plastic waste entering the environment, but also to reduce food waste and contribute to a more sustainable food production cycle.

Conclusions

Our studies suggest that the modification procedure for vermiculite delamination and transfer to organic solvents provides the ideal nanosheet filler for biodegradable food packaging.

These nanosheets simultaneously addresses two major problems facing widespread implementation of biodegradable polymers: poor barrier properties and high price. Our estimation suggests that the price of 1 kg of delaminated vermiculite on the lab scale is below 1 USD, which is cheaper than PBSA or PLA (\$3.5 and \$2 per kg in 2019). In this way, we resolve difficulties in the implementation of biodegradable materials by employing a strategy that the packaging industry already uses for commodity polymers, in which almost half of the mass of material consists of inert filler (carbon black or CaCO₃) to decrease the price of the final product. A nanocomposite with 50 wt% vermiculite is expected to have a price close to \$2 per kg for PBSA and \$1.5 per kg for PLA, making it comparable to polyethylene and polypropylene, which are commonly used in the packaging industry.

Experimental section

Materials

Unless otherwise stated, all the chemicals used in the present work were purchased from Sigma Aldrich and directly used without further purification. Butylamine (99.5%), phosphoric acid (≥85 wt% in H₂O), sulphuric acid (95.0–98.0%), hydrochloric acid (37 wt% in H₂O), NMF, Citric acid (99%), formic acid (99%), glacial acetic acid (99%).

The PBSA used in this work was purchased from Mitsubishi Chemicals (BioPBS FD92PM). PLA was supplied by Nature Works, USA as the Ingeo 4043D grade semi-crystalline poly-L-lactide.

Mechanically disintegrated CNF was prepared from bleached birch kraft pulp obtained from the Finnish pulp mill. The pulp suspension was pre-refined in a Masuko grinder (Supermasscolloider MKZA10-15J, Masuko Sangyo Co., Japan) at 1500 rpm and fluidized with six passes through a Microfluidizer (Microfluidics M-7115-30 Microfluidics Corp.) at 1800 bar. Self-standing CNF films were produced by solvent casting method and they were manufactured on a semipilot scale Coatema Coating Machinery GmbH with the patented method.^{61,70,71} A 1.6 wt% CNF dispersion, including sorbitol (30 wt% solids in dry film from Sigma), was casted on polypropylene substrate. After evaporation of water, the CNF film with a thickness of 35 μm was separated from the plastic substrate and cut into A4 sheets. The grammage and density of the CNF film is 60 g m⁻² and 0.93 g cm⁻³, respectively.

Starting material was Eucatex vermiculite. The structural formula of half unit cell is [Mg_{0.35}]^{inter}[Mg_{2.475} Al_{0.075} Fe_{0.305} Ti_{0.04} Mn_{0.005}]^{oct}[Si_{3.11} Al_{0.89}]^{tet}O₁₀H₂ and cation exchange capacity of 147 m equiv./100 g. Natural vermiculite flakes were ground into crystals of 50 μm size. A larger crystal size impedes swelling.

Preparation of ion exchange solutions

Butylamine was titrated in Millipore water to pH = 7 with appropriate acid to obtain the desired counter anion. The solutions were diluted to 1 mol L⁻¹.

Ion exchange procedure. 2 g of the clay was suspended in 200 mL of a 1 M solution of the organic salt (> 25-fold excess of the CEC, delamination is prevented by the high ionic strength) and refluxed for 12 h. Then the clay was washed 5 times with 50/50 vol% water/ethanol mixture and dried in the vacuum oven at 70 °C.

Delamination experiment

A known amount of ion-exchanged vermiculite powder was added to 10 mL of MilliQ water in a 15 mL centrifuge tube and was equilibrated in an overhead shaker for 24 h. The vermiculite was then centrifuged at 3000 g for 10 minutes, and the supernatant with the delaminated nanosheets was poured into a Petri dish with a known weight. The water from the supernatant was completely evaporated at 120 °C, and then the Petri dish was equilibrated at 43% RH for 24 h. After weighing the Petri dish, the delamination yield was determined by the ratio between the weight of the nanosheets left after evaporation to the initial weight of vermiculite added for the delamination experiment.

SAXS measurements

SAXS data was collected with a “Double Ganesha AIR” (SAXSLAB, Denmark). In this laboratory-based system, a focused X-ray beam is provided by a rotating copper anode (MicoMax 007HF, Rigaku Corporation, Japan). A position-sensitive detector (PILATUS 300 K, Dectris) was used in different positions to cover the range of the scattering vector $q = 0.004\text{--}0.6 \text{ \AA}^{-1}$. Before the measurement, the clay suspensions were added to 1 mm glass capillaries (Hilgenberg, code 4007610). The circularly averaged data was normalized to the incident beam, sample thickness, and measurement time. The scattering of a solvent filled capillary was used for background subtraction. Further evaluation was done with the software Scatter (version 2.5).⁷² The measurements for ESI† are performed in vacuum at room temperature on a Xeuss 3.0 (Xenocs SAS, Grenoble, France) equipped with a Cu K α source (wave length of $\lambda = 1.54 \text{ \AA}$) and a Dectris EIGER 2R 1M detector. Different sample to detector distances (50, 350, 900, 1200 and 1800 mm) were used to cover a wider range of scattering vectors q .

AFM measurements

The surface topography has been determined by atomic force microscopic measurements. The images were acquired with a Dimension Icon (Bruker Nano Inc.) in PeakForce tapping mode in air. ScanAsyst Air cantilever (Bruker Nano Inc.) with a typical spring constant of 0.4 N m⁻¹ and a resonant frequency of 70 kHz was used. The PeakForce amplitude was 60 nm and the PeakForce frequency was 2 kHz. The AFM images were processed with NanoScope Analysis 1.80 (Bruker Nano Inc.). The topography was flattened by subtracting a first-order polynomial background using a threshold to exclude platelets from flattening. Platelet heights were determined by means of ‘step tool’ in NanoScope Analysis software. The samples were prepared by slow evaporation of a few drops of a diluted suspension (0.02 g L⁻¹) on a Si-wafer under ambient conditions.



Particle size distribution

Particle size distribution was recorded by static light scattering (SLS) of aqueous dispersions using a Retsch Horiba LA-950 SLS instrument. The refractive index of the solid phase was set to a value of 1.5. A measurement routine called “mica in water” supplied by the manufacturer (Horiba) was applied. The routine determines transmission rates and optimizes the concentration of the suspensions.

Scanning electron microscopy (SEM). SEM images of the cross-section of the film were observed using a ZEISS LEO 1530 (Carl Zeiss AG, Germany) operating at 3 kV.

Foil fabrication

PLA-vermiculite solution was prepared by mixing 2.5 g of a 10 wt% PLA solution in γ -BL with 5 g of a 5 wt% vermiculite dispersion in a γ -BL/NMF (90:10) mixture. Total solid content was 6.67 wt%. This solution was mixed overnight on an overhead mixer before being coated onto a CNF substrate using a doctor blading unit (Zehntner ZAA 2300, Zehntner GmbH Testing Instruments, Switzerland). The substrate temperature was 60 °C, the blade speed was 1.5 cm s⁻¹, and the blade height was 250 μ m. For the PLA/CNF foil, the PLA solution was coating directly onto the CNF foil using the same conditions. The coated foils were dried overnight at room temperature then in 40 °C oven for two days. Complete solvent removal was confirmed using thermal gravimetric analysis (Fig. S9, ESI[†]).

Coating thickness of 5 μ m was determined using a high-accuracy Digimatic micrometer (Mitutoyo, Japan) with a measuring range of 0–25 mm and a resolution of 0.0001 mm. Thickness was also confirmed with SEM imaging (Fig. S6, ESI[†]).

Oxygen transmission rates (OTR)

OTR was determined on a Mocon OX-TRAN 2/21 M10x system (Mocon Inc., USA) with a lower detection limit of 5×10^{-4} cm³ m⁻² day⁻¹ atm⁻¹. The measurements were performed at 23 °C and 65% RH. A mixture of 98 vol% nitrogen and 2 vol% hydrogen was used as the carrier gas and pure oxygen as the permeant (> 99.95%, Linde Sauerstoff 3.5).

Water vapor transmission rates (WVTR)

WVTR was determined on a HiBarSens HBS 2.0 HT (Sempa Systems GmbH, Dresden, Germany) with a lower detection limit of 10^{-6} g m⁻² day⁻¹. The tests were conducted at 23 °C at a relative humidity of 75%.

Thermal gravimetric analysis (TGA)

Thermogravimetric analysis was performed at a TG 209 F1 Libra (Netzsch). Approximately 8 mg of the sample was precisely weighed into an aluminum crucible (Concavus) by the internal balance of the machine. The sample was measured in the range of 25–600 °C under nitrogen. The program Proteus Analysis version 8.0 was used to process the results.

X-Ray diffraction (XRD)

XRD patterns were obtained on a Bragg–Brentano-type diffractometer (Empyrean, Malvern Panalytical BV, The Netherlands) equipped with a PIXcel-1D detector using Cu K α radiation ($\lambda = 1.54187$ Å). All patterns were analyzed using Malvern Panalytical's HighScore Plus software.

Optical properties

Transmittance, haze, and clarity were measured on a BYK-Gardner Haze-Gard Plus (BYK-Gardner GmbH, Germany). An average of five measurements per film sample were taken.

Author contributions

V. D. and R. T. contributed equally to this work. J. B., S. A., T. T. conceived and supervised the research. V. D. optimized the vermiculite delamination and performed the transfer to organic solvents. V. D. and O. K. performed the characterization of the nanosheets. Investigation of delamination progress by SAXS was done by V. D. and S. R. R. T. and M. R. performed foil fabrication and barrier measurements. V. D., R. T., O. K., and J. B. wrote the manuscript. All authors discussed the results and commented on the manuscript.

Conflicts of interest

There are no conflicts to declare.

Acknowledgements

V. Dudko and R. Timmins contributed equally to this work. The project has been funded by the Deutsche Forschungsgemeinschaft (DFG, German Research Foundation) – project number 391977956 – SFB1357/C02. V. D. thanks the Elite Network of Bavaria for support. Tekla Tammelin gratefully acknowledges the Academy of Finland's Flagship Competence Center for Materials Bioeconomy, FinnCERES. The authors thank Marco Schwarzmann for preparing and taking the transmission electron microscopy images, Michael Thelen for AFM measurements, and Dr Matthias Daab for useful discussions. We appreciate the support of the Keylabs for Polymer Additives and Fillers, Optical and Electron Microscopy, Mesoscale Characterization: Scattering Techniques, Surface and Interface Characterization of the Bavarian Polymer Institute (BPI).

Notes and references

- 1 Food wastage footprint Impacts on natural resources, Food and Agriculture Organization of the United Nations, 2013.
- 2 S. Atkinson and I. Payne, A Throwaway World: the challenge of plastic packaging and waste, <https://www.ipsos.com/en/throwaway-world-challenge-plastic-packaging-and-waste>, 2022).



9 Spontaneous Delamination of Affordable Natural Vermiculite as a High Barrier Filler for Biodegradable Food Packaging

View Article Online

Paper

Materials Advances

- 3 Single-Use Plastics Prohibition Regulations, <https://www.gazette.gc.ca/rp-pr/p1/2021/2021-12-25/html/reg2-eng.html>, 2022).
- 4 Single-use plastics, https://ec.europa.eu/environment/topics/plastics/single-use-plastics_en, 2022).
- 5 C. J. Moore, *Environ. Res.*, 2008, **108**, 131–139.
- 6 N. D. Steenis, E. van Herpen, I. A. van der Lans, T. N. Ligthart and H. C. M. van Trijp, *J. Cleaner Prod.*, 2017, **162**, 286–298.
- 7 F. Riedewald, E. Wilson, Y. Patel, D. Vogt, I. Povey, K. Barton, L. Lewis, T. Caris, S. Santos and M. O'Mahoney, *Waste Manage.*, 2022, **138**, 172–179.
- 8 M. C. Heller, S. E. M. Selke and G. A. Keoleian, *J. Ind. Ecol.*, 2018, **23**, 480–495.
- 9 M. van Birgelen, J. Semeijn and M. Keicher, *Environment and Behavior*, 2008, **41**, 125–146.
- 10 H. Shaghaleh, X. Xu and S. Wang, *RSC Adv.*, 2018, **8**, 825–842.
- 11 G. de Souza, M. N. Belgacem, A. Gandini and A. J. F. Carvalho, *Cellulose*, 2021, **28**, 1617–1632.
- 12 P. Willberg-Keyrilainen, J. Vartiainen, J. Peltó and J. Ropponen, *Carbohydr. Polym.*, 2017, **170**, 160–165.
- 13 I. Leppänen, M. Vikman, A. Harlin and H. Orelma, *J. Polym. Environ.*, 2019, **28**, 458–470.
- 14 J.-W. Rhim, H.-M. Park and C.-S. Ha, *Prog. Polym. Sci.*, 2013, **38**, 1629–1652.
- 15 C. Habel, M. Schöttle, M. Daab, N. J. Eichstaedt, D. Wagner, H. Bakhshi, S. Agarwal, M. A. Horn and J. Breu, *Macromol. Mater. Eng.*, 2018, **303**, 1800333.
- 16 R. L. Timmins, A. Kumar, M. Röhr, K. Havlíček, S. Agarwal and J. Breu, *Macromol. Mater. Eng.*, 2021, 2100727, DOI: [10.1002/mame.202100727](https://doi.org/10.1002/mame.202100727).
- 17 Y. Cui, S. Kumar, B. Rao Kona and D. van Houcke, *RSC Adv.*, 2015, **5**, 63669–63690.
- 18 B. Tan and N. L. Thomas, *J. Membr. Sci.*, 2016, **514**, 595–612.
- 19 F. Wu, M. Misra and A. K. Mohanty, *Prog. Polym. Sci.*, 2021, **117**, 101395.
- 20 S. Singha and M. S. Hedenqvist, *Polymers*, 2020, **12**(5), 1095.
- 21 M. Stöter, D. A. Kunz, M. Schmidt, D. Hirsemann, H. Kalo, B. Putz, J. Senker and J. Breu, *Langmuir*, 2013, **29**, 1280–1285.
- 22 L. J. Michot, I. Bihannic, S. Maddi, S. S. Funari, C. Baravian, P. Levitz and P. Davidson, *Proc. Natl. Acad. Sci. U. S. A.*, 2006, **103**, 16101–16104.
- 23 M. Daab, N. J. Eichstaedt, A. Edenharter, S. Rosenfeldt and J. Breu, *RSC Adv.*, 2018, **8**, 28797–28803.
- 24 M. Daab, N. J. Eichstaedt, C. Habel, S. Rosenfeldt, H. Kalo, H. Schießling, S. Förster and J. Breu, *Langmuir*, 2018, **34**, 8215–8222.
- 25 J. E. F. C. Gardolinski and G. Lagaly, *Clay Miner.*, 2005, **40**, 547–556.
- 26 W. J. Roth, T. Sasaki, K. Wolski, Y. Song, D.-M. Tang, Y. Ebina, R. Ma, J. Grzybek, K. Kalahurska, B. Gil, M. Mazur, S. Zapotoczny and J. Cejka, *Sci. Adv.*, 2020, **6**, eaay8163.
- 27 L. Wang and T. Sasaki, *Chem. Rev.*, 2014, **114**, 9455–9486.
- 28 P. Davidson, C. Penisson, D. Constantin and J.-C. P. Gabriel, *Proc. Natl. Acad. Sci. U.S.A.*, 2018, **115**, 6662–6667.
- 29 J.-C. P. Gabriel, F. Camerel, B. J. Lemaire, H. Desvaux, P. Davidson and P. Batail, *Nature*, 2001, **413**, 504–508.
- 30 R. Liu, T. Gong, K. Zhang and C. Lee, *Sci. Rep.*, 2017, **7**, 1–9.
- 31 E. S. Tsurko, P. Feicht, C. Habel, T. Schilling, M. Daab, S. Rosenfeldt and J. Breu, *J. Membr. Sci.*, 2017, **540**, 212–218.
- 32 T. Schilling, C. Habel, S. Rosenfeldt, M. Röhr and J. Breu, *ACS Applied Polymer Materials*, 2020, **2**, 3010–3015.
- 33 V. Dudko, K. Ottermann, S. Rosenfeldt, G. Papastavrou and J. Breu, *Langmuir*, 2021, **37**, 461–468.
- 34 T. J. Brown, N. E. Idoine, C. E. Wrighton, E. R. Raycraft, S. F. Hobbs, R. A. Shaw, P. Everett, E. A. Deady and C. Kresse, *World Mineral Production 2015–2019*, British Geological Survey, Nottingham, UK, 2021.
- 35 H. Kalo, M. W. Möller, D. A. Kunz and J. Breu, *Nanoscale*, 2012, **4**, 5633–5639.
- 36 A. Meunier, *Clay Miner.*, 2006, **41**, 551–566.
- 37 S. Taruta, R. Obara, N. Takusagawa and K. Kitajima, *J. Mater. Sci.*, 2005, **40**, 5597–5602.
- 38 M. Daab, S. Rosenfeldt, H. Kalo, M. Stöter, B. Bojer, R. Siegel, S. Förster, J. Senker and J. Breu, *Langmuir*, 2017, **33**, 4816–4822.
- 39 W. G. Garrett and G. F. Walker, *Clays Clay Miner.*, 1960, **9**, 557–567.
- 40 G. F. Walker and W. G. Garrett, *Science*, 1967, **156**, 385–387.
- 41 J. A. Rausell-Colom and P. S. Salvador, *Clay Miner.*, 1971, **9**, 139–149.
- 42 L. F. Braganza, R. J. Crawford, M. V. Smalley and R. K. Thomas, *Clays Clay Miner.*, 1990, **38**, 90–96.
- 43 J. L. Pérez-Rodríguez, F. Carrera, J. Poyato and L. A. Pérez-Maqueda, *Nanotechnology*, 2002, **13**, 382–387.
- 44 S. Rosenfeldt, M. Stöter, M. Schlenk, T. Martin, R. Q. Albuquerque, S. Förster and J. Breu, *Langmuir*, 2016, **32**, 10582–10588.
- 45 M. J. Wilson, *Clay Miner.*, 1999, **34**, 7–25.
- 46 J.-J. Shao, K. Raidongia, A. R. Koltanow and J. Huang, *Nat. Commun.*, 2015, **6**, 1–7.
- 47 B. Rotenberg, J.-P. Morel, V. Marry, P. Turq and N. Morel-Desrosiers, *Geochim. Cosmochim. Acta*, 2009, **73**, 4034–4044.
- 48 K. N. Pearce, *Aust. J. Chem.*, 1980, **33**, 1511–1517.
- 49 J. W. Bunting and K. M. Thong, *Can. J. Chem.*, 1970, **48**(11), 1654–1656.
- 50 N. T. Skipper, A. K. Soper and J. D. C. McConnell, *J. Chem. Phys.*, 1991, **94**, 5751–5760.
- 51 L. Boldon, F. Laliberte and L. Liu, *Nano Rev.*, 2015, **6**(1), 25661.
- 52 E. Paineau, I. Bihannic, C. Baravian, A.-M. Philippe, P. Davidson, P. Levitz, S. S. Funari, C. Rochas and L. J. Michot, *Langmuir*, 2011, **27**, 5562–5573.
- 53 D. Goossens, *Sedimentology*, 2008, **55**, 65–96.
- 54 P. Das, J.-M. Malho, K. Rahimi, F. H. Schacher, B. Wang, D. E. Demco and A. Walther, *Nat. Commun.*, 2015, **6**, 1–14.
- 55 J. Barthel, R. Buchner and B. Wurm, *J. Mol. Liq.*, 2002, **98–99**, 51–69.
- 56 C. M. Hansen, *Hansen Solubility Parameters*, CRC Press, 2007.
- 57 K. Missoum, P. Sadocco, J. Causio, M. N. Belgacem and J. Bras, *Mater. Sci. Eng., C*, 2014, **45**, 477–483.
- 58 M. Lassoued, F. Crispino and E. Loranger, *Carbohydr. Polym.*, 2021, **254**, 117411.

Open Access Article. Published on 03 November 2022. Downloaded on 4/4/2023 11:29:52 AM.
This article is licensed under a Creative Commons Attribution 3.0 Unported Licence.



9 Spontaneous Delamination of Affordable Natural Vermiculite as a High Barrier Filler for Biodegradable Food Packaging

View Article Online

Materials Advances

Paper

- 59 A. Mautner, K. Y. Lee, P. Lahtinen, M. Hakalahti, T. Tammelin, K. Li and A. Bismarck, *Chem. Commun.*, 2014, **50**, 5778–5781.
- 60 K.-Y. Lee, T. Tammelin, K. Schultfer, H. Kiiskinen, J. Samela and A. Bismarck, *ACS Appl. Mater. Interfaces*, 2012, **4**, 4078–4086.
- 61 T. Mäkelä, M. Kainlauri, P. Willberg-Keyriläinen, T. Tammelin and U. Forsström, *Microelectron. Eng.*, 2016, **163**, 1–6.
- 62 H. C. Langowski, Presented in part at the Permeation durch Packstoffe, Freising, 2008.
- 63 J. E. Samuels, *High-barrier flexible polyvinylidene chloride composite applications*, ASTM International, 1986.
- 64 J. Lange and Y. Wyser, *Packag. Technol. Sci.*, 2003, **16**, 149–158.
- 65 M. Putkonen, P. Sippola, L. Svrđ, T. Sajavaara, J. Vartiainen, I. Buchanan, U. Forsström, P. Simell and T. Tammelin, *Philos. Trans. R. Soc. A*, 2018, **376**, 20170037.
- 66 M. Röhr, L. K. S. Federer, R. L. Timmins, S. Rosenfeldt, T. Dörres, C. Habel and J. Breu, *ACS Appl. Mater. Interfaces*, 2021, **13**, 48101–48109.
- 67 S. Spoljaric, A. Salminen, N. Dang Luong, P. Lahtinen, J. Vartiainen, T. Tammelin and J. Seppälä, *Polym. Compos.*, 2014, **35**, 1117–1131.
- 68 G. L. Robertson, *Food packaging: principles and practice*, CRC press, 2005.
- 69 G. L. Robertson, *Food packaging and shelf life: a practical guide*, CRC Press, 2009.
- 70 T. Tammelin, A. Harlin, M. Vehviläinen, P. Nousiainen and K. Kolppo, *BioResources*, 2011, **6**, 2386–2398.
- 71 T. Tammelin, A. Salminen and U. Hippi, *WIPO (PCT)*, WO2013/060934, 2012.
- 72 S. Förster, S. Fischer, K. Zielske, C. Schellbach, M. Sztucki, P. Lindner and J. Perlich, *Adv. Colloid Interface Sci.*, 2011, **163**, 53–83.

Open Access Article. Published on 03 November 2022. Downloaded on 4/4/2023 11:29:52 AM.
This article is licensed under a Creative Commons Attribution 3.0 Unported Licence.



9 Spontaneous Delamination of Affordable Natural Vermiculite as a High Barrier Filler for Biodegradable Food Packaging

Electronic Supplementary Material (ESI) for Materials Advances.
This journal is © The Royal Society of Chemistry 2022

Supporting Information

Spontaneous Delamination of Affordable Natural Vermiculite as a High Barrier Filler for Biodegradable Food Packaging

*Volodymyr Dudko, Renee L. Timmins, Olena Khoruzhenko, Maximilian Röhrl, Christopher Greve, Sabine Rosenfeldt, Tekla Tammelín, Seema Agarwal, Eva M. Herzig, Josef Breu**

9 Spontaneous Delamination of Affordable Natural Vermiculite as a High Barrier Filler for Biodegradable Food Packaging

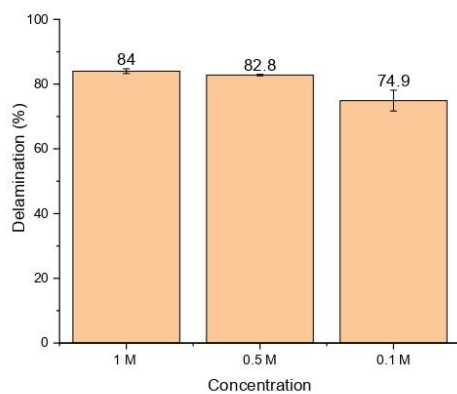


Figure S1. Comparison of the delamination yield depending on concentration of the cation.

9 Spontaneous Delamination of Affordable Natural Vermiculite as a High Barrier Filler for Biodegradable Food Packaging

CHN analysis

Table S1. Experimental wt% of C and N in exchanged organoclays

	$C_4 Cl^-$	Na to $C_4 Cl^-$	$C_4 Ac^{2-}$
C, wt %	3.9	4.78	7.6
N, wt %	1.08	1.31	2.21

$C_4 Cl^-$ is the sample prepared via single exchange using butylammonium cation and chlorine as a counter anion.

Na to $C_4 Cl^-$ denotes the two step sequential exchange with sodium and then with $C_4 Cl^-$.

$C_4 Ac^{2-}$ denotes the single exchange using the butylammonium cation and citrate as a counter anion.

9 Spontaneous Delamination of Affordable Natural Vermiculite as a High Barrier Filler for Biodegradable Food Packaging

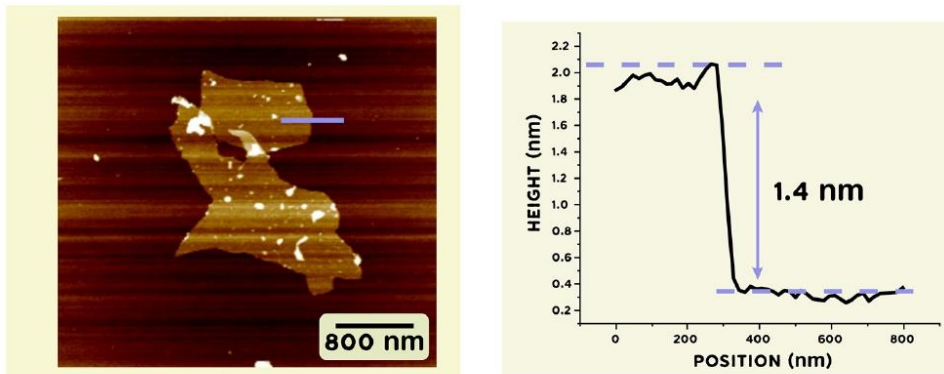


Figure S2. Topographic AFM image of a single nanosheet from an aqueous suspension with the height profile

9 Spontaneous Delamination of Affordable Natural Vermiculite as a High Barrier Filler for Biodegradable Food Packaging

Cussler's theory for permeability:

$$P_{rel} = P/P_0 = \left(1 + \mu \left(\frac{\alpha^2 \phi^2}{1 - \phi}\right)\right)^{-1} \quad \text{Equation S1}$$

Where P is the permeability of the nanocomposite, P_0 is the permeability of the neat polymer, ϕ is the filler content (volume fraction), α is the aspect ratio of the filler, μ is a geometrical factor dependent on filler shape (in case of platelet shape filler it is 4/9)^[1]

To calculate theoretical improvement factor for different nanosheet sizes: μ is 4/9, aspect ratio is 30 for Laponite, 150 for Montmorillonite, 4000 for Vermiculite.

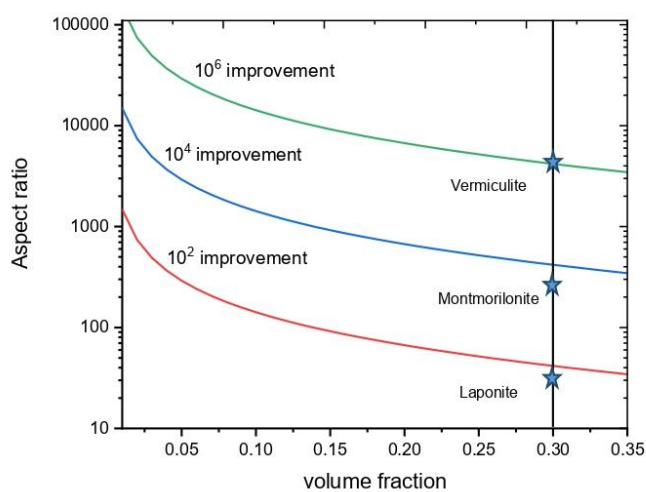


Figure S3. Improvement based on different aspect ratio nanosheets. The vertical line corresponds to a filler content as applied in the PLA-verm/CNF foil stressing the superiority of the vermiculite nanosheets compared to more common clay fillers.

9 Spontaneous Delamination of Affordable Natural Vermiculite as a High Barrier Filler for Biodegradable Food Packaging

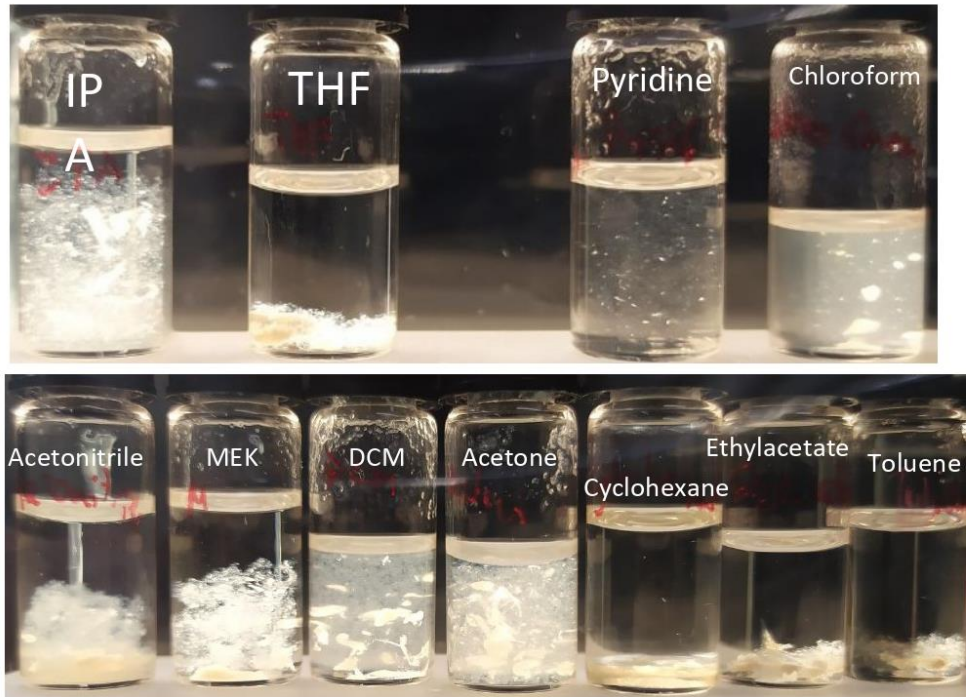


Figure S4. Photos of flocculated vermiculite samples in different solvents

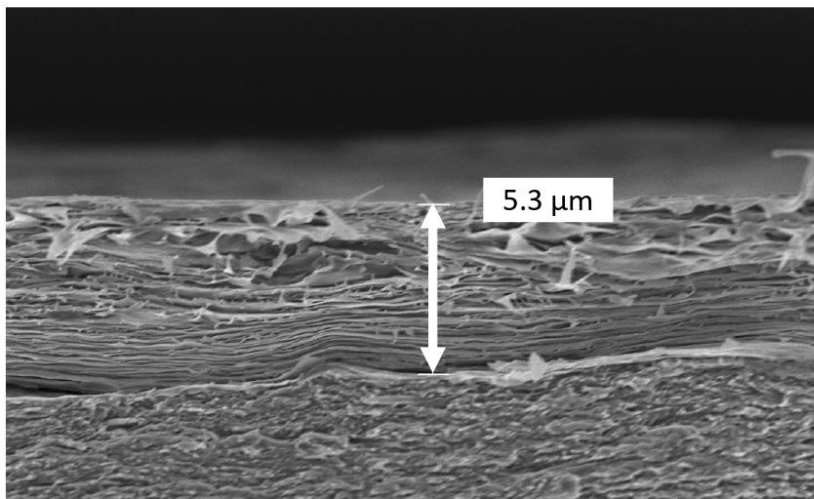


Figure S5. SEM photo of PLA-verm/CNF foil cross section. Marked bar denotes the thickness of the coating

9 Spontaneous Delamination of Affordable Natural Vermiculite as a High Barrier Filler for Biodegradable Food Packaging

Table S2. Summary of the solvent properties of the solvents used in the studies of natural vermiculite swelling

Solvents	Relative dielectric constant ^[2]	Dipole moment, D ^[2]	δD ^[3] [$Mpa^{1/2}$] ^[3]	δP [$Mpa^{1/2}$]	δH [$Mpa^{1/2}$]	Swelling
Ethanol	24.5	1.66	15.8	8.80	19.4	yes
Methanol	32.6	2.87	14.7	12.3	22.3	yes
DMac	37.8	3.72	16.8	11.5	9.40	yes
DMSO	46.7	4.10	18.4	16.4	10.2	yes
NMF	171 ^[4]	3.83	17.4	18.8	15.9	yes
Water	80.1	1.87	15.5	16.0	42.3	yes
N-methyl-acetamide	179 ^[4]	4.12	16.9	17.0	13.0	yes
FA	111	3.71	17.2	26.2	19.0	yes
γ -BL	41.0	4.27	18	16.6	7.40	yes
Propylene carbonate	64.9 ^[5]	4.94	20	18.0	4.10	yes
NMP	32.2	4.09	18	12.3	7.20	yes
DMF	36.7	3.79	17.4	13.7	11.3	yes
Isopropanol	19.9	1.59	15.8	6.10	16.4	no
Cyclohexane	1.88	0	16.8	0	0.20	no
Pyridine	12.5	2.37	19.0	8.80	5.90	no
Acetonitrile	38.8	3.44	15.3	18.0	6.10	no
Methylethyl ketone	18.5	2.78	16.0	9.00	5.10	no
Acetone	21.4	2.69	15.5	10.4	7.00	no
Toluene	2.38	0.31	18.0	1.4	2.00	no
Chloroform	4.81	1.15	17.8	3.1	5.70	no
Dichloro-methane	8.93	1.14	17.0	7.3	7.10	no
Tetra-hydrofuran	7.58	1.69	16.8	5.7	8.00	no
Ethylacetate	6.40	1.88	15.8	5.3	7.20	no

DMac-Dimethylacetamide, DMSO- Dimethyl sulfoxide, NMF- N-Methylformamide, FA-Formamide, γ -BL- gamma-Butyrolactone, NMP- N-Methyl-2-pyrrolidone, DMF- Dimethylformamide, δD dispersive, δP polar, δH hydrogen bond component of Hansen parameters.

9 Spontaneous Delamination of Affordable Natural Vermiculite as a High Barrier Filler for Biodegradable Food Packaging

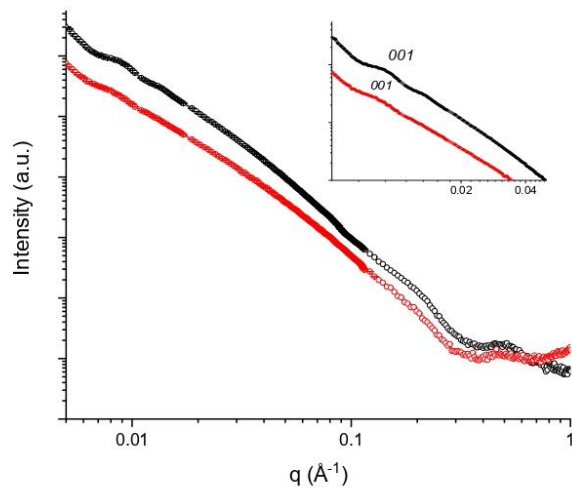


Figure S5. SAXS pattern of the vermiculite in gamma-bl (black) and vermiculite + PLA in gamma-bl (red), showing the *001* oscillation in similar position of q , showing that addition of PLA to vermiculite suspension do not compromise the colloidal stability of nanosheets. Insert shows the q range from 0.005 to 0.05 \AA^{-1} with higher magnifications.

9 Spontaneous Delamination of Affordable Natural Vermiculite as a High Barrier Filler for Biodegradable Food Packaging

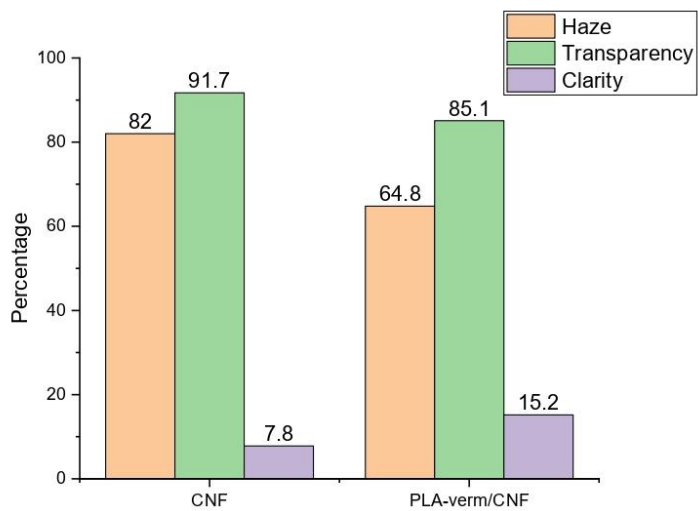


Figure S8. Optical properties (transmittance, haze, clarity) of the neat CNF substrate and CNF/Verm foil.

9 Spontaneous Delamination of Affordable Natural Vermiculite as a High Barrier Filler for Biodegradable Food Packaging

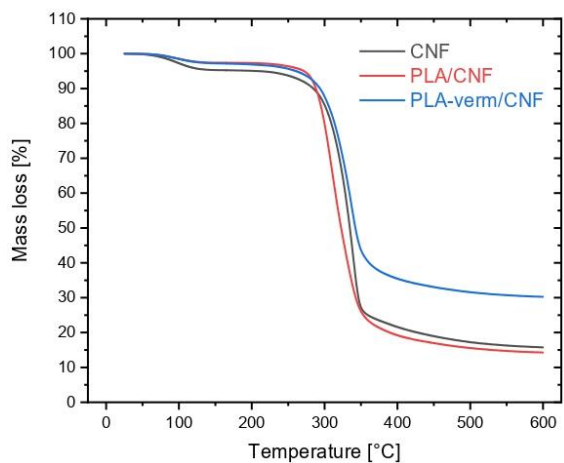


Figure S9. Thermal gravimetric analysis of CNF substrate (black), CNF coated with PLA (red), and CNF coated with PLA-verm nanocomposite (blue)

9 Spontaneous Delamination of Affordable Natural Vermiculite as a High Barrier Filler for Biodegradable Food Packaging

Calculation for barrier improvement factor

The OTRs for the coatings can be calculated by;

$$OTR_{coating} = \frac{1}{\frac{1}{OTR_{total}} - \frac{1}{OTR_{substrate}}}$$

Permeability (P) of both the neat polymer coating and the nanocomposite coating are calculated using their respective thicknesses (d);

$$P = OTR * d$$

For water vapor permeability, the water vapor partial pressure (Δp) must be considered. At 100% RH and 23°C, Δp is 0.0277 atm, which corresponds to $\Delta p = 0.020775$ atm at 75% RH and 23 °C. The new equation is;

$$P = \frac{OTR * d}{\Delta p}$$

Barrier improvement factor (BIF) is the ratio of the permeability of the neat polymer coating (P_{neat}) to the permeability of the nanocomposite coating (P_{nc});

$$BIF = \frac{P_{neat}}{P_{nc}}$$

Equation S2

9 Spontaneous Delamination of Affordable Natural Vermiculite as a High Barrier Filler for Biodegradable Food Packaging

Calculation for theoretical shelf life^[6]:

For 500 g of powder material that is 2 wt% water content,

$$weight_{dry} = 500 * 0.98 = 490 \text{ g}$$

$$weight_{water} = 500 * 0.02 = 10 \text{ g}$$

For a critical moisture content of 8 wt%, the final weight of water in the powder is,

$$weight_{max} = \frac{490}{0.92} - 490 = 42.6 \text{ g}$$

The weight of water to permeate into the powder is,

$$42.6 - 10 = 32.6 \text{ g}$$

For a rectangular package of dimensions 3 x 15 x 10 cm, the surface area is 0.045 m²

The amount of water permeating into the package per day is

$$weight_{water \text{ per day}} = 0.045 \text{ m}^2 * OTR$$

The time to reach the critical moisture content (i.e. shelf life) is,

$$shelf \ life = \frac{32.6 \text{ g}}{weight_{water \text{ per day}}}$$

9 Spontaneous Delamination of Affordable Natural Vermiculite as a High Barrier Filler for Biodegradable Food Packaging

References:

- [1] E. L. Cussler, S. E. Hughes, W. J. Ward, R. Aris, *J. Membr. Sci.* **1988**, 38, 161.
- [2] W. M. Haynes, *CRC Handbook of Chemistry and Physics*, CRC Press, **2011**.
- [3] C. M. Hansen, *Hansen Solubility Parameters*, CRC Press, **2007**.
- [4] J. Barthel, R. Buchner, B. Wurm, *J. Mol. Liq.* **2002**, 98-99, 51.
- [5] Y. Chernyak, *J. Chem. Eng. Data* **2006**, 51, 416.
- [6] G. L. Robertson, *Food packaging and shelf life: a practical guide*, CRC Press, **2009**.

10 List of publications and conferences

Publications used in the thesis

- Dudko, V., Ottermann, K., Rosenfeldt, S., Papastavrou, G., & Breu, J. (2021). Osmotic Delamination: A Forceless Alternative for the Production of Nanosheets Now in Highly Polar and Aprotic Solvents. *Langmuir*, 37(1), 461–468. doi: 10.1021/acs.langmuir.0c03113
- Dudko, V., Rosenfeldt, S., Siegel, R., Senker, J., Matejdes, M., & Breu, J. (2022). Delamination by Repulsive Osmotic Swelling of Synthetic Na-Hectorite with Variable Charge in Binary Dimethyl Sulfoxide–Water Mixtures. *Langmuir*, 38(35), 10781–10790. doi: 10.1021/acs.langmuir.2c00965
- Dudko, V., Timmins, R. L., Khoruzhenko, O., Röhr, M., Greve, C., Rosenfeldt, S., ...Breu, J. (2022). Spontaneous delamination of affordable natural vermiculite as a high barrier filler for biodegradable food packaging. *Mater. Adv.*, 3(24), 9052–9062. doi: 10.1039/D2MA00734G

Publication and manuscript not used in thesis

- Dudko, V., Khoruzhenko, O., Weiß, S., Daab, M., Loch, P., Schwieger, W., & Breu, J. (2023). Repulsive Osmotic Delamination: 1D Dissolution of 2D Materials. *Adv. Mater. Technol.*, 8(3), 2200553. doi: 10.1002/admt.202200553
- Michels-Brito, P. H., Dudko, V., Wagner, D., Markus, P., Papastavrou, G., Michels, L., ...Fossum, J. O. (2022). Bright, noniridescent structural coloration from clay mineral nanosheet suspensions. *Sci. Adv.*, 8(4), eabl8147. doi: 10.1126/sciadv.abl8147
- Schnupfhagn, C., Schumacher, T., Markus, P., Papastavrou, G., Aftenieva, O., König, T. A. F., Dudko, V. ...Lippitz, M. (2022). Disentangling the Orientations of Spectrally Overlapping Transition Dipoles in Dense Dye Layers. *Nano Lett.*, 22(18), 7499–7505. doi: 10.1021/acs.nanolett.2c02438
- Mayr, L., Amschler, S., Edenharter, A., Dudko, V., Kunz, R., Rosenfeldt, S., & Breu, J. (2020). Osmotic Swelling of Sodium Hectorite in Ternary Solvent Mixtures: Nematic Liquid Crystals in Hydrophobic Media. *Langmuir*, 36(14), 3814–3820. doi: 10.1021/acs.langmuir.0c00373

10 List of publications and conferences

- Liang, C., Dudko, V., Khoruzhenko, O., Hong, X., Zhong-Peng Lv , Breu, J., Zhang, H., Ikkala, O., Stiff and self-healing hydrogels by polymer entanglements in co-planar nanoconfinement, (2023) Submitted to Nature
- Hong, X.; Xu, Z.; Lv, Z.; Lin, Z.; Ahmadi, M.; Cui, L.; Liljeström, V.; Dudko, V.; Sheng, J.; Cui, X.; P. Tsapenko, A.; Breu, J.; Sun, Z.; Zhang, Q.; Kauppinen, E.; Peng, B.; Ikkala, O., High-permittivity solvents increase MXene stability and stacking order enabling ultraefficient Terahertz shielding, (2023) Submitted to ACS Nano
- Khoruzhenko, O., Dudko, V., Rosenfeldt, S., Breu, J., Fabricating defogging metasurfaces via a water-based colloidal route (2023) Submitted to Material horizons.

Acknowledgments

I would like to thank the following people, without whom I would not have been able to complete this thesis.

The formerly AC1 and now ICE² team at Bayreuth University, especially my supervisor Prof. Dr. Josef Breu, whose insight and knowledge into the subject matter steered me through this research.

My colleagues at the laboratory, have supported me and had to put up with my stresses and for the past years of study. Also to all the technicians, who had to do all the characterization, to Marco, Florian, and Michael.

I also would like to say thank you to all my collaborators, especially people at Aalto University, it was an enormous learning opportunity. Thank you, Hang Zhang, Chen Liang, and Olli Ikkala. Additionally, I would like to thank Marian Matejdes, for their fruitful work on the DMSO paper and thank you to Sabine Rosenfeldt for the SAXS expertise.

And my biggest thanks to my family for all the support you have shown me through this research. Especially for my wife Lena, thanks for all your support. Also thanks to Lena's family, who always was supportive,

(Eidesstattliche) Versicherungen und Erklärungen

(§ 9 Satz 2 Nr. 3 PromO BayNAT)

Hiermit versichere ich eidesstattlich, dass ich die Arbeit selbstständig verfasst und keine anderen als die von mir angegebenen Quellen und Hilfsmittel benutzt habe (vgl. Art. 64 Abs. 1 Satz 6 BayHSchG).

(§ 9 Satz 2 Nr. 3 PromO BayNAT)

Hiermit erkläre ich, dass ich die Dissertation nicht bereits zur Erlangung eines akademischen Grades eingereicht habe und dass ich nicht bereits diese oder eine gleichartige Doktorprüfung endgültig nicht bestanden habe.

(§ 9 Satz 2 Nr. 4 PromO BayNAT)

Hiermit erkläre ich, dass ich Hilfe von gewerblichen Promotionsberatern bzw. -vermittlern oder ähnlichen Dienstleistern weder bisher in Anspruch genommen habe noch künftig in Anspruch nehmen werde.

(§ 9 Satz 2 Nr. 7 PromO BayNAT)

Hiermit erkläre ich mein Einverständnis, dass die elektronische Fassung meiner Dissertation unter Wahrung meiner Urheberrechte und des Datenschutzes einer gesonderten Überprüfung unterzogen werden kann.

(§ 9 Satz 2 Nr. 8 PromO BayNAT)

Hiermit erkläre ich mein Einverständnis, dass bei Verdacht wissenschaftlichen Fehlverhaltens Ermittlungen durch universitätsinterne Organe der wissenschaftlichen Selbstkontrolle stattfinden können.

.....
Ort, Datum, Unterschrift